

TEXTE

106/2018

Impacts of Heavy Metal Emission on Air Quality and Ecosystems across Germany – Sources, Transport, Deposition and potential Hazards

Part 1: Assessment of the atmospheric heavy metal deposition to terrestrial ecosystems in Germany
Final Report

TEXTE 106/2018

Environmental Research of the
Federal Ministry for the
Environment, Nature Conservation
and Nuclear Safety

Project No. (FKZ) 3713 63 253
Report No. (UBA-FB) 002635/E

Impacts of Heavy Metal Emission on Air Quality and Ecosystems across Germany – Sources, Transport, Deposition and potential Hazards

Part 1: Assessment of the atmospheric heavy metal deposition to
terrestrial ecosystems in Germany

Final Report

by

Prof. Dr. Martijn Schaap, Carlijn Hendriks, Sander Jonkers,
Prof. Dr. Peter Builtjes
TNO, Utrecht

On behalf of the German Environment Agency

Imprint

Publisher:

Umweltbundesamt
Wörlitzer Platz 1
06844 Dessau-Roßlau
Tel: +49 340-2103-0
Fax: +49 340-2103-2285
info@umweltbundesamt.de
Internet: www.umweltbundesamt.de

 /umweltbundesamt.de

 /umweltbundesamt

Study performed by:

TNO, Netherlands Organisation for Applied Scientific Research
Princetonlaan 6
3584 CB Utrecht, The Netherlands

FU Berlin, FB Geosciences,
Institute for Meteorology
Carl-Heinrich-Becker-Weg 6-10
12165 Berlin

Study completed in:

April 2017

Edited by:

Section II 4.3 Air Pollution and Terrestrial Ecosystems
Gudrun Schütze

Publication as pdf:

<http://www.umweltbundesamt.de/publikationen>

ISSN 1862-4804

Dessau-Roßlau, December 2018

The responsibility for the content of this publication lies with the author(s).

Abstract

Atmospheric deposition of heavy metals (HM) may cause serious problems for ecosystem integrity through various (eco)toxicological hazards. To be able to assess the risk for ecosystems and human health it is important to estimate the atmospheric deposition of various metals to ecosystems in Germany. This report describes an empirical assessment of dry and wet deposition fluxes for rural, industrial and urban conditions as well as a modelling study using the chemistry transport model LOTOS-EUROS. The lowest total deposition is estimated for Cadmium with $40 \mu\text{g}/\text{m}^2/\text{year}$ on average. Typical deposition fluxes for Pb and Cu were estimated to be 1160 and $2300 \mu\text{g}/\text{m}^2/\text{year}$, respectively, while the highest deposition is estimated for Zn with $62000 \mu\text{g}/\text{m}^2/\text{year}$. Highest fluxes are found in industrialized regions. For all metals the deposition fluxes reported here are lower than previously estimated. The uncertainty in the reported deposition estimates is considered to be high due to the limited experimental basis for the empirical assessment and the high uncertainty in the emission inventories underlying the modelling work.

For mercury the current understanding of its sources, atmospheric transformation and deposition was performed. Based on measurement at Waldhof a background flux of $11 \mu\text{g}/\text{m}^2/\text{a}$ was derived. Near point sources the locally derived Mercury input may be significant. As a case study the regional deposition of two power plants in Bavaria was discussed. Furthermore, our current understanding of Mercury deposition was compared to atmospheric deposition estimates used in water quality assessments for two river catchments. Although the central values compared well, a few recommendations were made to improve the spatial allocation of the Mercury deposition flux.

Kurzbeschreibung

Die Zielstellung dieser Studie war es, die atmosphärische Deposition von Schwermetallen in terrestrische Ökosysteme in Deutschland zu ermitteln. Die Quantifizierung der Schwermetalleinträge stützt sich auf zwei methodische Säulen. Erstens wurde für alle Metalle ein empirischer Ansatz basierend auf Schwermetallgehalten im Feinstaub und Schwermetallkonzentrationen im Regenwasser verfolgt. Die Depositionsflüsse wurden für vier verschiedene Stationstypen (städtisch, ländlich, Verkehr und Industrie) ermittelt. Zweitens wurden auf Basis von verfügbaren Emissionsinventaren für verschiedene Metalle (V, Cu, Ni, Zn, As, Cd und Pb) die Depositionsfelder über Deutschland mit dem chemischen Transportmodell LOTOS-EUROS berechnet. Die niedrigste mittlere Gesamtdeposition wird mit $40 \mu\text{g}/\text{m}^2 \cdot \text{Jahr}$ für Cadmium geschätzt. Für Pb (1160) und Cu (2300) sind die Einträge deutlich höher, während die höchsten Einträge mit $62000 \mu\text{g}/\text{m}^2 \cdot \text{Jahr}$ für Zn geschätzt wurden. Diese Depositionsflüsse sind deutlich niedriger als bisher geschätzt wurde. Da für die meisten Schwermetalle die Anzahl der Konzentrations- und Depositionsmesswerte in Deutschland begrenzt ist, sind mit dem empirischen Verfahren zur Schätzung der trockenen und nassen Deposition erhebliche Unsicherheiten verbunden. Gleiches gilt für die Ergebnisse der Modellierung und zwar aufgrund der eingeschränkten Qualität und Detailliertheit der Emissionsdaten und damit der begrenzten Möglichkeiten zur Validierung.

Der vorliegende Bericht umfasst weiterhin auch eine Literatur- und Modellierungsstudie, die als spezieller Beitrag der Bestimmung von Quecksilberdepositionen dient. Für Hintergrundbedingungen in Deutschland schätzen wir die Hg-Deposition auf Basis von Messungen an der Station Waldhof auf etwa $11 \mu\text{g} / \text{m}^2 \cdot \text{a}$. In der Nähe von Emissionsquellen könnte die Gesamtdeposition deutlich höher sein. Als Fallstudie wurde die regionale Deposition von zwei Kraftwerken in Bayern anhand indikativer Berechnungen mit dem LOTOS-EUROS-Modell und einem lokalen Dispersionsmodell diskutiert. Die heutigen Stand des Wissens wurde verglichen zu die Quecksilbereinträge die in der Modellierung von Wasserqualität verwendet wird. Obwohl die zentralen Werte gut übereinstimmen, empfehlen wir, die Methodik zur Bestimmung der räumlichen Verteilung zu aktualisieren.

Table of Contents

List of Figures.....	VII
List of Tables.....	IX
List of Abbreviations.....	X
1 Introduction.....	1
2 Quantifying atmospheric deposition of heavy metals.....	2
2.1 Introduction.....	2
2.2 Simple assessment approach.....	2
2.2.1 Introduction.....	2
2.2.2 Dry deposition estimation.....	3
2.2.2.1 Data availability in UBA database and site classification	3
2.2.2.2 Average concentrations based on UBA database	5
2.2.2.3 Expanded literature search for heavy metal concentration data	6
2.2.2.4 Establishing representative concentrations	7
2.2.2.5 Size fractionation	8
2.2.2.6 Effective dry deposition velocity	9
2.2.2.7 Empirical dry deposition fluxes	10
2.2.3 Empirical wet deposition fluxes.....	11
2.2.3.1 Observation locations	11
2.2.3.2 Post processing of the wet deposition observations	12
2.2.3.3 Observation analysis	12
2.2.4 Empirical total deposition fluxes.....	16
2.3 Chemistry transport modelling.....	20
2.3.1 LOTOS-EUROS model description and application.....	20
2.3.2 Emission data.....	22
2.3.3 Model results.....	22
2.3.3.1 Cadmium and lead distributions	22
2.3.3.2 Modelled spatial distributions for wet deposition	24
2.3.3.3 Concentration modelling	34
2.3.3.4 Assessment of effective dry deposition velocity	38
2.4 Discussion on emissions.....	42
2.5 Conclusions.....	45
3 Case Study: Mercury.....	47
3.1 Introduction.....	47
3.2 Mercury components.....	48

3.3	Mercury budget.....	49
3.3.1	Emissions	49
3.3.1.1	Primary sources	49
3.3.2	Atmospheric transformation processes	55
3.3.2.1	Oxidation	56
3.3.2.2	Reduction	56
3.3.2.3	Mercury partitioning between aerosol and gas phase	56
3.3.3	Removal processes	57
3.3.3.1	Wet deposition	57
3.3.3.2	Dry deposition	57
3.4	Atmospheric mercury levels in Germany	59
3.4.1	Atmospheric concentration levels.....	59
3.4.2	Dry deposition	59
3.4.3	Wet deposition of mercury.....	60
3.4.4	Total deposition estimate for Germany	61
3.5	Establishing the mercury input of two plants in Bavaria to the catchments of the Isar and Salzach.....	62
3.5.1	Plants under consideration.....	62
3.5.2	Local scale dispersion calculations	64
3.5.3	Regional calculation with LOTOS-EUROS.....	67
3.5.4	Comparison to deposition estimates used in MoRe for Salsach and Isar	68
3.6	Conclusions.....	70
4	References	73
5	List of Annexes.....	77
Annex 1:	Dry deposition fluxes (in $\mu\text{g}/\text{m}^2/\text{year}$) based on empirical approach and modelled deposition velocities.....	78
Annex 2:	Total deposition fluxes (in $\mu\text{g}/\text{m}^2/\text{yr}$) based on empirical approach and modelled deposition velocities.....	80

List of Figures

Figure 1:	Number of stations with data on heavy metal concentrations in PM ₁₀ for the years 2009, 2010 and 2011 from the UBA database (source: this work)	3
Figure 2:	Annual mean concentrations (in ng/m ³) of cadmium and lead in PM ₁₀ averaged for all sites according to the UBA station classification for background (Bg), industrial (Ind) and traffic (Tr) sites. Values for 2009, 2010 and 2011 are plotted (source: this work)	4
Figure 3:	Empirical annual dry deposition flux on arable land (ara), coniferous forest (cnf), deciduous forest (dec), urban land (urb) and seminatural vegetation (sem) for rural areas (source: this work)	10
Figure 4:	Empirical dry deposition flux on arable land (ara), coniferous forest (cnf), deciduous forest (dec), urban land (urb) and seminatural vegetation (sem) for urban areas (source: this work)	11
Figure 5:	Locations of observation stations (wet deposition and air concentration) throughout Germany (source: this work)	12
Figure 6:	Observed annual total wet depositions [µg/m ² /year] left : UBA stations; right : Länder stations (source: this work)	13
Figure 7:	Summary of empirically derived wet deposition for metals in Germany based on Länder observations as well as UBA observations. Data averaged over the years 2009,2010 and 2011. (Source: this work).....	16
Figure 8:	Contribution of dry deposition to total deposition for several metals and land use classes (source: this work)	17
Figure 9:	Total deposition for selected land use classes based on empirical data.....	17
Figure 10:	Comparison between the central total deposition estimates obtained in this study and those by Knappe (2008)	18
Figure 11:	Deposition velocities for fine and coarse particles used in this study and those used by Knappe (2008)	18
Figure 12:	Average measured concentration in air (ng/m ³) for Pb, Cr and Cd based on this study and Knappe (2008)	19
Figure 13:	A sketch of an Eulerian chemistry transport model such as LOTOS-EUROS (source: ctocog.org).....	20
Figure 14:	Modelled 5 year mean concentration distribution (upper left) and dry deposition flux to arable land (upper right) for lead as well as the comparison to observed concentration data (lower panel) (source: this work)	23
Figure 15:	Modelled 5 year mean concentration distribution (upper left) and dry deposition flux to arable land (upper right) for cadmium as well as the comparison to observed concentration data (lower panel) (source: this work)	24
Figure 16:	Modelled annual total wet deposition fluxes [µg/m ² /year] (source: this work)	25

Figure 17:	Scatter plots of modelled versus observed annual wet deposition totals for Arsenic. Top: Länder data, Bottom : UBA data. Note the difference in scales. Source: this work	27
Figure 18:	Scatter plots of modelled versus observed annual wet deposition of cadmium in 2009. Top: Länder data, Bottom : UBA data. Note the difference in scales. Source: this work	28
Figure 19:	Scatter plots of modelled versus observed annual wet deposition of nickel in 2009. Top: Länder data, Bottom : UBA data. Note the difference in scales. Source: this work	29
Figure 20:	Scatter plots of modelled versus observed annual wet deposition of zinc. Top: Länder data, 2009; Bottom: UBA data, 2010. Note the difference in scales. Source: this work	30
Figure 21:	Scatter plots of modelled versus observed annual wet deposition of lead in 2009. Top: Länder data; Down: UBA data. Note the difference in scales. Source: this work.....	31
Figure 22:	Scatter plot of modelled versus observed annual wet deposition of vanadium in 2009 from Länder data. Source: this work	32
Figure 23:	Scatter plots of modelled versus observed annual wet deposition of copper. Top: Länder data, 2009; Bottom: UBA data, 2010. Note the difference in scales. Source: this work	33
Figure 24:	Scatter plots of modelled versus observed annual average concentration including all stations (urban, rural, traffic and industrial). Source: this work.....	35
Figure 25:	Effective dry deposition velocity per land use category based on each individual year and the 5 year period for the fine and coarse fractions of lead and cadmium (source: this work)	39
Figure 26:	Comparison of the long term average effective dry deposition velocity for fine and coarse cadmium (source: this work)	41
Figure 27:	Effective v_d for fine cadmium particles: comparison of the 5-yr mean to the 4-yr mean excluding 2010 (source: this work).....	42
Figure 28:	Overview of the atmospheric mercury budget (source: www.ii.cnr.it).....	49
Figure 29:	Global emission of mercury by activity sector in 2005 (source: Rafaj et al., 2013)	51
Figure 30:	Officially reported annual emission of mercury to air for the EU28 in 2010 (tonnes/yr). Source: this work	52
Figure 31:	Reported and expert emission estimates for Germany (source: EMEP, 2015).....	53
Figure 32:	Mercury emissions by country according to several emission databases. Efs = emission factors. Source: this work	54
Figure 33:	The implemented chemical model for mercury in Polyphemus (source: Polyphemus website). In this picture the gaseous and aqueous phases are marked by white and grey.	57

Figure 34:	Mercury concentrations in air (left; ng/m ³) and precipitation (right; ng/L) from the EMEP network (www.emep.int).	59
Figure 35:	Google earth picture of SWM Heizkraftwerk Nord	63
Figure 36:	Google earth picture of GDF SUEZ Kraftwerk.....	63
Figure 37:	Locations of Kraftwerk Zolling and Heizkraftwerk Nord. In pink : the German Länder borders; light grey: the Isar area, brown: the Salzach area. Source: this project.....	64
Figure 38:	Local scale dispersion modelling results (source: this work).....	66
Figure 39:	Modelled mercury concentrations (ng/m ³) with LOTOS-EUROS.....	68
Figure 40:	Mercury deposition rates as used within MoRe.....	69

List of Tables

Table 1:	Metals considered in this work, in order of decreasing effort spent on the assessment	2
Table 2:	Number of measurement stations recording Cd and Pb air concentrations, per station type, for the years 2009-2011.....	5
Table 3:	Summary of UBA measurements of heavy metals for rural, urban background, industrial and traffic stations. * = stations for which three years of data was available. Average concentrations in ng/m ³	5
Table 4:	Overview of data availability for heavy metal measurements in Germany and surrounding countries. Between brackets: station types for which data is available (I = Industrial; R = Rural; T = Traffic, U = Urban)	6
Table 5:	Representative values for heavy metal concentrations over Germany. N = number of measurements on which the concentration is based.	8
Table 6:	Size fractions (PM _{2.5} /PM ₁₀ ratio) used in this study	9
Table 7:	Effective dry deposition velocity in cm/s for each land use category used in this study	9
Table 8:	Land use categories	21
Table 9:	Specification of the emission data applied in the modelling	22
Table 10:	Comparison of the 2005 emission totals for heavy metals as used in LOTOS-EUROS (Denier van der Gon et al., 2005; Builtjes et al., 2012) and officially reporting by Germany in 2016 (www.emep.int).....	43
Table 11:	Comparison of Cadmium and Lead emissions for the year 2000 from TNO-official and ESPREME-official and ESPREME-expert inventories.....	43
Table 12:	Emissions of Copper and PM ₁₀ (tonnes/yr) from brake wear from transport as well as the implied percentage (%) of Copper.	45
Table 13:	Overview of global anthropogenic Hg emissions (Mg/yr)	51
Table 14:	Overview of German mercury emissions (tonnes) in the period 1990-2015 (UBA, 2017).....	52

Table 15:	Emission factors from IIASA and Zyśk et al. (2011) for Hg (kg.PJ ⁻¹)	53
Table 16:	Specific splitting factors of total mercury into its main forms – literature review	55
Table 17:	Estimated effective and average dry deposition velocities for GOM and PBM based on Schaap et al. (2015).	58
Table 18:	Mercury levels (pg/m ³) for 2009-2011 at Waldhof (Weigelt et al., 2013).	59
Table 19:	Estimates of mercury deposition to forest and grassland in the surrounding of Waldhof.	60
Table 20:	Mean Hg-concentration in precipitation at four locations in Germany (www.emep.int).....	61
Table 21:	Estimates of typical total deposition for reactive mercury in background and polluted conditions as well as GEM deposition for the German situation [ug/m ²].	62
Table 22:	Reported mercury emissions (kg/yr) for the two selected point sources in Bavaria.	63

List of Abbreviations

PM	Particulate Matter
UBA	Umweltbundesamt
HM	Heavy metals
CLC2006	Corine Land Cover 2006 database
ECMWF	European Centre for Medium-Range Weather Forecasts
EMEP	European Monitoring and Evaluation Programme
TNO	Netherlands Organisation for applied scientific research TNO
GEM	Gaseous elemental mercury
GOM	Gaseous oxidized mercury
PBM	Particle bound mercury
CTM	Chemistry transport model
E-PRTR	European Pollutant Release and Transfer Register
MoRe	Modelling of Regionalized Emissions; system to quantify Hg input to surface water

1 Introduction

Enhanced atmospheric deposition and subsequent enhanced concentrations of heavy metals (HM) may cause serious problems for ecosystem integrity through various (eco)toxicological hazards (Becker et al. 2013; Truhaut 1977). Total atmospheric deposition of heavy metals encompasses dry, wet and occult deposition. Although wet deposition fluxes are monitored throughout Europe, experimental data for occult and dry deposition are hardly available. Hence, to assess these inputs to terrestrial ecosystems one relies on chemistry transport modelling or on empirical estimates based on the heavy metal content of particulate matter. Alternatively or complementarily, monitoring organisms (bioindicators, biomonitors) are used for monitoring and mapping spatial patterns of element concentrations (e.g. Harmens et al., 2010). Although the moss concentration data provide no direct quantitative measurement of total deposition, this information can be derived by statistical approaches relating element concentrations in mosses to deposition monitoring data (Harmens et al. 2010, 2011). Further biomonitoring data of HM in biota (i.e. needles or leaves) has been produced in international monitoring programmes (ICP Forests) and on national level (German Environmental Specimen Bank).

This project aims at extending established methods of modelling and mapping heavy metal deposition in Germany and risk assessing, respectively (Bultjes et al. 2011). In this framework, three different groups of HM are investigated: Group A (Cd, Hg and Pb) dealt with highest priority; Group B (As, Cr, Cu, Ni and Zn) considered with medium intensity; Group C comprises other HM (V, Mn, Sb, Ti, Th, Co, Mo and Pt). The first goal of this project part was **to establish the atmospheric deposition for a range of heavy metals to terrestrial ecosystems in Germany**. For this purpose the total deposition was assessed using empirical data and chemistry transport modelling and the results were compared to an earlier study by Knappe (2008).

An important distinction between mercury and other atmospheric pollutants is that environmental and health impacts are only indirectly related to ambient atmospheric concentrations of Mercury. Once deposited to land or oceans, mercury can be converted by microorganisms to the extremely toxic methylmercury (MeHg), which begins its rise in the food chain inflicting increasing levels of harm on higher order species such as predatory fish and fish eating birds and mammals. The experimental data on atmospheric mercury to assess its deposition to ecosystems is very limited, making it very difficult to provide an empirical assessment of mercury deposition. In this study we aim **to summarize the current understanding of atmospheric Mercury and provide a first order estimate of the mercury deposition for conditions in Germany**. Specific additional questions relevant for UBA were:

- What are the most important sources of Mercury in the atmosphere?
- How large is the contribution of anthropogenic emissions from Germany to international long range transport?
- Which part of its direct anthropogenic emissions deposits in Germany?
- How large is the re-emission in comparison to the total emission?

Additionally, a case study aimed **to quantify in how far regional emission sources are relevant to the mercury deposition in a river catchment area** was performed. The focus of this case study was on two catchments in Bavaria.

The deposition information described in this part of the project report were compared to and evaluated with available data on HM concentration in various biomonitors (mosses, leaves, needles). Furthermore, the modelled data were integrated with these observations using regression analysis and geostatistical methods. Finally, a risk assessment was performed. These activities are described in part 2 of the project report.

2 Quantifying atmospheric deposition of heavy metals

2.1 Introduction

Quantifying the atmospheric deposition of heavy metals to ecosystems remains a challenge as experimental observation data for many metals are few and, if present, emission estimates are highly uncertain. This study aims to establish the atmospheric deposition of heavy metals to terrestrial ecosystems in Germany and to identify ecosystems at risk. In total, 16 metals are in focus. As the information availability on the different metals differs substantially, the metals have been divided in three groups, indicating the effort put into their assessment from high to low (Table 1).

Table 1: Metals considered in this work, in order of decreasing effort spent on the assessment

Group A	Group B	Group C
Cd, Pb, Hg	As, Cr, Cu, Ni, Zn	V, Mn, Sb, Ti, Th, Co, Mo, Pt

To quantify the atmospheric heavy metal input to ecosystems two methodologies were used. For all metals a first order assessment was made based on experimental data. Available air concentration and wet deposition data were classified as function of station type. Through combination of air concentrations with effective dry deposition velocities typical ranges for dry deposition fluxes can be estimated for each land use class for rural, urban, traffic and industrial areas. Combination with wet deposition data provides first order estimates for the total deposition.

In the second methodology the chemical transport model LOTOS-EUROS was used to calculate land use dependent dry deposition distributions across Germany for the metals that allow explicit modeling. Calculations were performed using existing emission databases or through the modeling of PM in combination with metal contents. An example for the latter is the estimation of vanadium levels based on modeled primary PM from heavy oil combustion. The observations from methodology 1 were used for validation. To correct for systematic biases in the modelling, the model results are connected with the moss monitoring data in part 2, chapter 4, of the project report.

In this report the assessment of the atmospheric input to German terrestrial ecosystems is detailed. Below, we first describe the empirical assessment that forms a basis for all metals. The second section of this chapter describes the explicit modelling exercise for selected metals.

2.2 Simple assessment approach

2.2.1 Introduction

The simple assessment approach to estimate the atmospheric input to terrestrial ecosystems in Germany is based on empirical data. The total deposition will be estimated based on separate assessments for dry and wet deposition fluxes:

$$F_{tot} = F_{wet} + F_{dry}$$

For the wet deposition flux we will evaluate the rain water composition data available from the deposition network of the UBA and federal states in section 2.2.3.

For the assessment of the dry deposition flux a more elaborate approach is needed as no measurements of the dry deposition flux exist. Hence, we rely on measured concentration (C) data in combination with established dry deposition velocity to estimate the dry deposition flux. As heavy metals are generated by wear and combustion processes it is well known that the metals occur in both the coarse and fine particulate matter fractions. As the deposition velocities (Vd) of these fractions it is important to assess the size fractionation (a) for each metal. The dry deposition is estimated using the following formula:

$$F_{dry} = C * \{ a * Vd_{fine} + (1-a) Vd_{coarse} \}$$

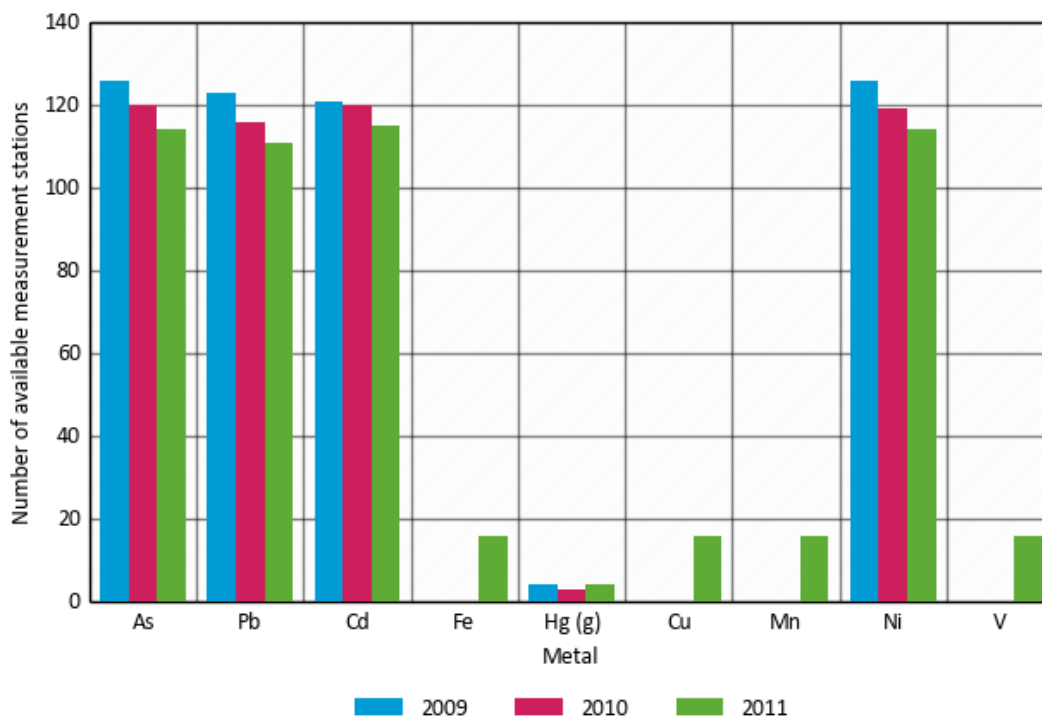
In the following sections we describe how we apply this formula to estimate the dry deposition flux of HMs to selected eco-systems. Afterwards the wet deposition estimates are presented and added together to arrive at the total deposition estimates.

2.2.2 Dry deposition estimation

2.2.2.1 Data availability in UBA database and site classification

The first step in the assessment of the dry deposition flux to ecosystems is to establish the typical concentration of a metal and its variability. UBA delivered their measurement database for heavy metal contents in PM₁₀ to the project partners. The database consisted of annual mean concentrations of gaseous Hg and 7 components of PM₁₀: Cd, Pb, Ni, V, Fe, Cu and Mn. In Figure 1 we show the number of stations available from this database. For four of these metals the number of stations exceed 100 for each year in 2009, 2010, and 2011. For the other four elements the data availability is confined to a few stations in Hessen, 2011. We have used the large dataset for Cd, Pb, Ni and As to make a first assessment of the variability of the concentrations and establish a strategy for the other elements.

Figure 1: Number of stations with data on heavy metal concentrations in PM₁₀ for the years 2009, 2010 and 2011 from the UBA database (source: this work)



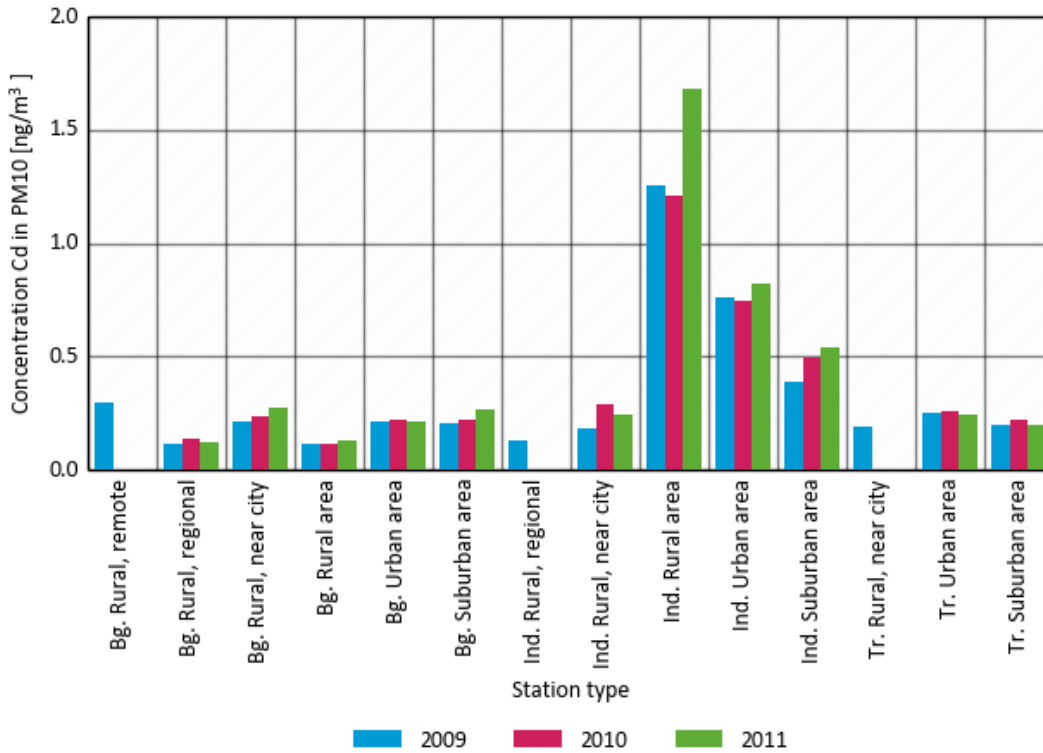
The UBA measurement database uses the official site classification system defined by the EU (European Commission, DG Environment, 2013) with 14 classifications for the station surroundings. In Figure 2 we summarize the observed annual concentrations as function of these categories for cadmium and lead. Table 2 shows the number of stations available for each station type and year. It can directly be observed that the highest concentrations occur in industrial areas for both metals. The high averages for industrial stations in rural areas for both metals are caused by one station with very high values: at Braubach (Rheinland-Pfalz) measured values for cadmium and lead are more than a factor 10 larger than at other stations with the same qualifications. The same, but to a smaller extent, is true for Stollberg Heinrichböhlplatz (Nordrhein-Westfalen) and industrial stations in urban area.

Although for four metals the segregation in 14 station types seems possible, this is not the case for the others. Moreover, we can observe that some classes show very similar concentrations. Hence, we have adopted a more simplistic station categorization in this study. We look at four different stations types: rural, urban, traffic and industrial. These station types are assumed to reflect background, as well as more polluted and near source conditions.

Figure 2: Annual mean concentrations (in ng/m^3) of cadmium and lead in PM10 averaged for all sites according to the UBA station classification for background (Bg), industrial (Ind) and traffic (Tr) sites. Values for 2009, 2010 and 2011 are plotted (source: this work)

Cadmium in PM10

Annual average



Lead in PM10

Annual average

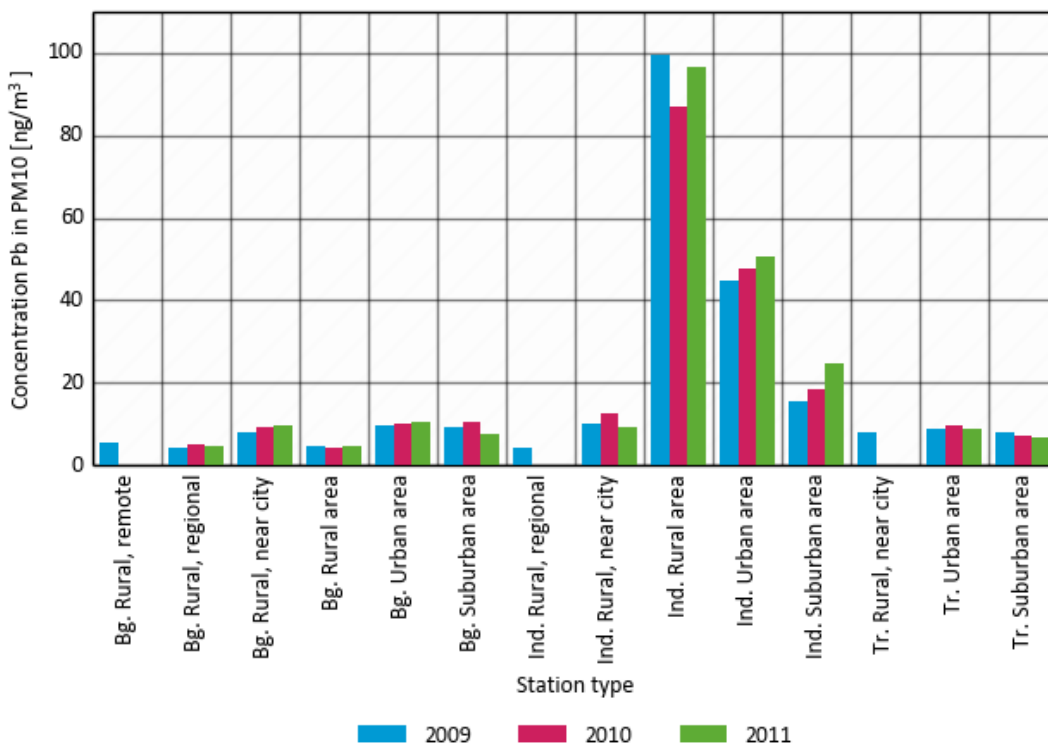


Table 2: Number of measurement stations recording Cd and Pb air concentrations, per station type, for the years 2009-2011

Station type	Cadmium			Lead		
Rural, remote	2			2		
Rural, regional	6	8	7	7	8	7
Rural, near city	4	4	3	4	4	3
Rural area	9	7	8	9	7	8
Urban area	24	28	26	27	28	26
Suburban area	10	6	5	10	6	4
Rural, regional	1			1		
Rural, near city	2	1	1	2	1	1
Rural area	2	3	3	3	3	3
Urban area	13	14	13	13	14	13
Suburban area	9	11	9	9	11	9
Rural, near city	1			1		
Urban area	37	37	38	34	33	35
Suburban area	1	1	2	1	1	2

2.2.2.2 Average concentrations based on UBA database

In this section we provide the mean concentrations of the individual HMs for the 2009-2011 time period. The annual means of the available years were averaged to obtain these values. Hence, data for Cd, Pb, Ni and As reflect three year averages whereas the other data are representative for Hessen, 2011. Comparison of the annual mean concentration per station type in Figure 2 shows that the inter-annual variability in the concentration averaged over a number of sites is not very large.

In Table 3 we present the average concentration for all years for the four groups of stations. For rural stations, the average of all stations classified as 'rural background' is taken, whereas urban background represents all stations with classification 'suburban background' and 'urban background'.

 Table 3: Summary of UBA measurements of heavy metals for rural, urban background, industrial and traffic stations. * = stations for which three years of data was available. Average concentrations in ng/m³

	Rural		Urban background		Industrial		Traffic	
	N	Average concentration	N	Average concentration	N	Average concentration	N	Average concentration
As*	19	0.59	34	0.80	28	1.63	40	0.95
Pb*	20	2.32	34	9.95	28	40.59	36	9.04
Cd*	19	0.15	33	0.22	27	0.70	39	0.25
Cu	3	6.87	10	15.51	1	30.62	2	35.32

	Rural		Urban background		Industrial		Traffic	
	N	Average concentration	N	Average concentration	N	Average concentration	N	Average concentration
Mn	3	5.92	10	12.64	1	225.9	2	10.8
Ni*	19	1.12	34	2.14	27	7.13	39	2.24
V	3	0.47	10	0.58	1	2.51	2	0.62

2.2.2.3 Expanded literature search for heavy metal concentration data

The UBA database does not include all heavy metals targeted by this study. Hence, to expand on the data from the UBA database, a literature search into heavy metal concentration measurements for Germany and its neighbouring countries for the period 1990-2013 was conducted (Andersen et al., 2007; Beuck et al., 2011; Cyrus et al., 2003; Gu et al., 2011; Hueglin et al., 2005; John et al., 2001; Kuhlbusch and John, 2000; Scheider and Lorbeer, 2002; Richard et al., 2011; Rogula et al., 2011; Swielicki and Krejci, 1996; Vallius et al., 2005, VMM, 2010; 2011; 2013).

The measurement sites were divided into four classes: Industrial, Rural, Traffic and Urban. All sites with direct influence of air quality by industry were classified as industrial, i.e. this category contains both rural industrial and urban industrial stations. When available, the station classification of the studies was adopted, in other cases the classification was based on the description of the measurement site in the studies. The number of studies available varies per metal, which is illustrated in Table 4. This table gives an overview of the data availability for the heavy metals considered in this study. For most metals 4-8 German and 7-11 international studies were found. For thallium and platinum-group elements no data were found, whereas for tin, cobalt and molybdenum only few German studies were found. Note that most studies only give the metal concentration in the PM₁₀ fraction. Only a few report the concentration in PM_{2.5} or PM_{2.5-10}, which we need to determine the size fraction.

Table 4: Overview of data availability for heavy metal measurements in Germany and surrounding countries. Between brackets: station types for which data is available (I = Industrial; R = Rural; T = Traffic, U = Urban)

Metal	German studies	International studies
Cd	5 (IRTU)	7 (IRTU)
Pb	8 (IRTU)	10 (IRTU)
Hg	1 (IR)	0
As	4 (IRTU)	9 (IRTU)
Cr	5 (RTU)	8 (IRTU)
Cu	7 (IRTU)	11 (IRTU)
Ni	8 (IRTU)	12 (IRTU)
Zn	7 (IRTU)	10 (IRTU)
V	5 (IRTU)	11 (IRTU)
Mn	6 (IRTU)	11 (IRTU)
Sb	2 (RU)	8 (IRTU)
Ti	5 (RUT)	10 (IRTU)
Th	0	0
Co	2 (U)	3 (RUT)

Metal	German studies	International studies
Mo	1 (RU)	8 (IRTU)
Pt	0	0

2.2.2.4 Establishing representative concentrations

Representative concentrations of each metal in PM₁₀ for the several stations types for Germany were established using the following procedure:

- When measurements from at least four German stations of a certain type were available for the period 2003-2013, the average of these measurements was taken (approach A).
- When for a certain station type the previous requirement was not met, first measurements from surrounding countries in the period 2003-2013 are included (approach B).
- If this still yields too little measurement sites, older data from Germany and its neighboring countries is also taken into account (approach C).
- If data is lacking almost completely and the 'representative' concentration is based on less than four stations in total, the approach is called D (including German stations) or E (no German measurements available).

The thus obtained 'representative' heavy metal concentrations for Germany and the approaches are listed in Table 5. The concentration gradients between the station types shows variation between different groups of metals depending on the main source sector. For example, many metals (As, Cd, Pb, Ni, Mn) are industry-derived and show high levels at industrial sites, lower but very comparable concentrations at urban and traffic sites and lowest values at rural sites. Metals with traffic (Sb) and both industrial and traffic sources (Cu) show maxima at traffic locations. Cr and Zn show little variation with the station type. For most metals either approach A or B has been followed. This is not a surprise as the procedure was set up in a practical sense.

Average concentrations of substances for which measurements were performed at a large number of stations in Germany (e.g. Cd, Pb, As, Ni) can be used with quite some confidence, although the standard deviation across the stations can sometimes be large. The latter is especially true for industrial areas as the concentrations of individual metals depend very much on the type of industry located in a specific industrial zone. For the metals for which a mixture of German and foreign data was used (B) the question rises how representative the data for neighboring countries are for German conditions. On the other side, when few locations are available for Germany in procedure A these could also be biased to a certain region. These representativity issues are difficult to answer, but for vanadium a strange feature is observed in the data. Procedure A was followed for rural and urban locations and procedure B was followed traffic and industrial sites. The derived vanadium concentrations, however, are a factor 5-10 different between the categories for the two different procedures. Therefore, we compare the average metal concentrations from German studies to those from foreign studies to get an indication.

Table 5: Representative values for heavy metal concentrations over Germany. N = number of measurements on which the concentration is based.

	Industrial			Rural			Traffic			Urban		
	repr. conc. (ng/m ³)	N	Approach	repr. conc. (ng/m ³)	N	Approach	repr. conc. (ng/m ³)	N	Approach	repr. conc. (ng/m ³)	N	Approach
Cd	0.70	40	A	0.15	24	A	0.25	50	A	0.23	47	A
Pb	40.59	40	A	5.61	24	A	9.04	49	A	10.15	46	A
Hg	1.29	1	D	1.67	4	A	n.a.	-	-	n.a.	-	-
As	1.63	40	A	0.59	24	A	0.95	53	A	0.84	46	A
Cr	5.40	5	B	3.36	10	B	4.81	10	B	5.09	14	B
Cu	15.07	6	B	5.96	4	A	30.64	12	B	18.78	12	A
Ni	7.13	40	A	1.17	24	A	2.24	53	A	2.28	47	A
Zn	52.00	5	B	54.42	10	B	53.43	10	B	58.86	14	B
V	5.65	6	B	0.63	4	A	3.37	12	B	0.73	11	A
Mn	46.81	6	B	5.71	4	A	13.00	12	B	14.32	12	A
Sb	2.23	4	B	1.21	8	B	3.56	10	B	2.97	11	B
Ti	11.82	5	B	4.82	10	B	9.88	10	B	8.74	14	B
Th	n.a.	-	-									
Co	n.a.	-	-	0.27	3	E	0.50	1	E	0.37	2	D
Mo	2.22	4	B	1.02	8	B	2.06	10	B	2.12	10	B
Pt	n.a.	-	-									

2.2.2.5 Size fractionation

Ideally, one should use only reported data on PM_{2.5} and PM₁₀ that were measured simultaneously to determine the fractionation between the fine and coarse fraction. The only studies in which such a size fractionation is reported are Kuhlbusch and John (2000) and Schneider and Lorbeer (2002). In practice, in PM-speciation campaigns different samples are taken for PM_{2.5} and PM₁₀. Issues like sampler failure, filter braking or analysis errors will occur occasionally. Therefore, studies tend to report PM_{2.5} and PM₁₀ contents based on different number of samples. Fortunately, the difference in numbers is mostly small. Thus, to include more metals and more recent data in the assessment, results from John et al. (2001), Hueglin et al. (2005) and Schaap et al. (2010), who report PM_{2.5} and PM₁₀ are taken into account as well.

If the size fraction (PM_{2.5}/PM₁₀ ratio) from Kuhlbusch and John (2000) is available for a species and station type, this fraction is taken. If not, an estimate based on the other studies is taken. The studies give very different size fractions, e.g. for rural stations the Cd size fraction ranges from 0.4 to 1. Therefore, establishing reliable size fractions is difficult and the numbers presented here (see Table 7) should be used carefully as the uncertainties are large and difficult to quantify.

Table 6: Size fractions (PM_{2.5}/PM₁₀ ratio) used in this study

Metal	Industrial	Rural	Traffic	Urban
Cd	0.4	0.6	0.9	0.9
Pb	0.7	0.6	0.7	0.9
Hg	n.a.	n.a.	n.a.	n.a.
As	0.7	0.8	0.7	0.8
Cr	n.a.	0.8	0.8	0.6
Cu	n.a.	0.8	0.3	0.5
Ni	0.3	0.6	0.6	0.8
Zn	0.5	0.4	0.9	0.9
V	n.a.	0.9	0.9	0.8
Mn	n.a.	0.4	0.3	0.4
Sb	n.a.	0.7	0.2	0.5
Ti	n.a.	0.4	0.3	0.4
Th	n.a.	n.a.	n.a.	n.a.
Co	n.a.	n.a.	n.a.	n.a.
Mo	n.a.	n.a.	n.a.	n.a.
Pt	n.a.	n.a.	n.a.	n.a.

2.2.2.6 Effective dry deposition velocity

The next piece of information we need is the effective dry deposition velocity of fine and coarse particles to different land use classes. To establish the effective dry deposition velocity for heavy metals simulations were made with the LOTOS-EUROS model for Cd and Pb for the years 2007-2011. These model simulations and determination of the effective deposition velocities are described in detail in 0. The effective dry deposition velocities are available for 9 land use classes used in the dry deposition module of LOTOS-EUROS, see Table 7. Largest dry deposition velocities are modelled for the rough surfaces such as forests and urban areas.

Table 7: Effective dry deposition velocity in cm/s for each land use category used in this study

Effective vd	Fine particles	Coarse particles
Grassland	0.07	0.29
Arable land	0.09	0.31
Permanent crops	0.10	0.40
Coniferous forest	0.17	0.88
Deciduous forest	0.17	0.41
Water	0.09	0.26
Urban	0.15	0.36
Other	0.04	0.26
Semi-natural	0.08	0.30

2.2.2.7 Empirical dry deposition fluxes

In the sections above we have described all the necessary information needed to derive empirical dry deposition fluxes for different land use categories in rural, urban and industrial areas as well as near major roads using the relation

$$F_{dry} = C * \{ a * Vd_{fine} + (1-a) Vd_{coarse} \}.$$

The resulting empirical dry deposition fluxes for all metals for which sufficient data was available, all land use classes and all station types (industrial, urban, rural and traffic) are listed in Annex 1. For rural stations, the dry deposition fluxes for arable land, coniferous and deciduous forest and urban areas are displayed in Figure 3. Figure 4 shows the same for urban regions. The higher deposition flux over coniferous forest is caused by the higher effective deposition velocity for this land use class.

Figure 3: Empirical annual dry deposition flux on arable land (ara), coniferous forest (cnf), deciduous forest (dec), urban land (urb) and seminatural vegetation (sem) for rural areas (source: this work)

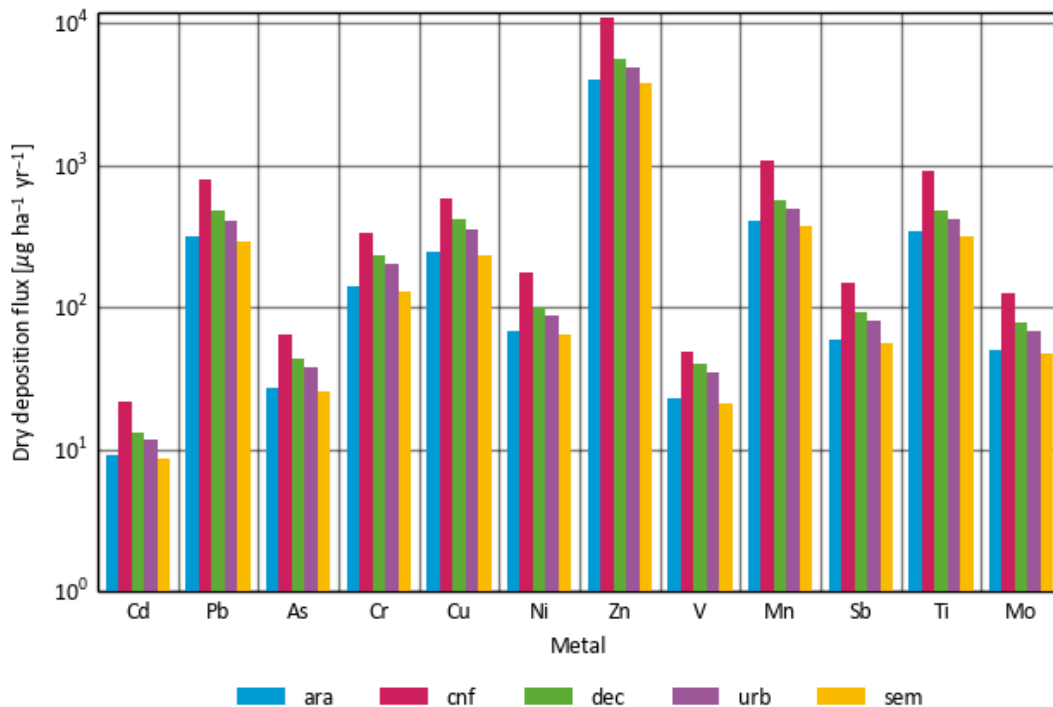
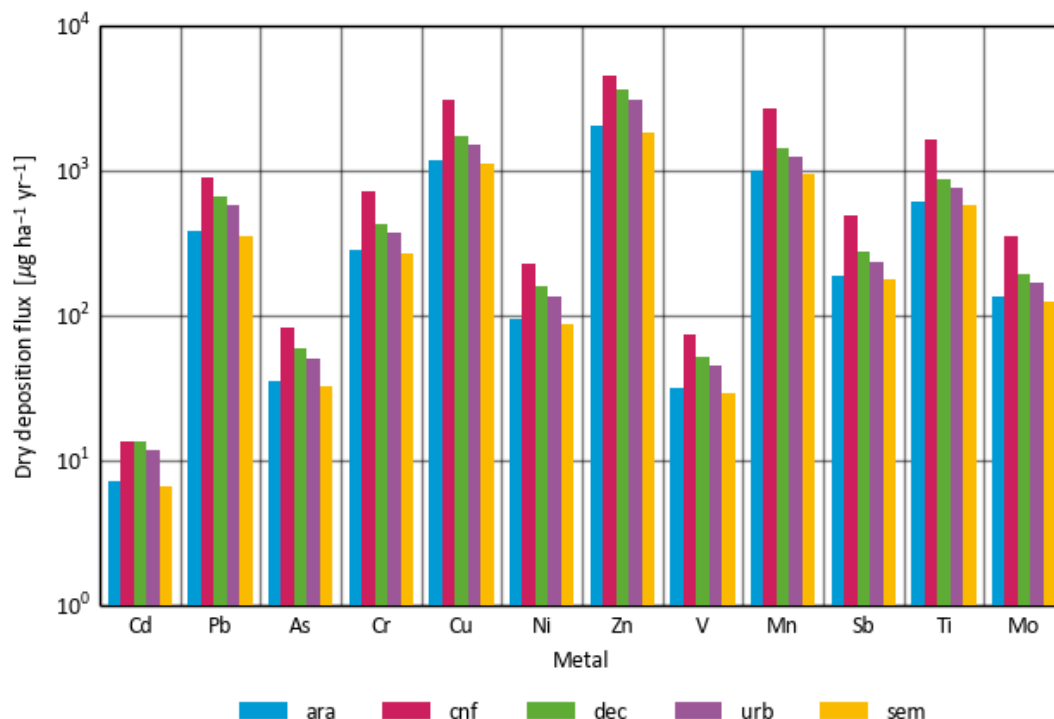


Figure 4: Empirical dry deposition flux on arable land (ara), coniferous forest (cnf), deciduous forest (dec), urban land (urb) and seminatural vegetation (sem) for urban areas (source: this work)



The differences in dry deposition flux between rural and urban areas depends on the metal of concern. Copper, for example, is emitted by traffic and the concentrations and deposition fluxes in urban areas are elevated compared to rural areas. For Zinc, the empirically derived deposition fluxes are higher for rural areas while measured concentrations are about the same for both station types. Zinc in rural areas is more often found in the coarse mode than for urban areas, making deposition in rural situations more effective. For most metals the difference in deposition flux between urban and rural areas is small, considering the uncertainties surrounding the empirical deposition flux estimation that are mainly due to limited availability of concentration and fine/coarse ratio measurements.

2.2.3 Empirical wet deposition fluxes

2.2.3.1 Observation locations

The wet deposition flux is observed throughout Germany by both the individual Länder and UBA. The locations of the observation stations are shown in Figure 5. The observation method of the Länder is often different from that of UBA. The networks in the Länder mostly apply the bulk sampling method. In a bulk deposition sampler, rain water, containing pollutants, is collected. However, in dry periods, air pollutants can still deposit into the water as the water collector is open continuously. Hence, to determine the heavy metal rainwater concentration, the concentration in the collected water is corrected, using the Gauger correction (Gauger et al., 2000). The observations of UBA are performed with wet-only samplers. The water collector opens automatically during rainy periods and showers and is sealed otherwise. Therefore, the heavy metal concentration in the collected water can be interpreted directly as the rain water concentration. Figure 5 displays the observation location of the states (Länder) and UBA throughout Germany.

Figure 5: Locations of observation stations (wet deposition and air concentration) throughout Germany (source: this work)

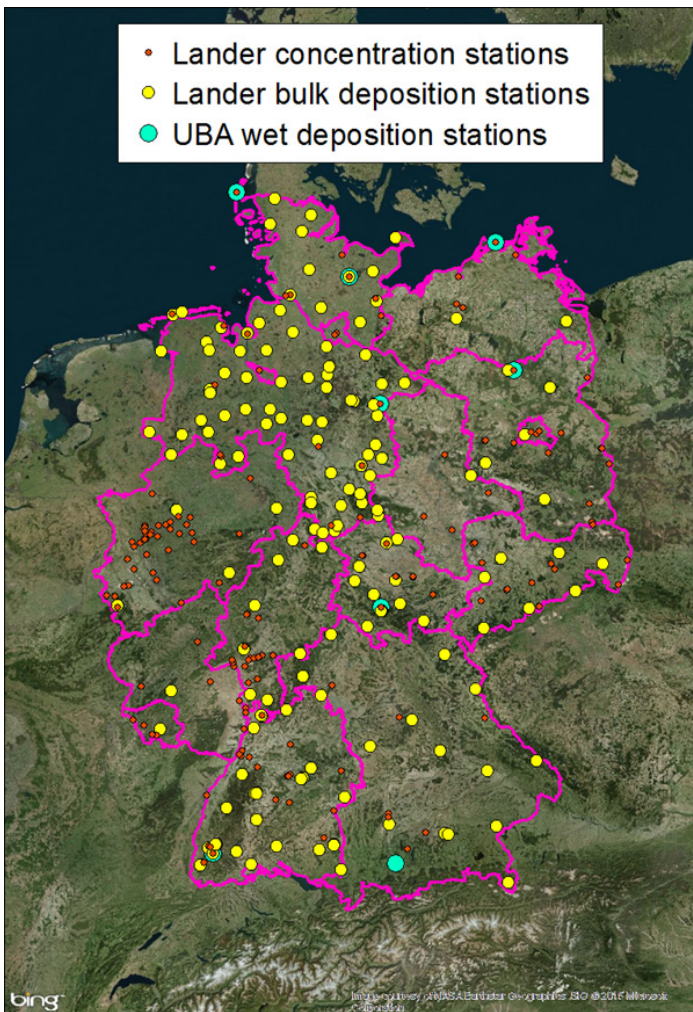


Figure 5 shows that the observation locations are not equally distributed. Some Länder have very few deposition stations, compared to others. Moreover, the UBA stations are few in number throughout the whole of Germany. It is noted that at each station only a selection of the aforementioned heavy metals is observed and the number of available stations varies slightly per year.

2.2.3.2 Post processing of the wet deposition observations

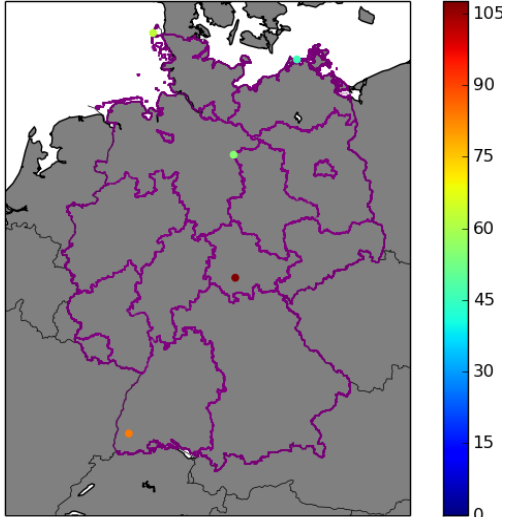
Before the observation data are used to validate the modelling, checks and corrections on the data are done. First, the data was checked on completeness: stations with a coverage lower than 80% of time are omitted in the analysis. Data at stations with availability in between 80 and 100% per year are extrapolated to annual totals. Next, all observations are converted in consistent units of $\mu\text{g}/\text{l}$. Finally, spikes were removed from the observations.

2.2.3.3 Observation analysis

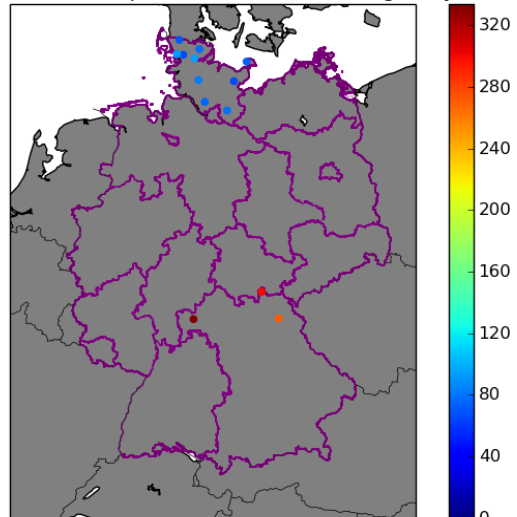
To examine the spatial variability of the annual total wet deposition, dot maps of the 2009 observations are displayed in Figure 6. Maps for 2010 and 2011 are made as well, but only shown if the 2009 data is unavailable as indicated. As we noted remarkable differences in between the observations from the Länder and UBA, these are shown separately. The maps are shown for As, Cd, Ni, Zn, Pb, V and Cu.

Figure 6: Observed annual total wet depositions [$\mu\text{g}/\text{m}^2/\text{year}$] left : UBA stations; right : Länder stations (source: this work)

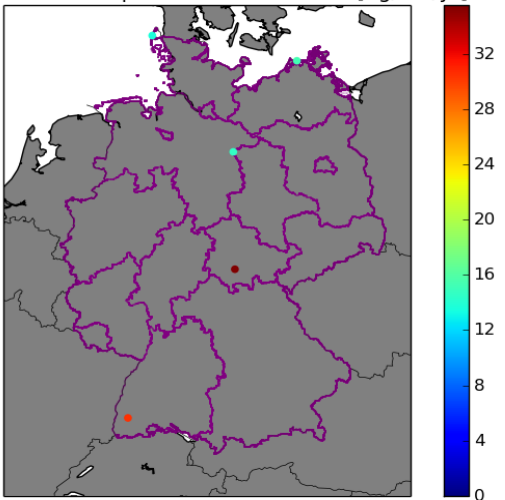
observed wet deposition of As in 2009 [$\mu\text{g}/\text{m}^2/\text{yr}$]



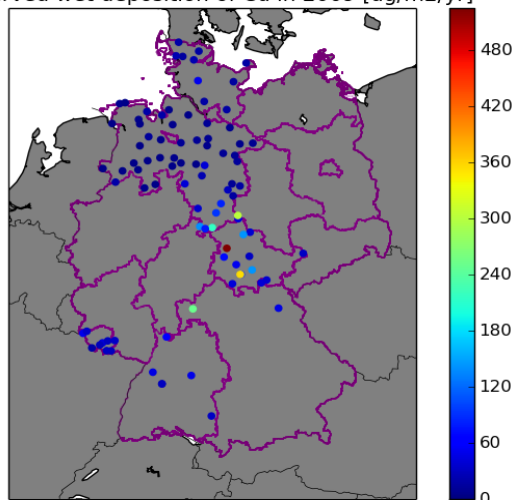
observed wet deposition of As in 2009 [$\mu\text{g}/\text{m}^2/\text{yr}$]



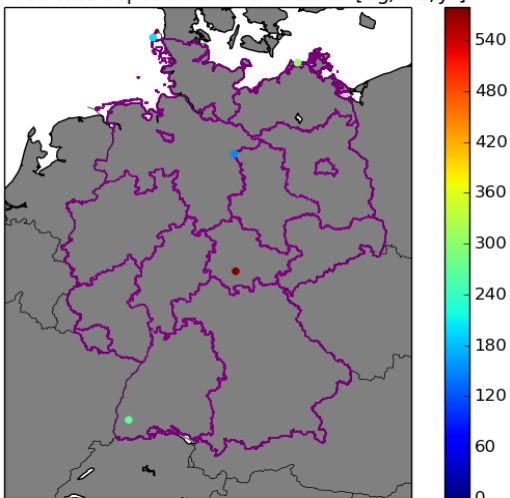
observed wet deposition of Cd in 2009 [$\mu\text{g}/\text{m}^2/\text{yr}$]



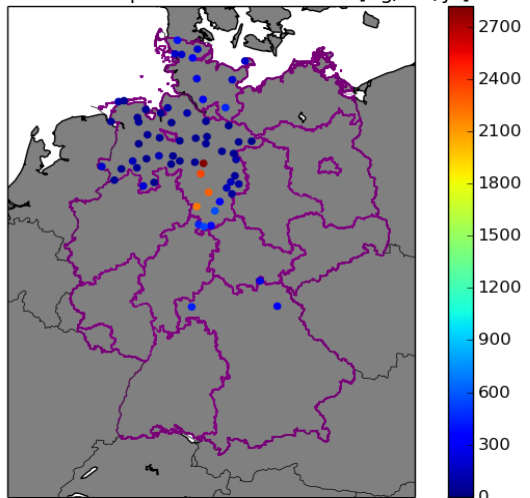
observed wet deposition of Cd in 2009 [$\mu\text{g}/\text{m}^2/\text{yr}$]



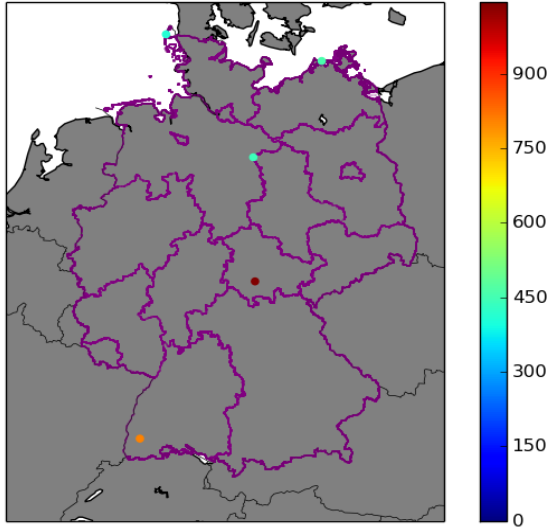
observed wet deposition of Ni in 2009 [$\mu\text{g}/\text{m}^2/\text{yr}$]



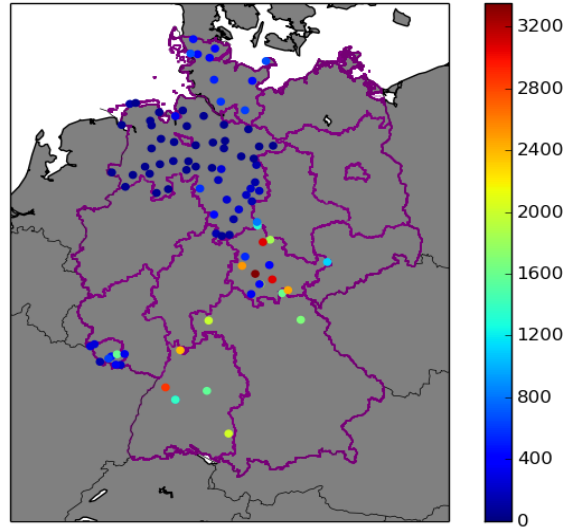
observed wet deposition of Ni in 2009 [$\mu\text{g}/\text{m}^2/\text{yr}$]



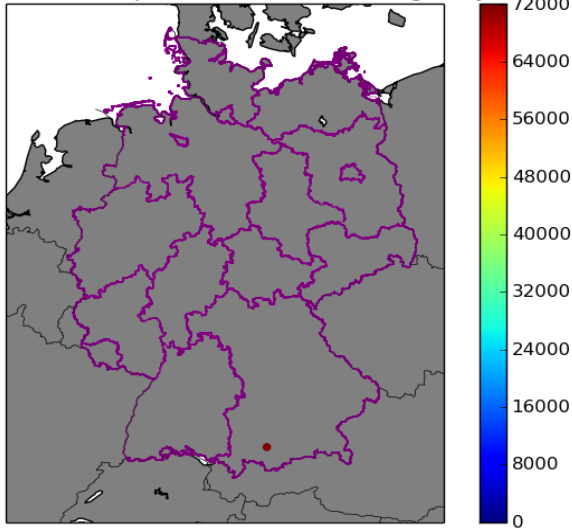
observed wet deposition of Pb in 2009 [ug/m2/yr]



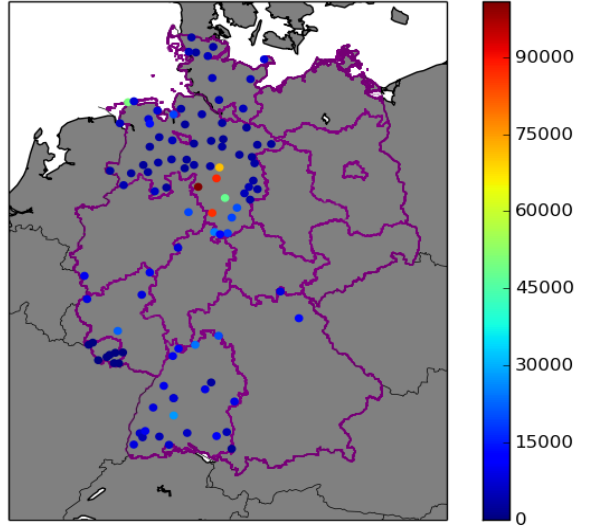
observed wet deposition of Pb in 2009 [ug/m2/yr]



observed wet deposition of Zn in 2010 [ug/m2/yr]

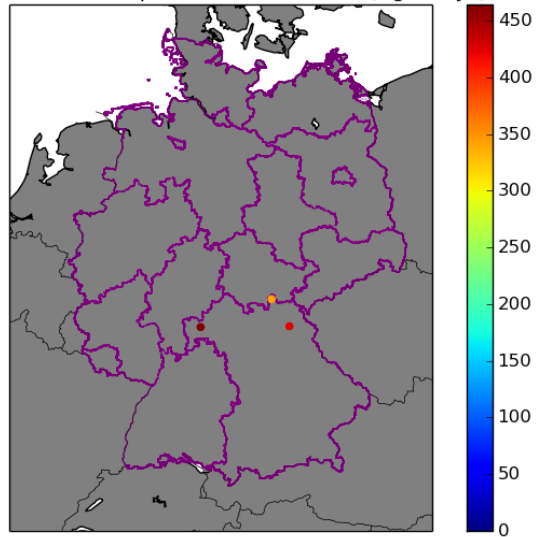


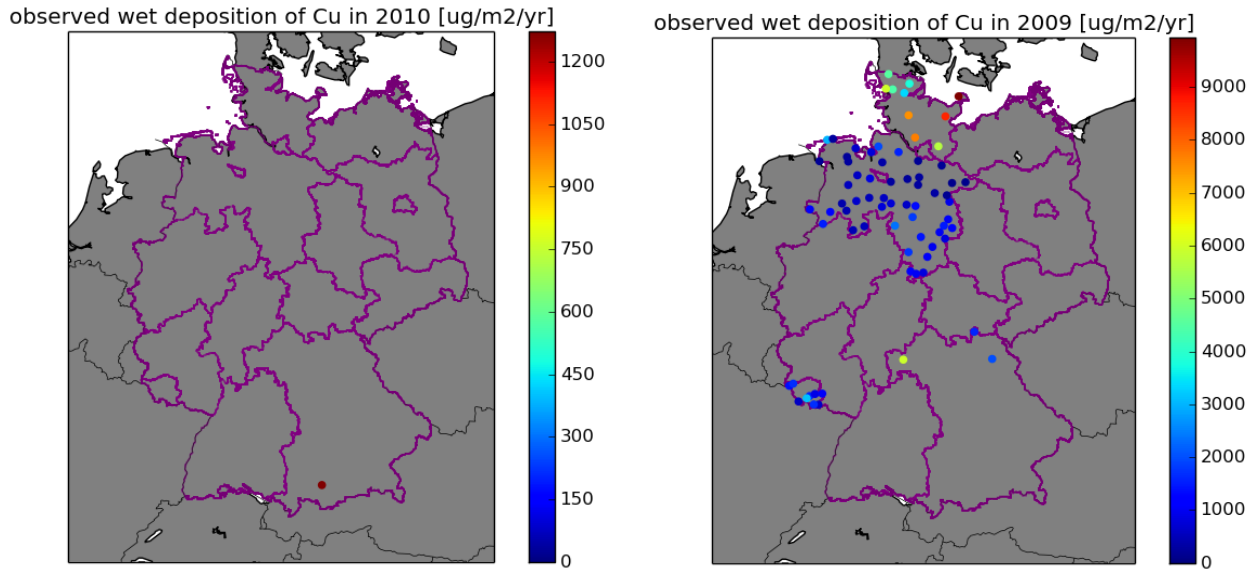
observed wet deposition of Zn in 2009 [ug/m2/yr]



Wet deposition of Vanadium is not observed by any of the UBA stations

observed wet deposition of V in 2009 [ug/m2/yr]





The wet deposition is not dependent on land use type and the data coverage is not available in sufficient detail to be able to make a distinction between urban, rural and industrial regions. The data shown in Figure 6 clearly show a few main features.

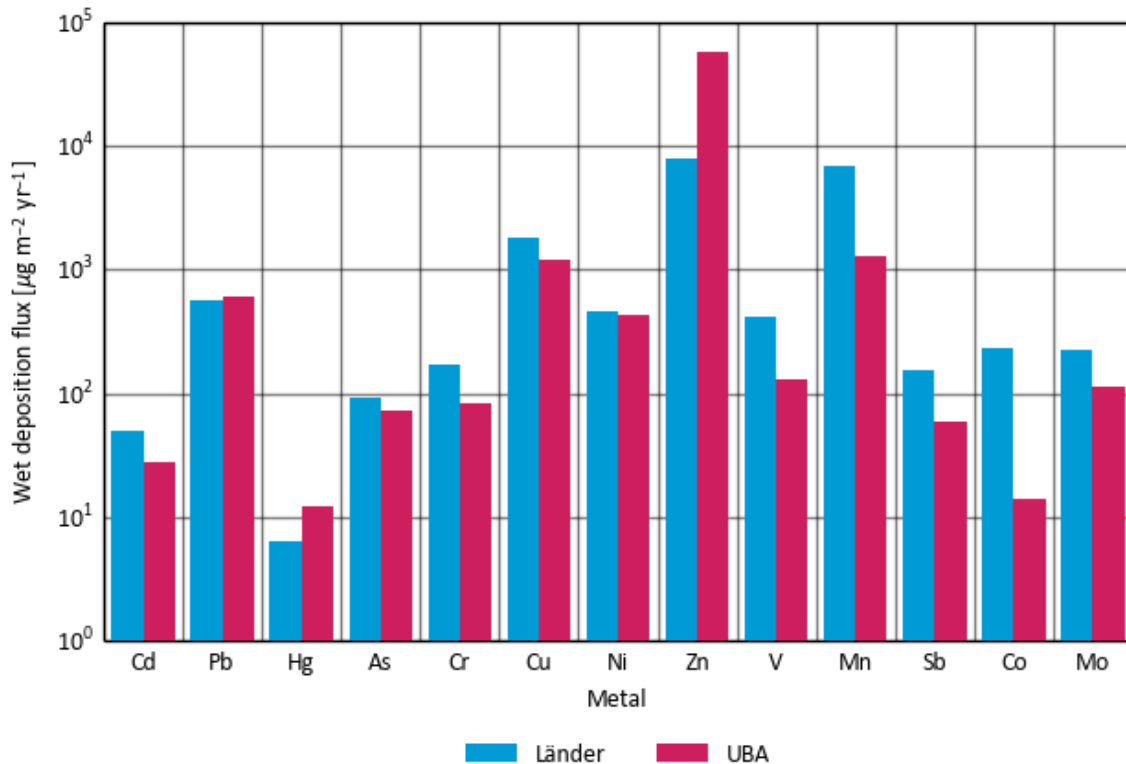
First of all, as also observed for the air concentration data is the data availability for many metals rather limited and in case more data are available they are restricted to a number of states. For instance, arsenic data are mostly available for Schleswig-Holstein. Cadmium and lead are determined for Schleswig-Holstein, Niedersachsen, Thüringen and Saarland. Baden-Württemberg has data for Cd, Pb and surprisingly many sites with Zn. Bayern has 2-3 sites with data, whereas NRW as an important source area is not represented. Similarly, many regions in eastern Germany are not covered.

Secondly, the observations of the Länder show a much higher range than those from UBA. The fluxes reported for stations in the Länder networks vary within about a factor of 10, whereas the fluxes at the UBA stations are typically within a factor 3 of each other.

Thirdly, there appear to be inconsistencies between networks. For example, compare Copper for Niedersachsen and Schleswig-Holstein and Lead in northern and southern Germany. For Zinc and Nickel 4 stations in the eastern part of Niedersachsen show much higher values than surrounding stations.

As a consequence, the means of the Länder observations are systematically higher than the UBA data, see Figure 7. This is the case for all components, except Pb, Hg and Zn. The higher variability is expected as the UBA stations are located at real background locations and rainout of metals is expected to be higher near source areas as concentrations are higher. However, these are expected near industrial locations and regions, which are hardly covered in the database. The inconsistencies show that methodological challenges remain and that the Länder data should be interpreted as maximum values.

Figure 7: Summary of empirically derived wet deposition for metals in Germany based on Länder observations as well as UBA observations. Data averaged over the years 2009,2010 and 2011. (Source: this work).



2.2.4 Empirical total deposition fluxes

Adding the empirically derived wet and dry deposition fluxes described above gives the empirical total deposition flux. As both dry and wet fluxes are not available for all metals targeted in this study, for some metals only the dry or wet flux is available. In Annex 2 the total deposition for all metals for which data was available are listed for all land use classes considered in this study for industrial, rural, urban and traffic-influenced areas.

Figure 8 shows the proportion of dry to total deposition for a selection of land use classes. For urban and traffic stations, the dry deposition on urban areas is displayed. For the deposition on coniferous and deciduous forest, the data from rural stations is used. The bars labelled ‘rural’ show the calculated deposition using ‘rural’ concentrations on arable land.

This figure shows that the relative importance of dry deposition for the total deposition changes widely across metals. For zinc, almost all deposition is wet deposition, whereas for example chromium is mainly deposited through the dry deposition mechanism. Figure 9 shows the total deposition for a selection of land use classes.

Figure 8: Contribution of dry deposition to total deposition for several metals and land use classes (source: this work)

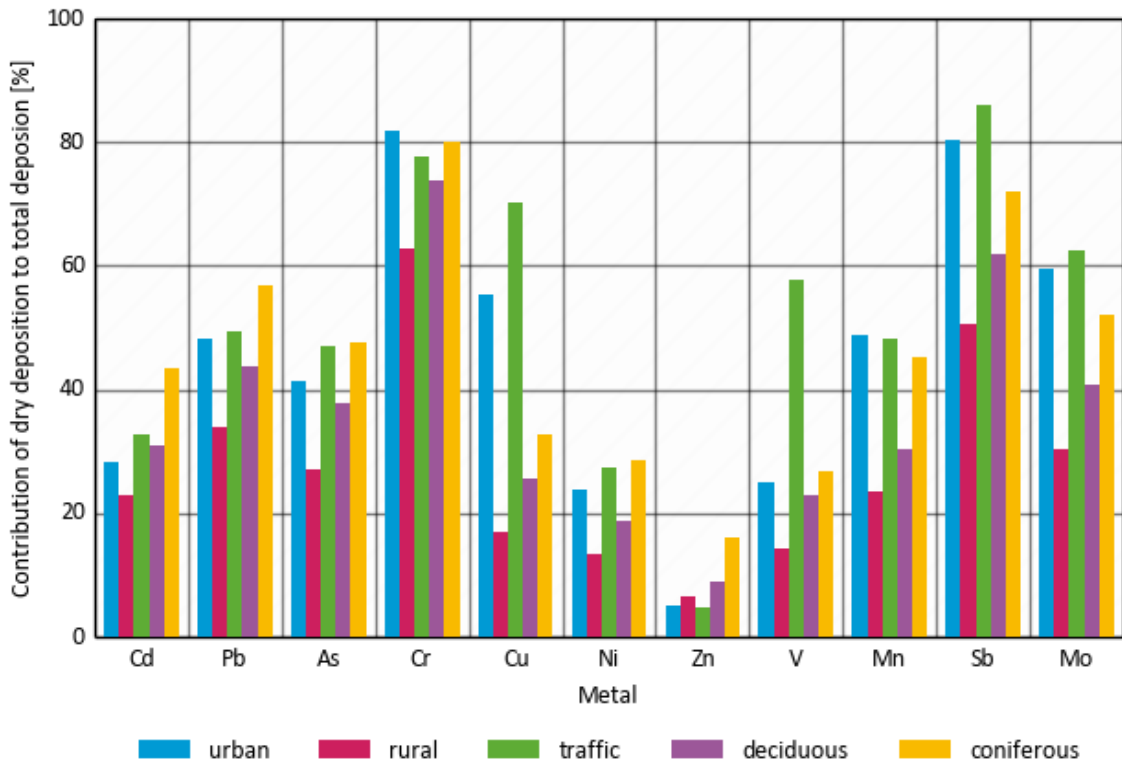


Figure 9: Total deposition for selected land use classes based on empirical data

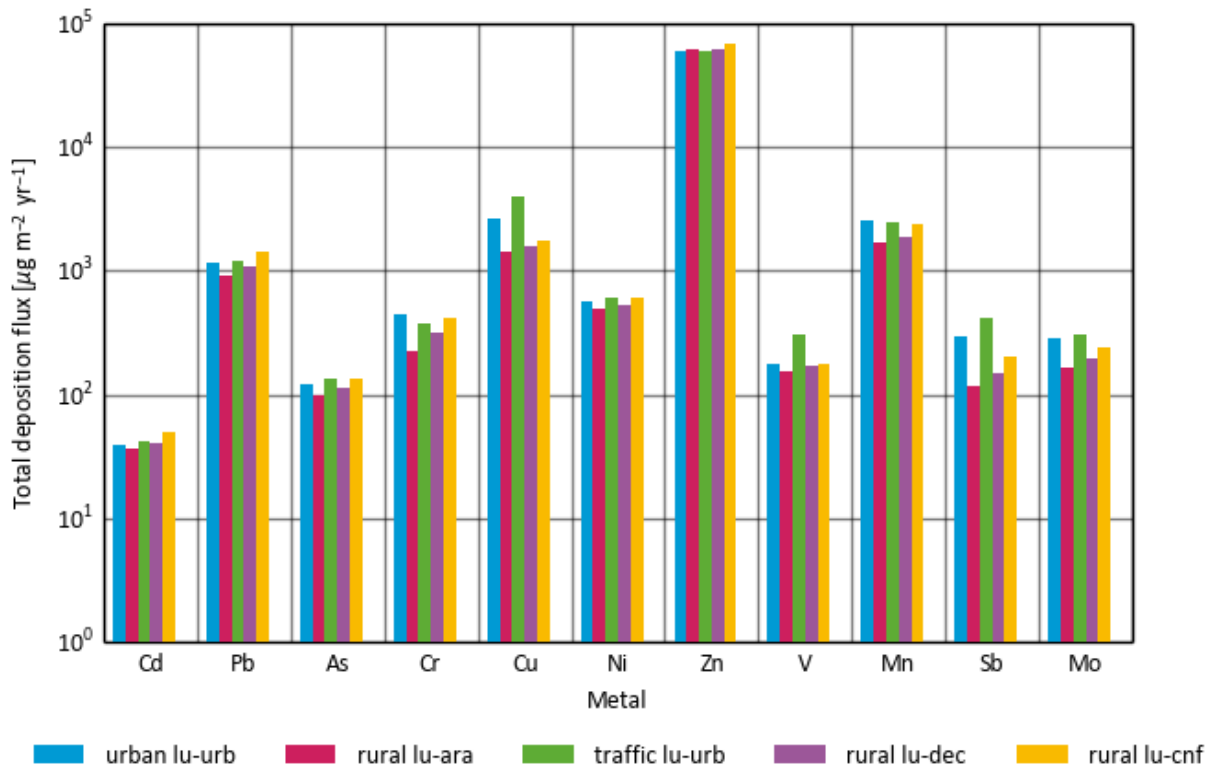


Figure 10: Comparison between the central total deposition estimates obtained in this study and those by Knappe (2008)

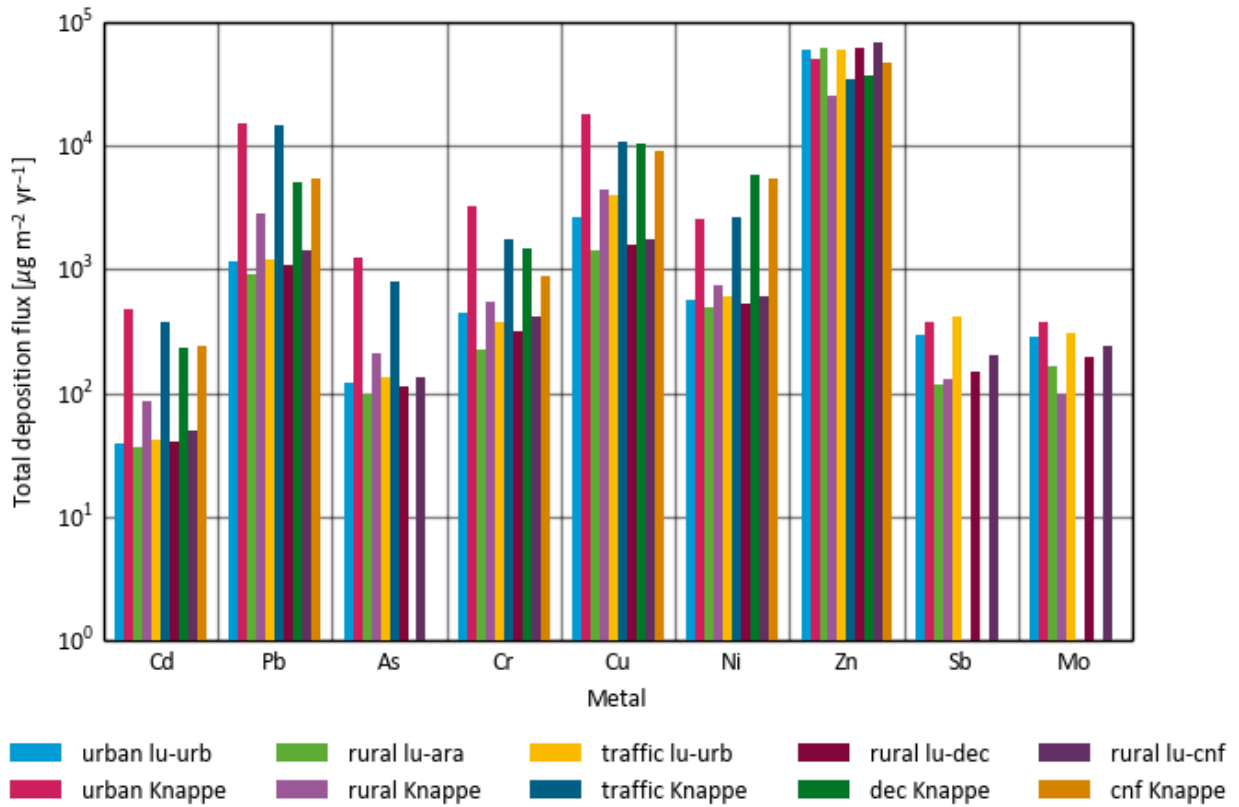
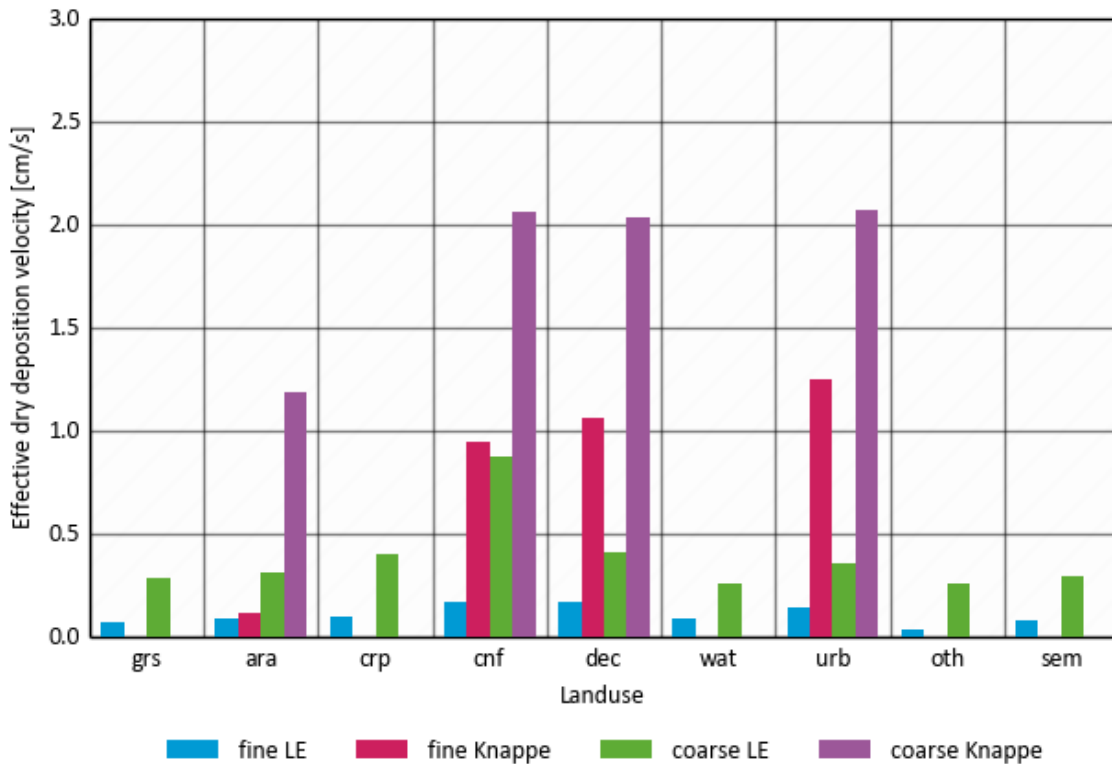
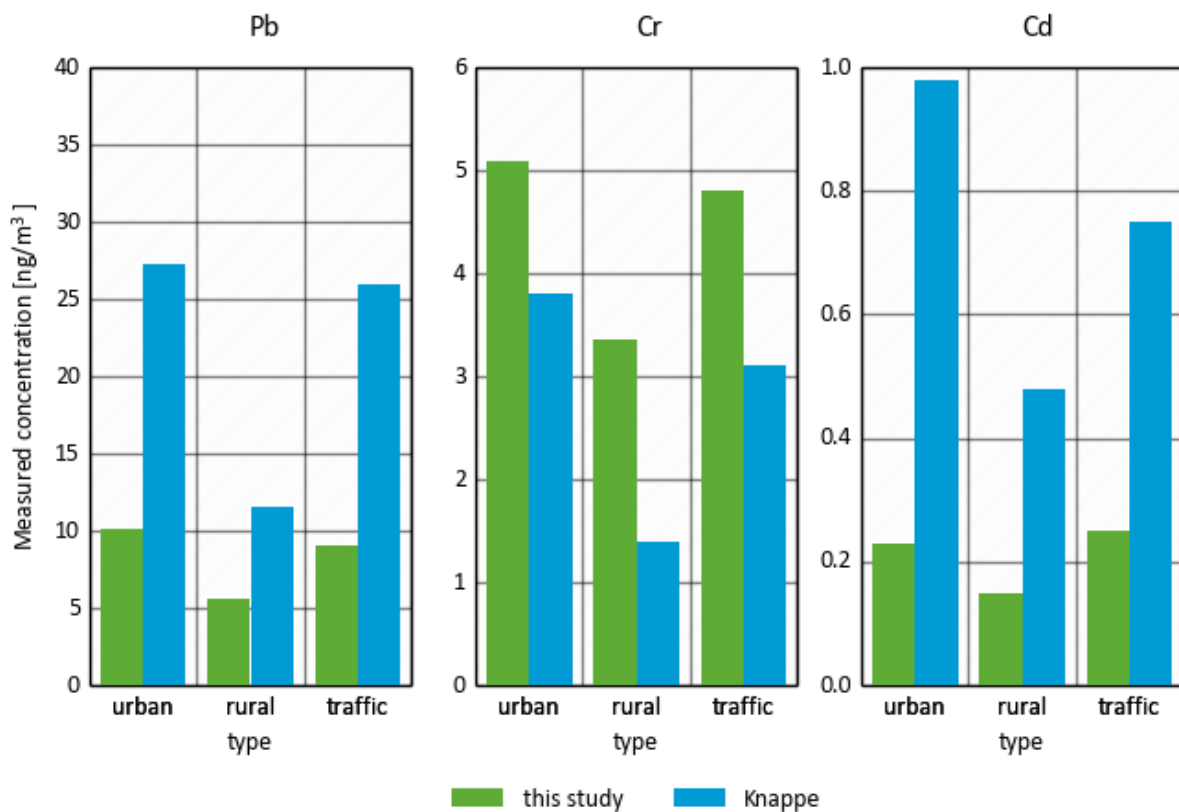


Figure 11: Deposition velocities for fine and coarse particles used in this study and those used by Knappe (2008)



In this study, deposition estimates are based on a.o. concentration measurements. For some metals and station types this information was scarce, and the available measurements are used to calculate an estimated deposition for Germany as a whole. This means that uncertainties associated with the results are large. To get a feeling of the importance of these uncertainties, we compare our results with Knappe (2008), who used more or less the same approach but used different data to base deposition estimates on. Figure 10 shows the total deposition for urban, rural, traffic-influenced, deciduous and coniferous areas from this study compared to Knappe (2008). This comparison shows that for several metals the difference between the two studies can be up to a factor 10 (e.g. Cd, Pb, As), especially for urban and traffic stations. For rural locations the difference is a factor 2-5 depending on the land use considered. For other metals (e.g. Zn) the studies are much more aligned (e.g. Zn). There is no direct connection between a large difference and low availability of concentration measurements for this study. The origin of the difference is found in the dry deposition; wet deposition estimates from this study and Knappe (2008) are much more alike.

Figure 12: Average measured concentration in air (ng/m³) for Pb, Cr and Cd based on this study and Knappe (2008)



The difference in the calculated dry deposition is partly caused by the much higher deposition velocities for particles used by Knappe (2008), who uses deposition velocities from Gauger (2002). This is illustrated in Figure 11. Figure 12 shows that for some metals, the average measured concentrations calculated by Knappe (2008) are much higher than the average concentrations resulting from the dataset used in this study, while for other species the differences are smaller and sometimes even higher in this study. This figure illustrates the uncertainties involved in using a limited set of measurements to calculate a 'typical' concentration per station type for Germany.

The higher deposition velocities combined with (for most metals) higher concentrations explains the much higher deposition flux estimates by Knappe (2008).

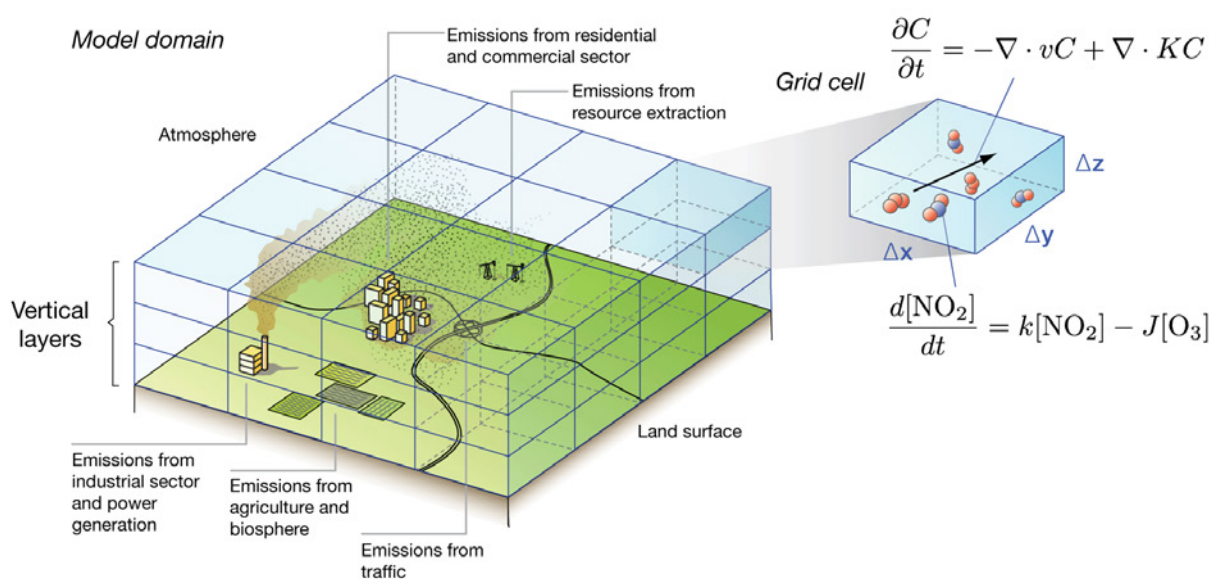
2.3 Chemistry transport modelling

2.3.1 LOTOS-EUROS model description and application

To assess the land use specific dry deposition distributions and determine effective dry deposition velocities across Germany one has to apply a modelling system. In this study we use the LOTOS-EUROS model. Below we describe the model, its application and its results.

The 3-D regional chemistry transport model LOTOS-EUROS (Schaap et al., 2008) is aimed at the simulation of air pollution in the lower troposphere. The model is of intermediate complexity in the sense that the relevant processes are parameterized in such a way that the computational demands are modest enabling hour-by-hour calculations over extended periods of several years within acceptable computational time. The model is a so-called Eulerian grid model, which means that the calculations are performed on a fixed three dimensional grid. On this grid the concentration changes due to advection, vertical mixing, chemical transformations and removal by wet and dry deposition are performed. A sketch of such a model system is given in Figure 13. The process calculations require information about anthropogenic emissions, land use and meteorological conditions, which have to be prescribed to the model system. The results of the model are stored in output files that contain modelled air pollutant concentrations and deposition fluxes.

Figure 13: A sketch of an Eulerian chemistry transport model such as LOTOS-EUROS (source: ctcog.org)



Many scientific studies have been carried out with previous (and the current) versions of the LOTOS-EUROS model studying secondary inorganic aerosol (Schaap et al., 2004b; 2011; Erisman and Schaap, 2004; Banzhaf et al., 2015), sea salt (Manders et al., 2010), particulate matter (Manders et al., 2009; Hendriks et al., 2013), ozone (Curier et al., 2012; Beltman et al., 2013), nitrogen dioxide (Schaap et al., 2013; Curier et al., 2014) and ammonia (Wichink Kruit et al., 2012a; Van Damme et al., 2014). For details of the model we refer to these publications.

With respect to Germany LOTOS-EUROS is used to assess nitrogen deposition to terrestrial ecosystems within the PINETI projects (Wichink Kruit et al., 2014; Schaap et al., 2015). Recently, a national assessment of ozone damage to crops and forests was supported by providing stomatal ozone deposition fluxes (Bender et al., 2015).

Earlier applications for Germany within MAPESI also included calculations for cadmium and lead (Bultjes et al., 2011). The dry deposition flux is calculated from the ambient concentration at a reference height and several resistances:

$$F = \frac{C}{R_a + R_b + R_c} = v_d \cdot C \quad (\text{Eq. 1})$$

The reciprocal of the sum of the resistances is also called the deposition velocity, i.e., v_d . The land use specific deposition velocities are calculated using land use specific roughness lengths and atmospheric stability parameters based on Zhang et al. (2001). The land use dependent dry deposition of HMs are saved as separate outputs.

The LOTOS-EUROS model currently uses the land use dataset Corine Land Cover for the year 2006, CLC2006, for concentration and deposition calculations. This land use data set is a vector based data set, which is aggregated to a $1/60^\circ \times 1/60^\circ$ latitude/longitude resolution, i.e., about $1.2 \times 1.8 \text{ km}^2$. The available land use classes in CLC2006 are aggregated to 9 land use classes. Table 8 shows these 9 DEPAC land use classes and their corresponding roughness lengths. The fractions of each land use class within one grid cell of $7 \times 7 \text{ km}^2$ in LOTOS-EUROS are calculated from the aggregated CLC2006 database.

Table 8: Land use categories

DEPAC categories (abbreviation)
Grassland (grs)
Arable land (ara)
Mixed forest (mix)
Coniferous forest (cnf)
Deciduous forest (dec)
Water (wat)
Urban (urb)
Semi-natural vegetation (sem)
Other (oth)

For the model simulations in this study two domains were used. First a European domain with a grid size resolution of 0.5° longitude by 0.25° latitude, approximately $36 \times 28 \text{ km}^2$ is used for large scale calculations. In case the required input information was present a second simulation using a equirectangular projection with a grid size resolution of 0.125° longitude by 0.0625° latitude, approximately $7 \times 7 \text{ km}^2$ at the latitude under consideration here, was performed. For its boundary conditions, this 'zoom' run makes use of a larger European run.

In the vertical, the model is based on the well mixed dynamic boundary layer concept, i.e., there are three dynamic layers and a surface layer. The lowest dynamic layer is the mixing layer, followed by two reservoir layers. The height of the mixing layer is obtained from the ECMWF meteorological input data used to drive the model. The meteorological data are obtained at the model resolution from ECMWF (i.e. interpolation performed by ECMWF procedures) and are provided on an 3-hourly basis. The data are interpolated to the hours of the day. The height of the reservoir layers is determined by the difference between ceiling and mixing layer height. A surface layer with a fixed depth of 25 m is included as part of the mixing layer to monitor ground-level concentrations. The total vertical model extend is 3.5 km above the Earth's surface.

Below we describe the emission input used to drive the model.

2.3.2 Emission data

In this study there was no room for improving emission inventories. Hence, emission inventories were taken from the literature and previous projects. As a consequence, the inventories used for the individual metals differ. The origin of the emission inventories is summarized in Table 9.

The spatial resolution of the EMEP emission database is 50 km, The TNO data have a 7 km spatial resolution. The higher resolution is available for Cd, Pb, V and Cu only. The emission of Vanadium was estimated to be 2% of the primary PM₁₀ emission due to heavy fuel combustion.

Table 9: Specification of the emission data applied in the modelling

Component	Emission data	Base year	Resolution (km)	Source
Ni	EMEP	2000	50x50	Denier van der Gon et al., 2005
Zn	EMEP	2000	50x50	Denier van der Gon et al., 2005
As	EMEP	2000	50x50	Denier van der Gon et al., 2005
Cd	TNO-MAPESI	2005	7x7	Builtjes et al., 2012
Pb	TNO-MAPESI	2005	7x7	Builtjes et al., 2012
V	TNO-ENERGEO	2005	7x7	EnerGEO project
Cu	TNO	2005	7x7	Denier van der Gon et al., 2007

2.3.3 Model results

2.3.3.1 Cadmium and lead distributions

For cadmium and lead the largest modelling effort was performed as the high resolution emission information and many validation stations were available. Therefore, the model results for these metals are used to establish the effective dry deposition velocities used for the empirical assessment of dry deposition fluxes.

The modelled concentration and dry deposition distributions for lead and cadmium are shown in Figure 14 and Figure 15. Lead emissions are mostly associated to industrial process emissions, showing maximum concentrations in the areas with metal processing industries. Cadmium on the other hand is also emitted by combustion of solid fuels and therefore shows a more gradual concentration and dry deposition field as lead. For both metals the industrial hotspots stand out, with maximum concentrations in the Ruhr area. Modelled wet deposition fields are presented in the next section and show similar gradients (although smoothed out).

Comparing the modelled concentrations to observations at rural and urban background stations shows that the modelled data are in general agreement outside the direct source areas. In the Ruhr area the modelled concentrations are higher than those observed which may be due to the artificial mixing of the concentrations near a large source over the model grid cell as well as the uncertainties in the emission data which may not reflect technological improvements after 2005. Only in Sachsen there is an indication the modelled concentrations underestimate the observed values, which may be due to incorrect representation of (the transport from) important sources in the Czech Republic.

Figure 14: Modelled 5 year mean concentration distribution (upper left) and dry deposition flux to arable land (upper right) for lead as well as the comparison to observed concentration data (lower panel) (source: this work)

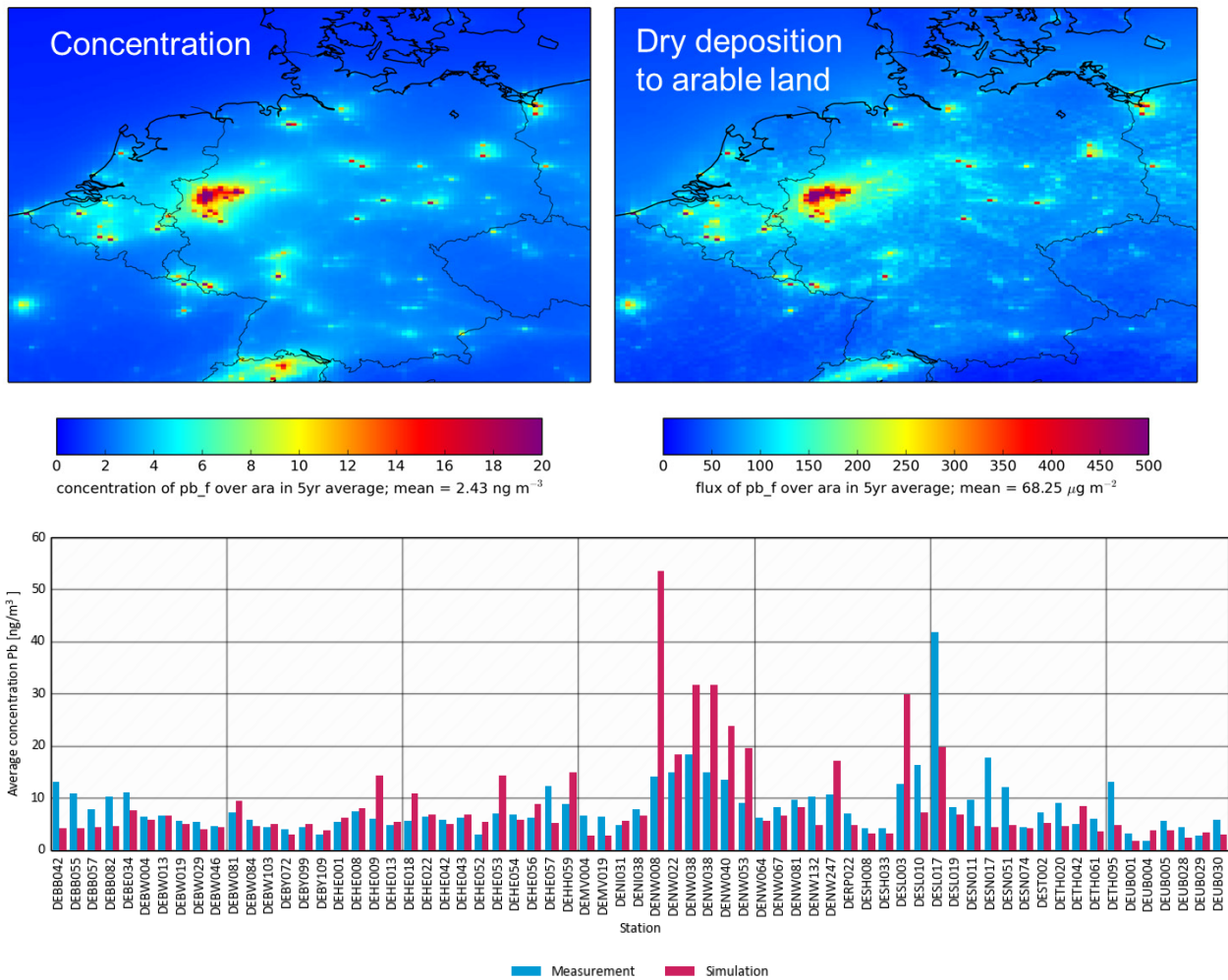
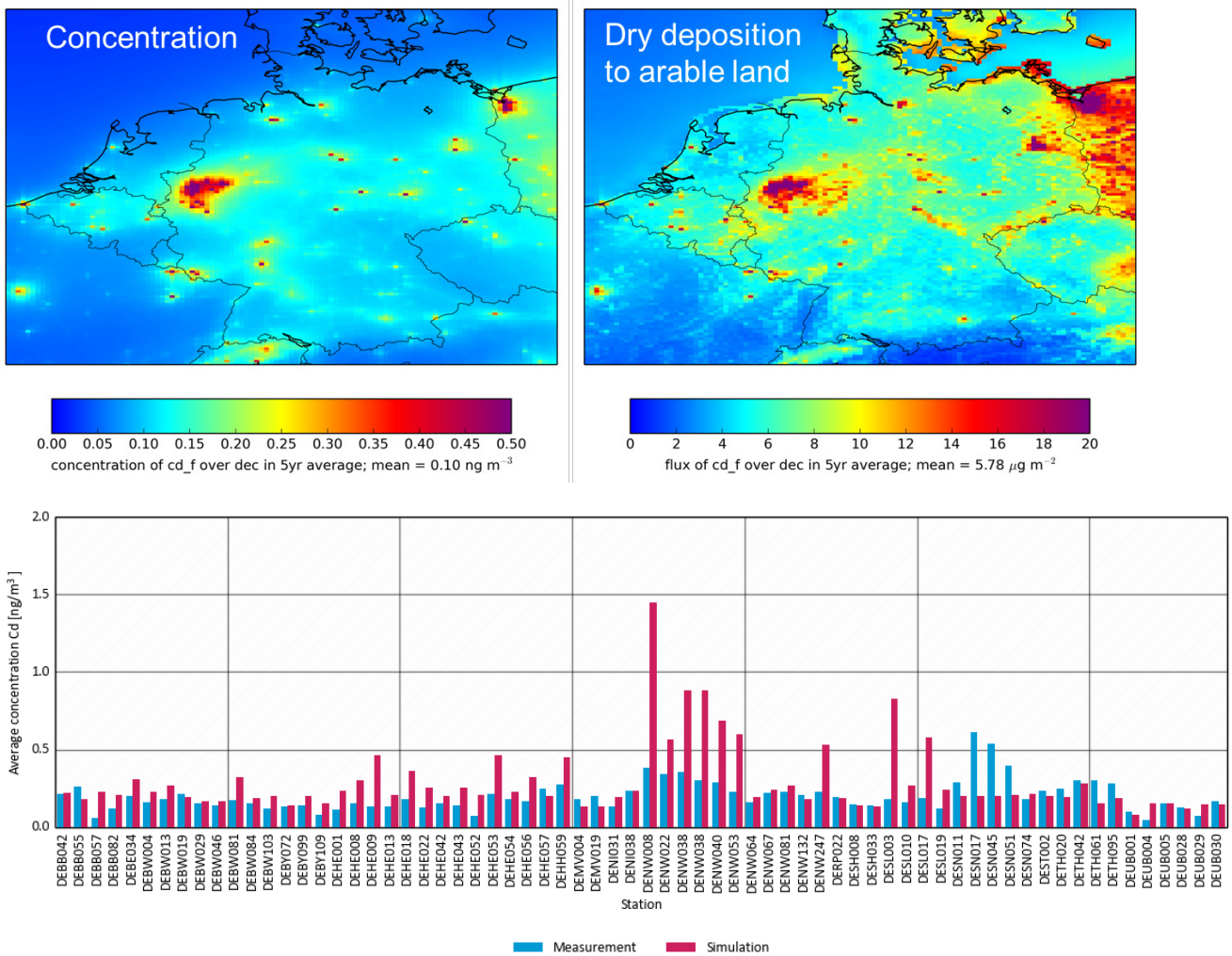


Figure 15: Modelled 5 year mean concentration distribution (upper left) and dry deposition flux to arable land (upper right) for cadmium as well as the comparison to observed concentration data (lower panel) (source: this work)

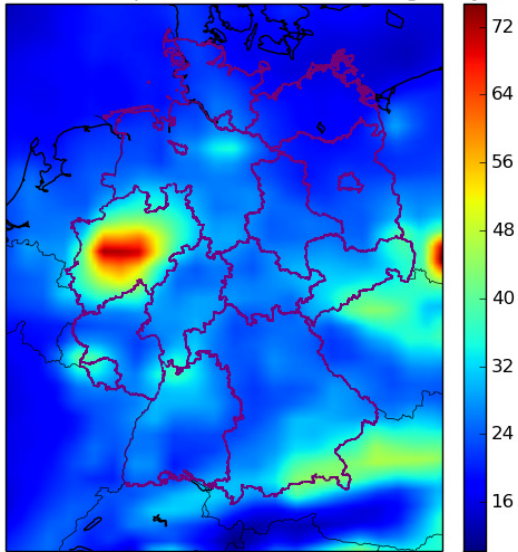


2.3.3.2 Modelled spatial distributions for wet deposition

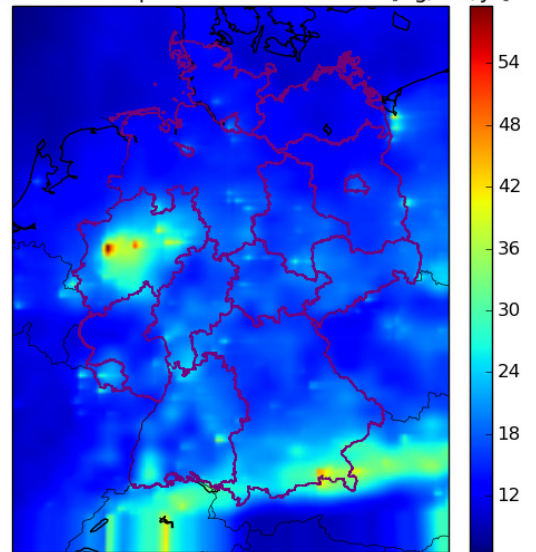
Maps of the 2009 year total wet deposition are displayed in Figure 16. The maps are shown for As, Cd, Ni, Zn, Pb, V and Cu. Years 2010 and 2011 are modelled as well, but not shown in this report. All modelled components show that the largest increase in wet deposition is to be found in the Ruhr area. This is the case for all components, except vanadium, which is increased in the vicinity of sea shipping lanes. Copper shows a clear increase in the Ruhr area, but is increased as well in areas with intense road traffic. The maps of Cadmium and Lead clearly show increased spatial detail, due to higher resolution of the emission inventories that were used. Furthermore, towards the south of Germany, the wet deposition increases for all components. This is caused by the higher annual precipitation sums in these areas.

Figure 16: Modelled annual total wet deposition fluxes [$\mu\text{g}/\text{m}^2/\text{year}$] (source: this work)

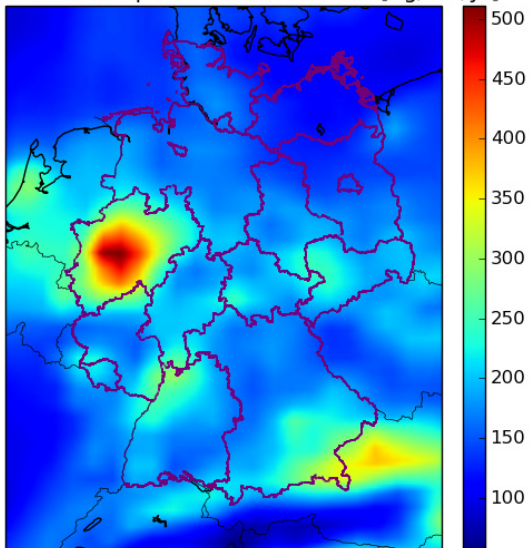
modelled wet deposition of As in 2009 [$\mu\text{g}/\text{m}^2/\text{yr}$]



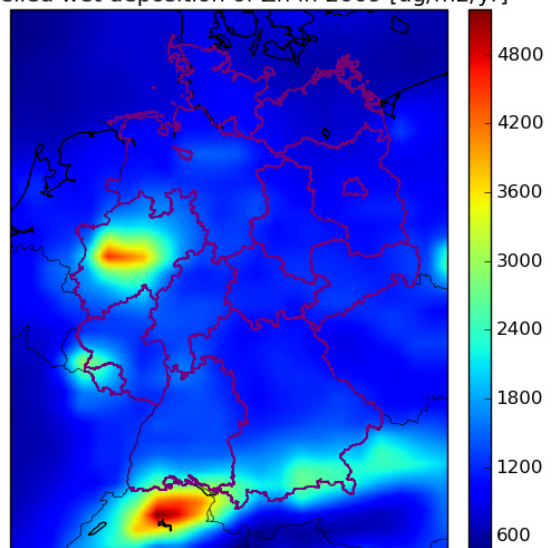
modelled wet deposition of Cd in 2009 [$\mu\text{g}/\text{m}^2/\text{yr}$]



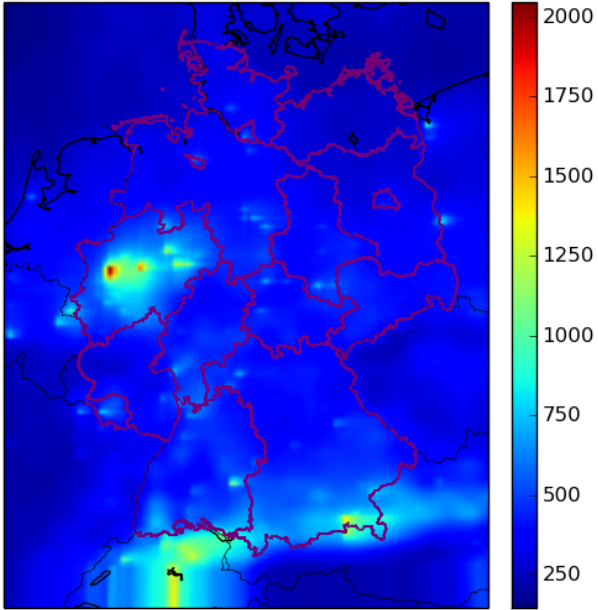
modelled wet deposition of Ni in 2009 [$\mu\text{g}/\text{m}^2/\text{yr}$]



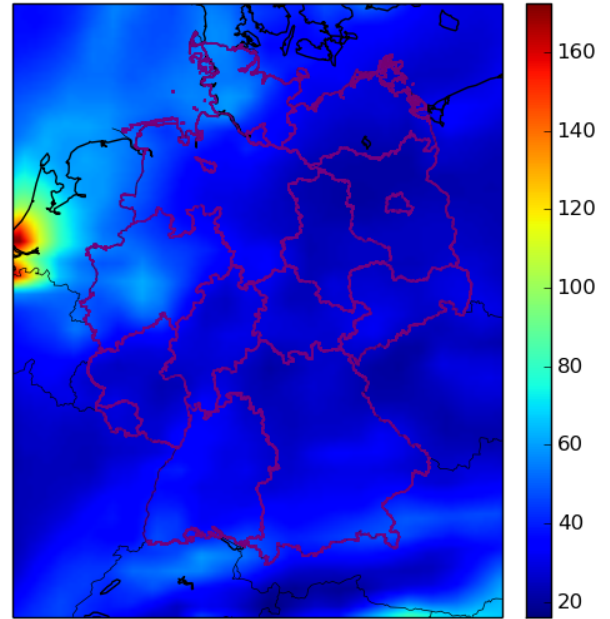
modelled wet deposition of Zn in 2009 [$\mu\text{g}/\text{m}^2/\text{yr}$]



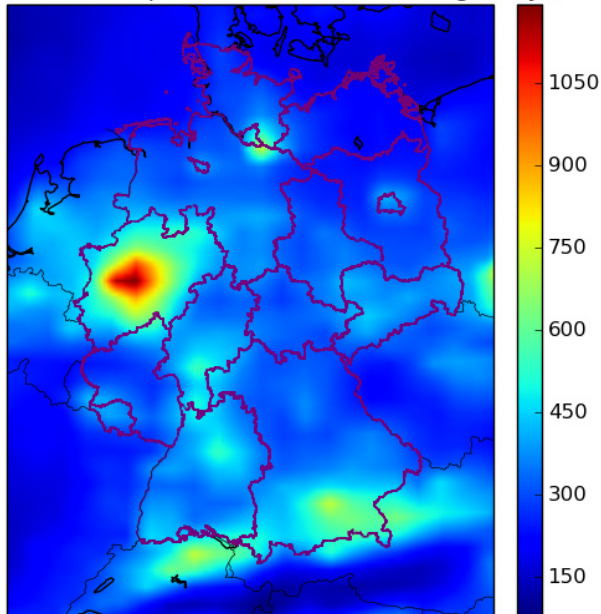
modelled wet deposition of Pb in 2009 [ug/m2/yr]



modelled wet deposition of V in 2009 [ug/m2/yr]



modelled wet deposition of Cu in 2009 [ug/m2/yr]

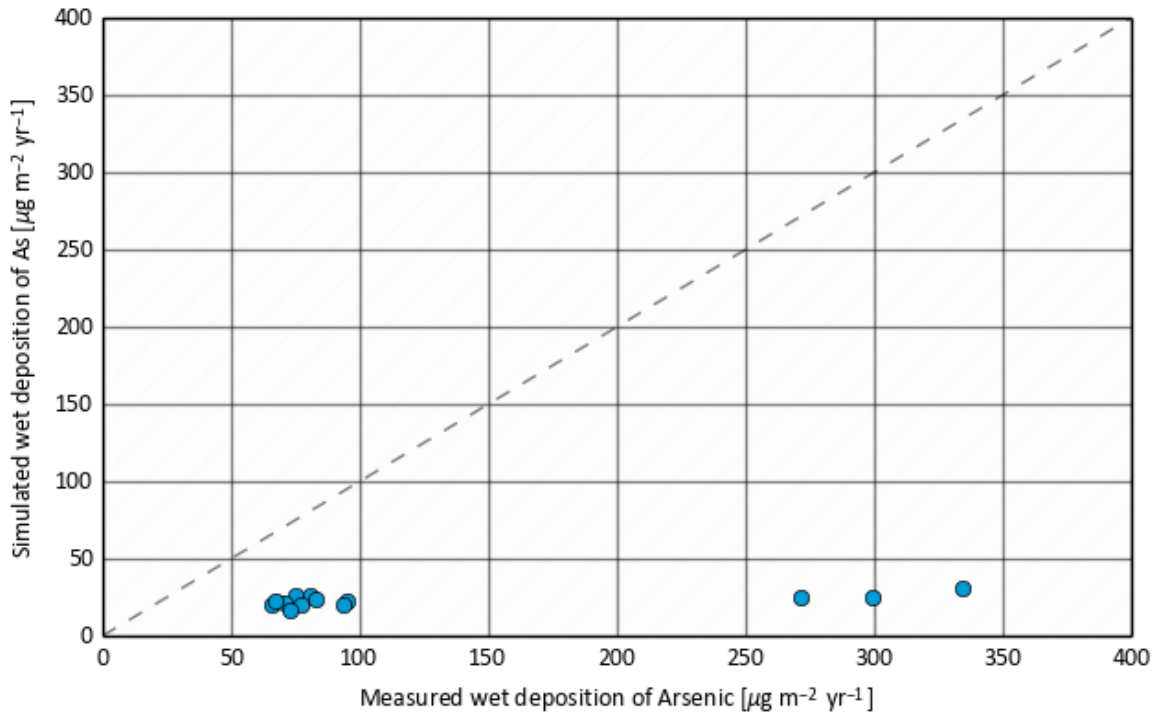


Figures 17-23 show modelled versus observed year total wet deposition scatterplots. Again, plots are shown for As, Cd, Ni, Zn, Pb, V and Cu. As the Länder observations are significantly different from the UBA dot maps, the scatter plots are shown for both.

Figure 17: Scatter plots of modelled versus observed annual wet deposition totals for Arsenic. Top: Länder data, Bottom : UBA data. Note the difference in scales. Source: this work

Wet deposition of Arsenic in 2009

Measurement data from Lander stations



Wet deposition of Arsenic in 2009

Measurement data from UBA stations

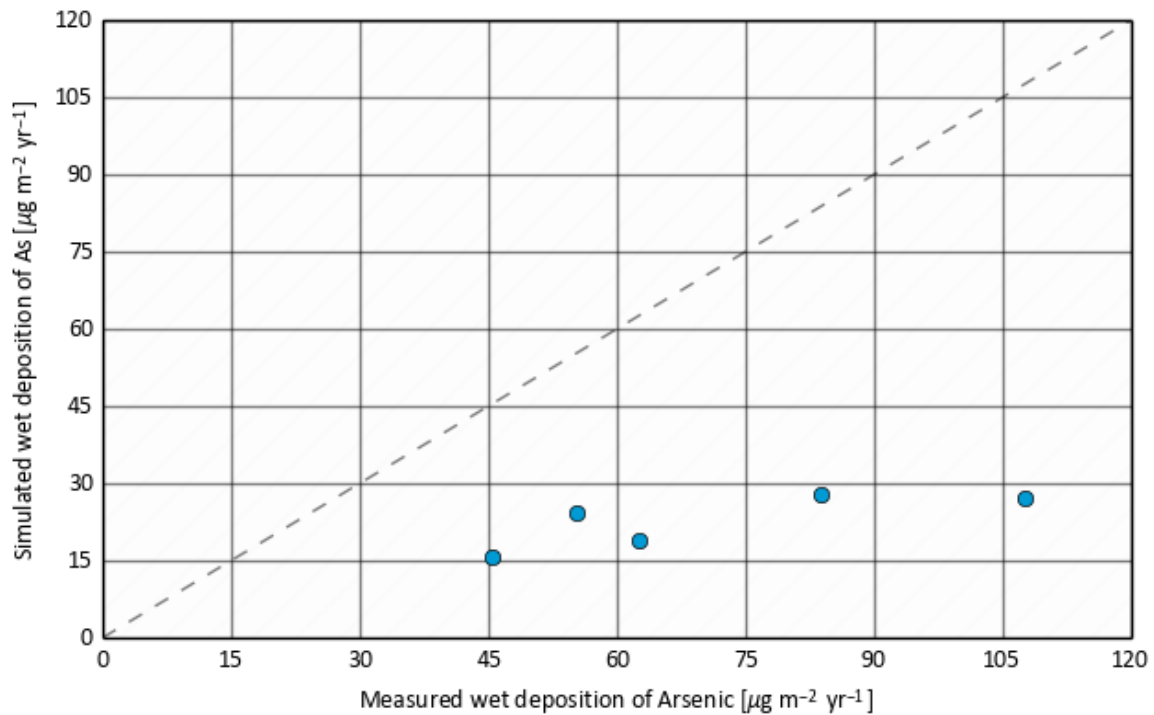
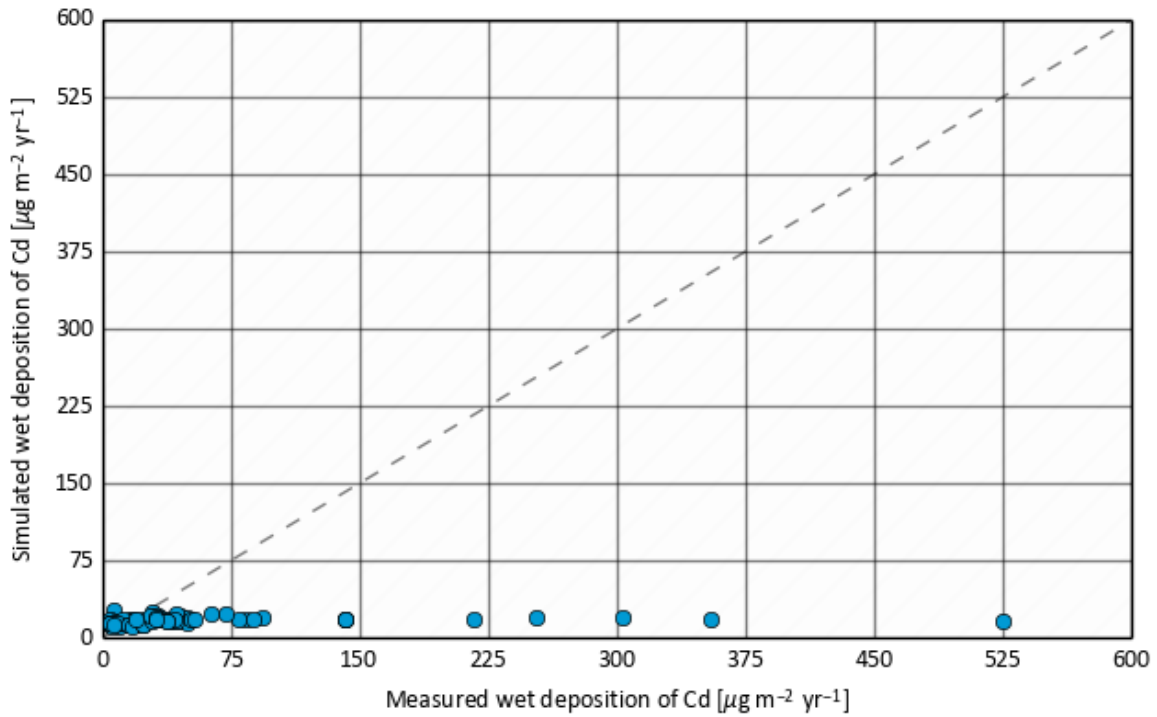


Figure 18: Scatter plots of modelled versus observed annual wet deposition of cadmium in 2009. Top: Länder data, Bottom : UBA data. Note the difference in scales. Source: this work

Wet deposition of Cadmium in 2009

Measurement data from Lander stations



Wet deposition of Cadmium in 2009

Measurement data from UBA stations

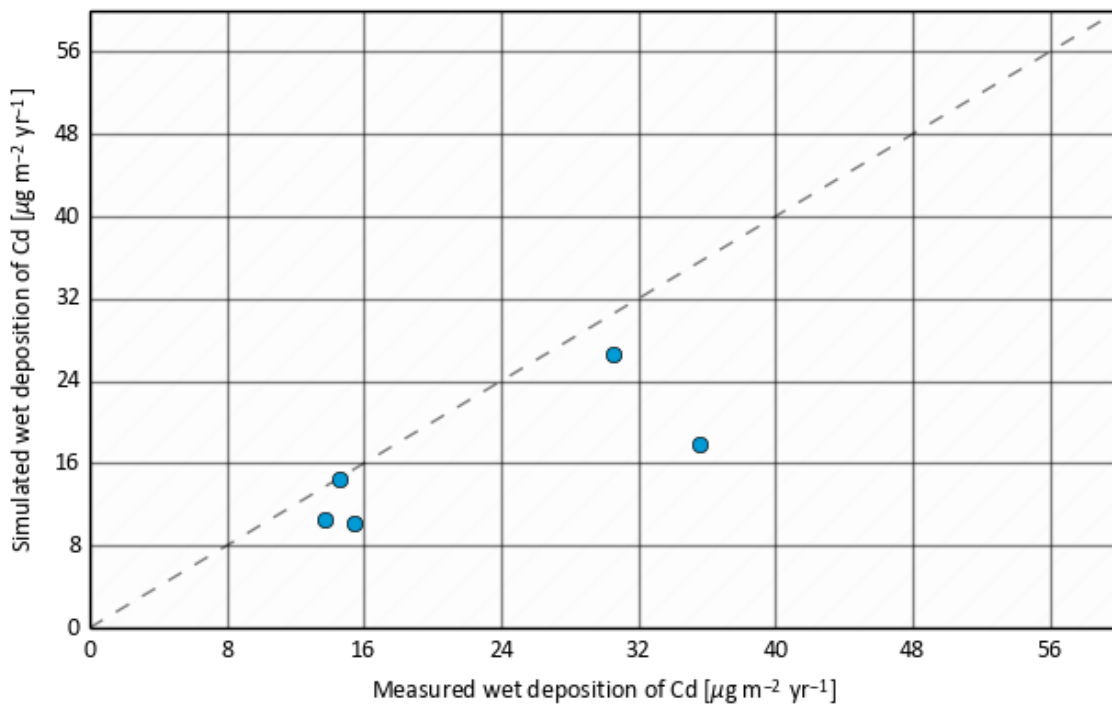
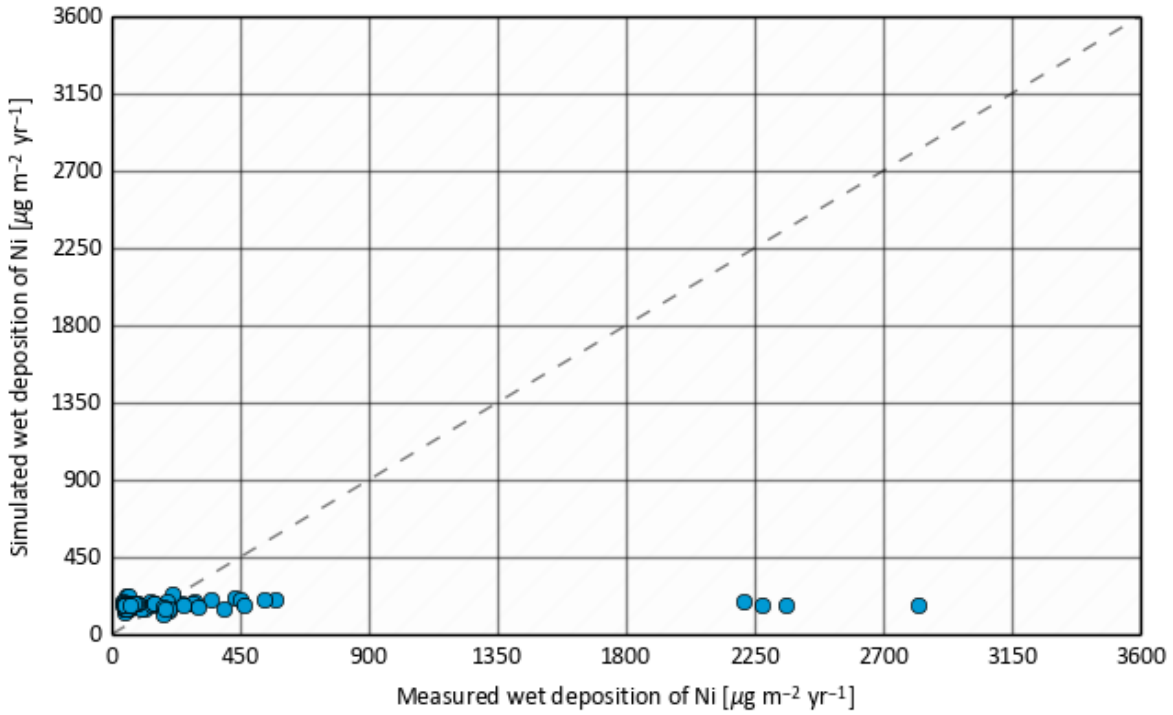


Figure 19: Scatter plots of modelled versus observed annual wet deposition of nickel in 2009. Top: Länder data, Bottom : UBA data. Note the difference in scales. Source: this work

Wet deposition of Nickel in 2009

Measurement data from Lander stations



Wet deposition of Nickel in 2009

Measurement data from UBA stations

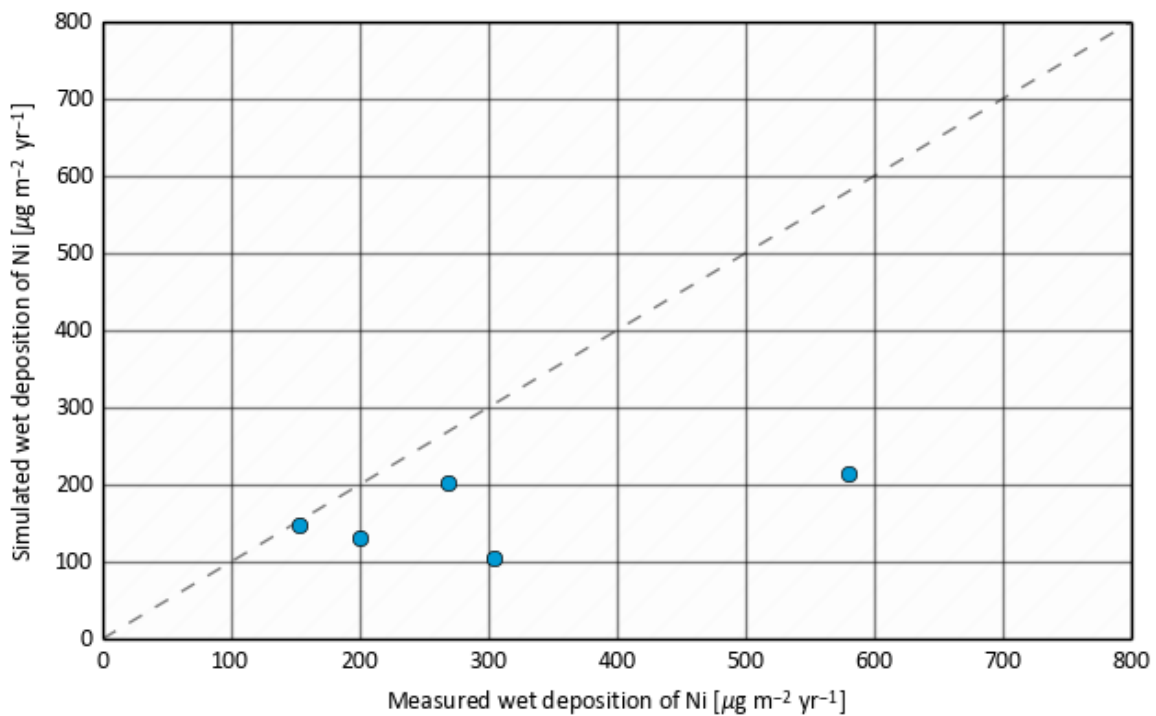
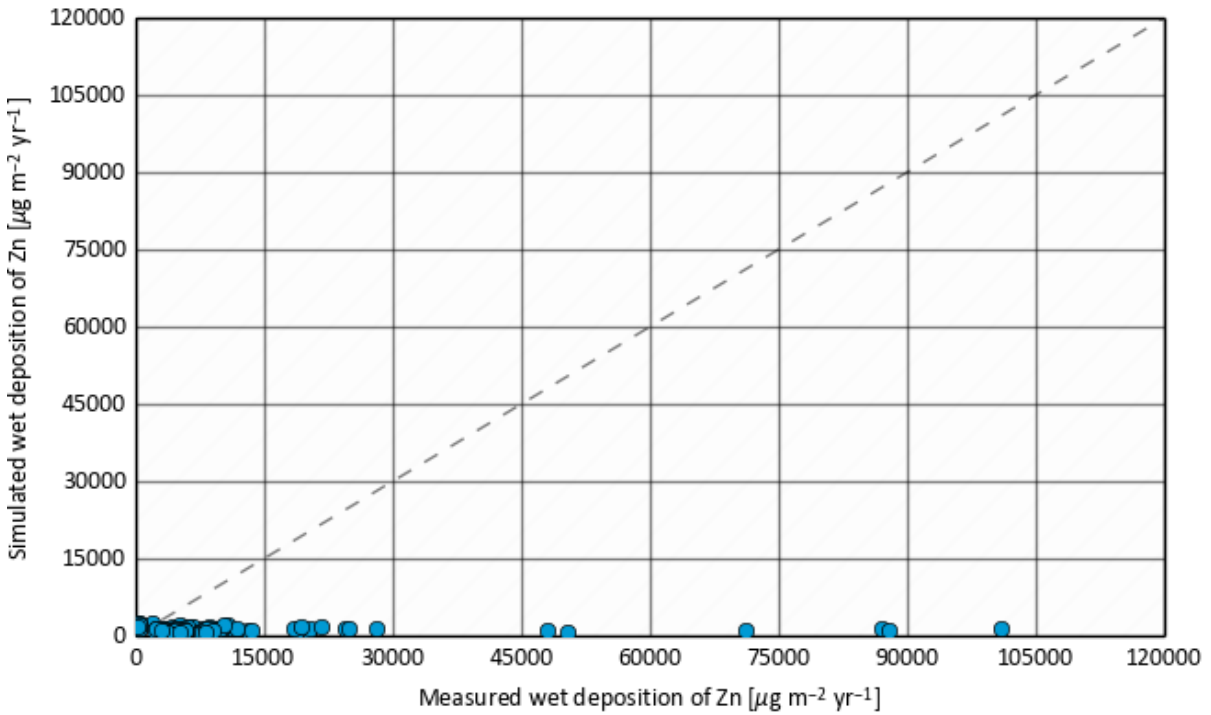


Figure 20: Scatter plots of modelled versus observed annual wet deposition of zinc. Top: Länder data, 2009; Bottom: UBA data, 2010. Note the difference in scales. Source: this work

Wet deposition of Zinc in 2009

Measurement data from Lander stations



Wet deposition of Zinc in 2010

Measurement data from UBA stations

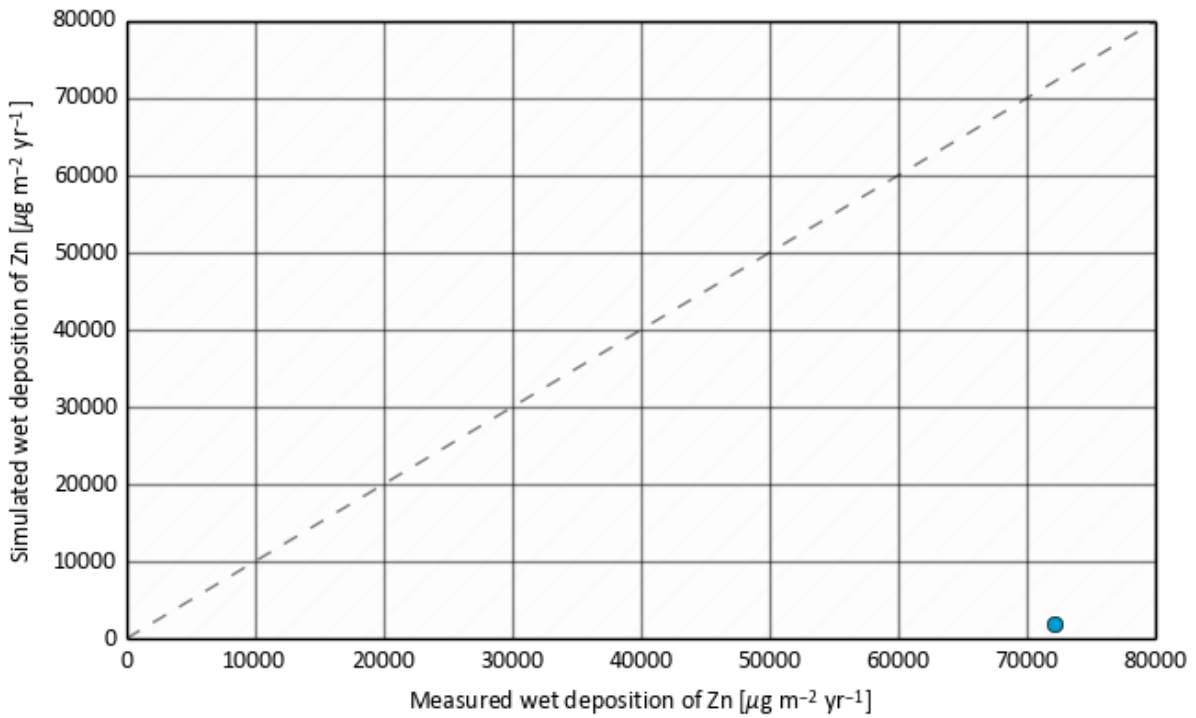
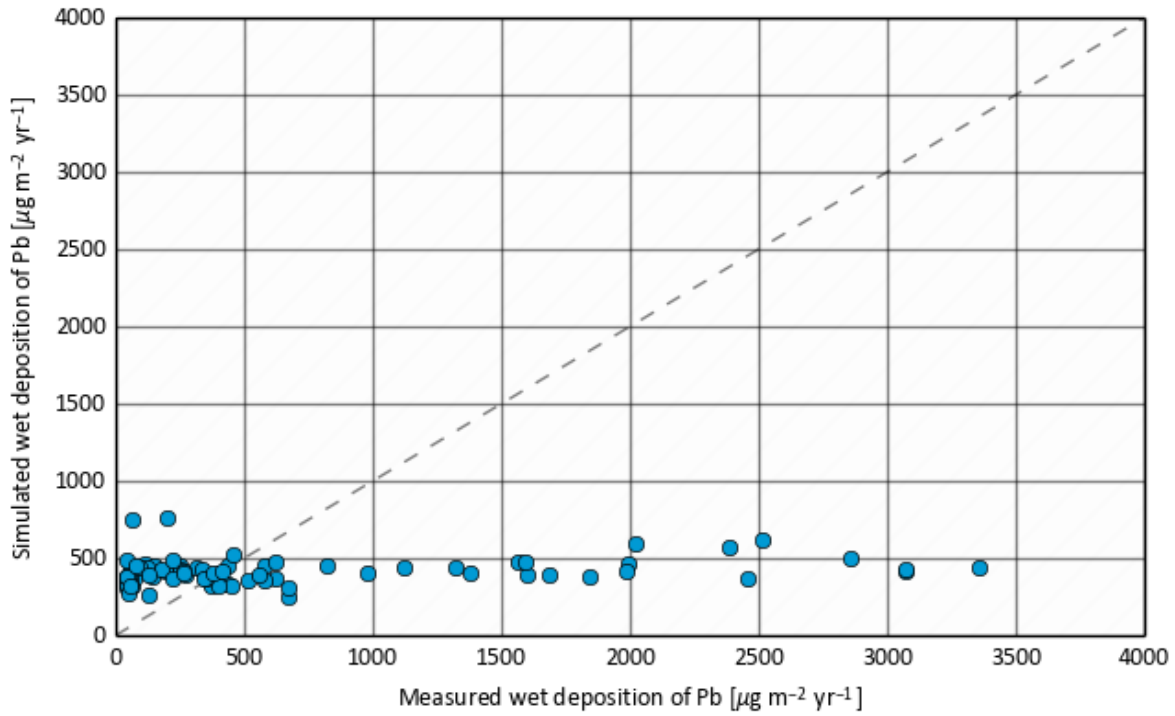


Figure 21: Scatter plots of modelled versus observed annual wet deposition of lead in 2009. Top: Länder data; Down: UBA data. Note the difference in scales. Source: this work

Wet deposition of Led in 2009

Measurement data from Lander stations



Wet deposition of Led in 2010

Measurement data from UBA stations

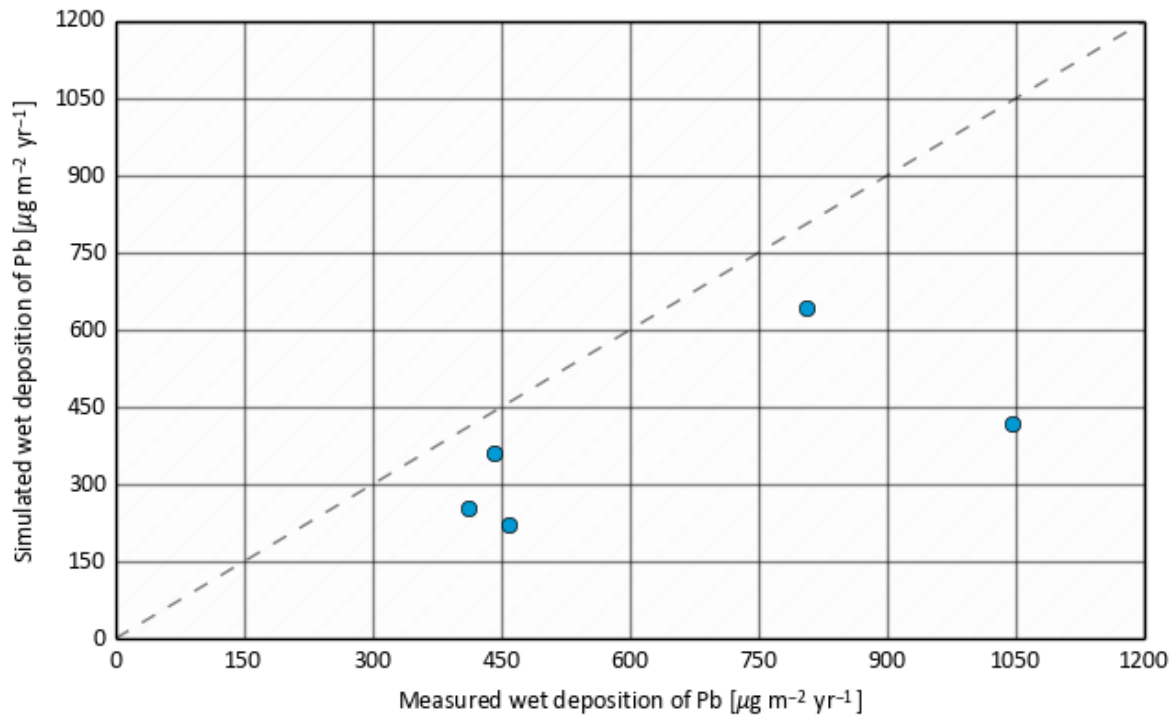


Figure 22: Scatter plot of modelled versus observed annual wet deposition of vanadium in 2009 from Länder data. Source: this work

Wet deposition of Vanadium in 2009

Measurement data from Lander stations

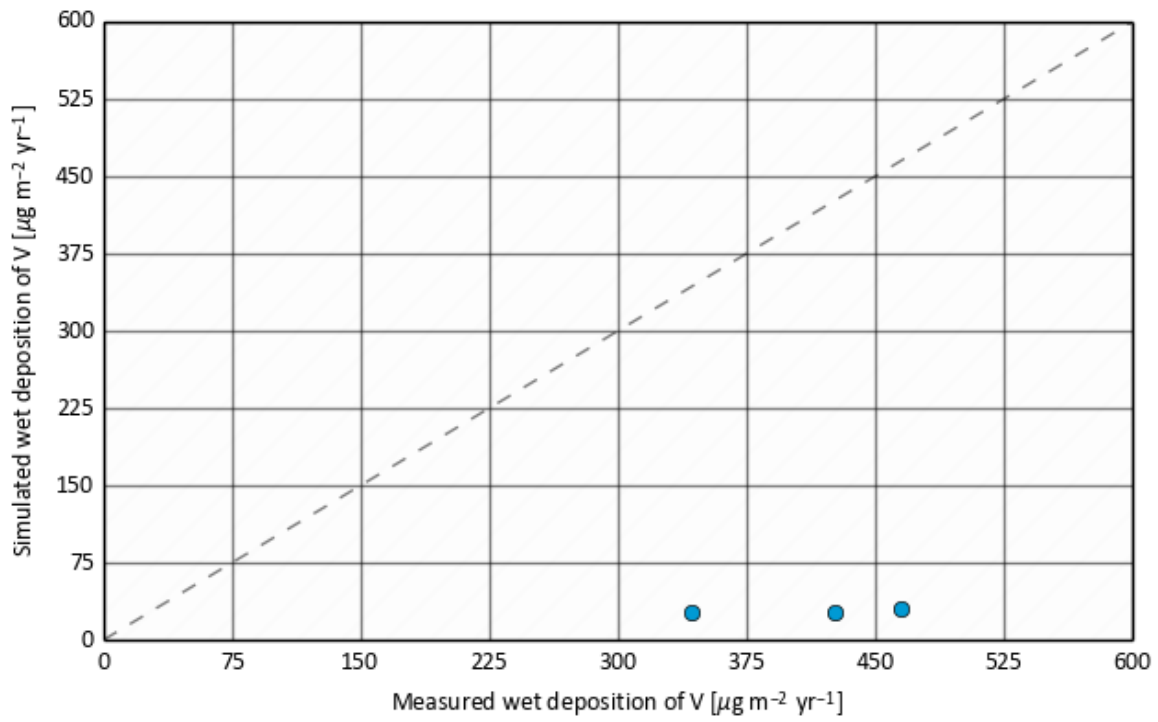
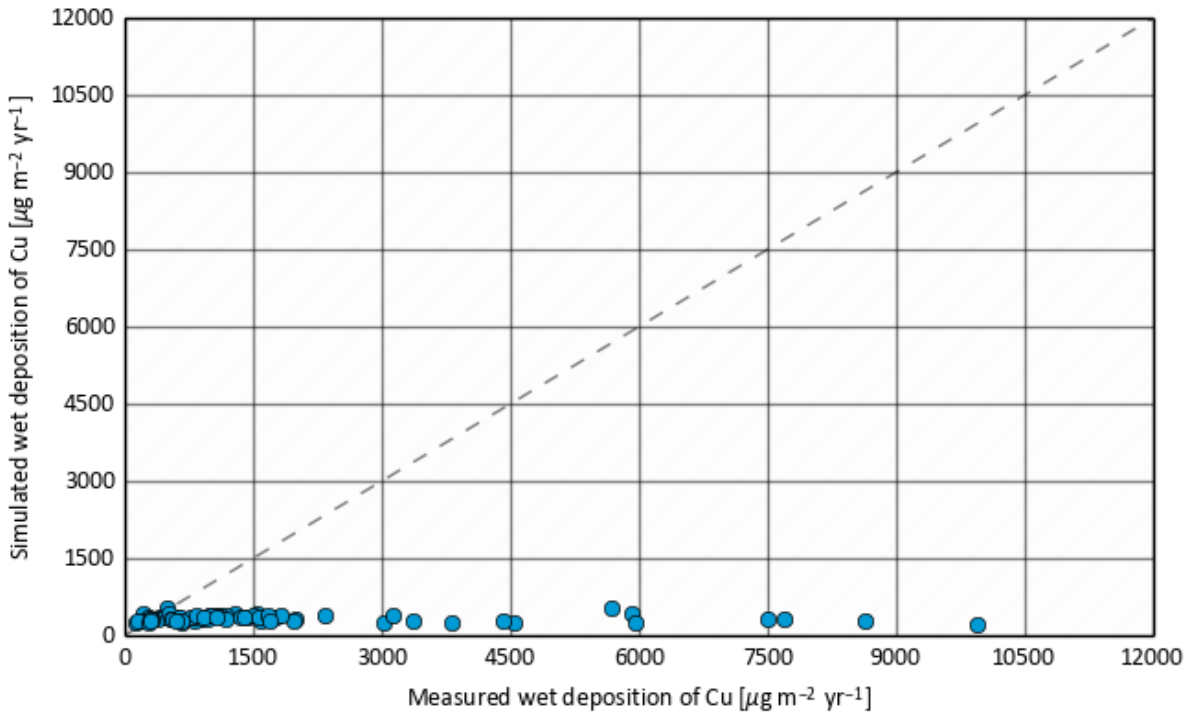


Figure 23: Scatter plots of modelled versus observed annual wet deposition of copper. Top: Länder data, 2009; Bottom: UBA data, 2010. Note the difference in scales. Source: this work

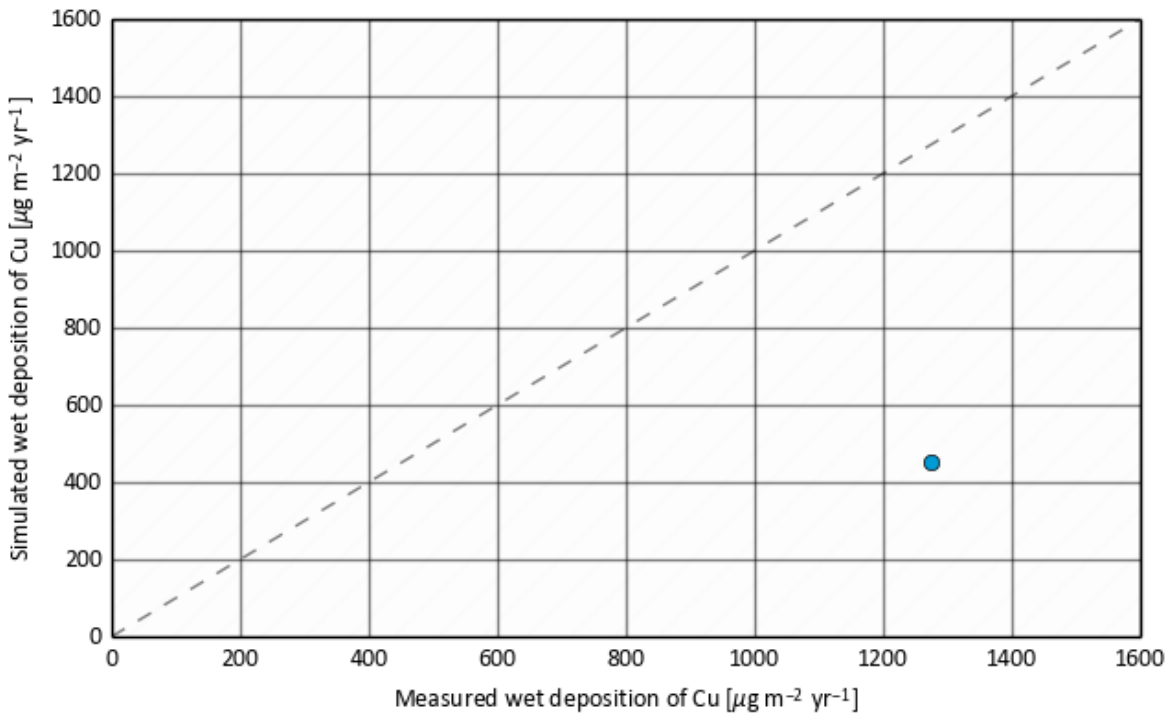
Wet deposition of Copper in 2009

Measurement data from Lander stations



Wet deposition of Copper in 2010

Measurement data from UBA stations



Clearly, the modelled wet deposition fluxes underestimate the size and spatial variability of the measured wet deposition fluxes. This underestimation is very obvious when the Länder observations are correlated to the model. The observed maximum from the Länder data is for most of the components more than 10 times the modelled maximum. The model shows better agreement when compared to the UBA observations, especially for components lead and cadmium. For these components, the observed wet deposition fluxes are underestimated too, but to a much lesser extent. In addition, the model predicts the spatial variability quite reasonably as the locations with high and low deposition coincide. Unfortunately, the number of stations operated by UBA is so low that strong conclusions are hard to make. As only for Cd and Pb 7 km spatial resolution emission data were applied, instead of 50 km, part of the poor model to observation agreement of the other metals can be explained from the emission data. For components As, Ni and Zn, the available EMEP emission inventories have not sufficient spatial detail to reproduce the observed gradients.

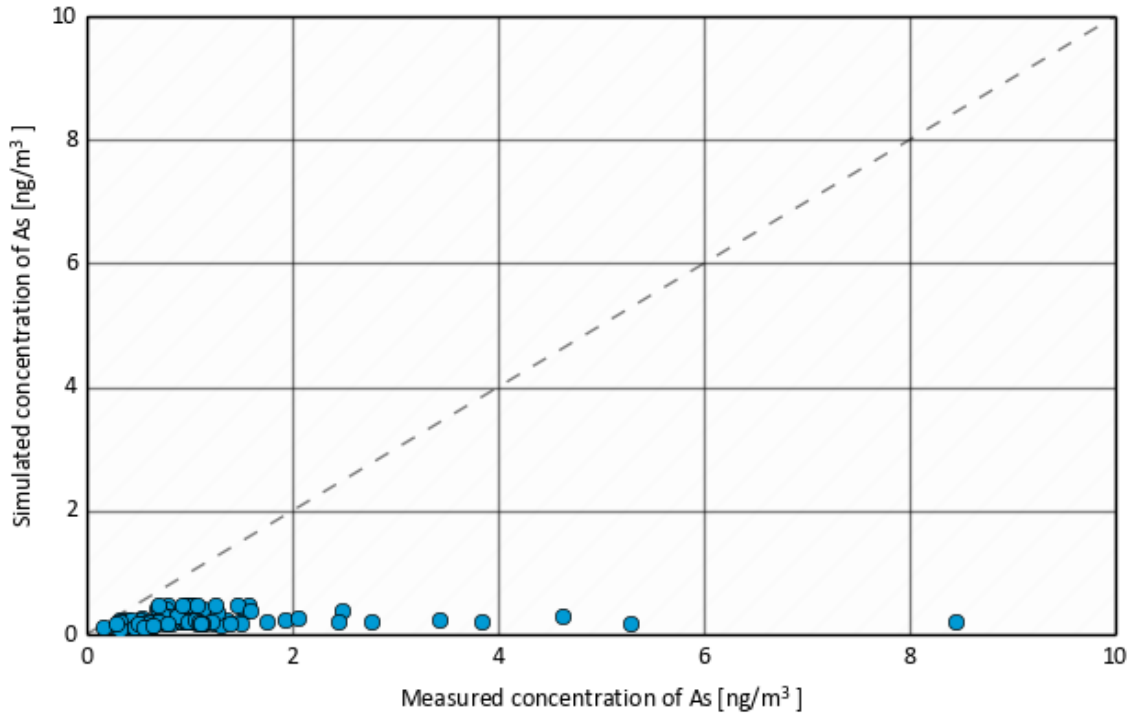
2.3.3.3 Concentration modelling

Modelled concentrations are compared to observations as well. This is done for the Länder stations only. Comparison of the concentration data provides complementary information on the model performance. Figure 24 shows the 2009 results for As, Cd, Ni, Pb, V and Cu. For zinc no concentration observations are available. For vanadium, the 2011 result is shown.

Figure 24: Scatter plots of modelled versus observed annual average concentration including all stations (urban, rural, traffic and industrial). Source: this work.

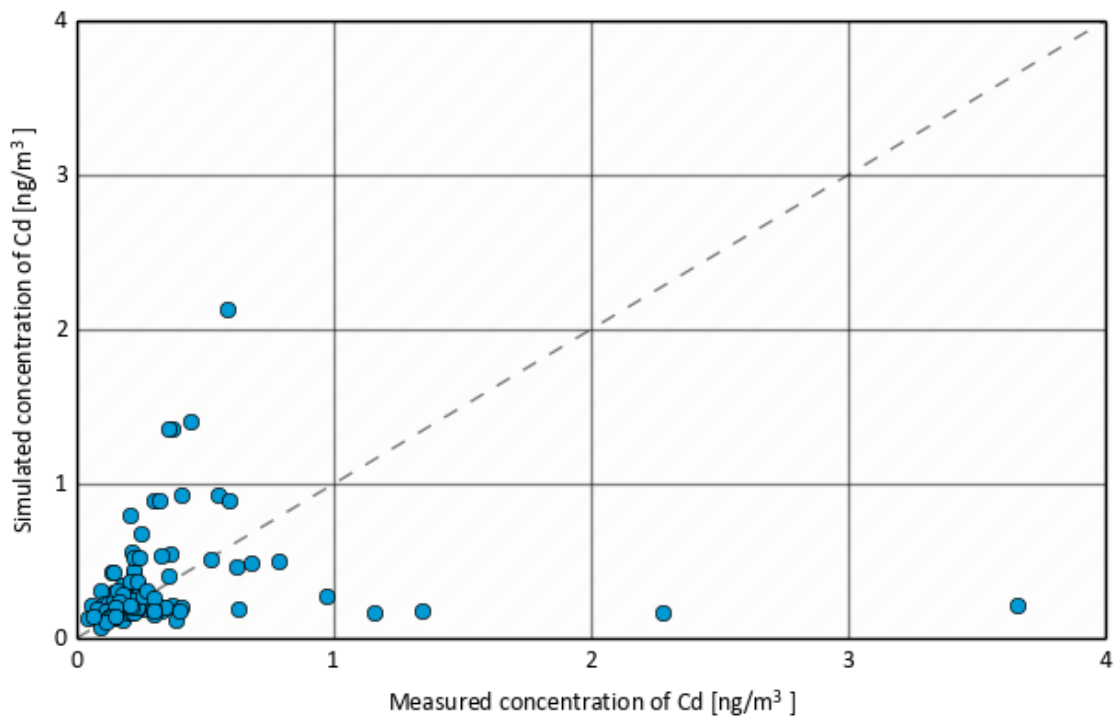
Annual concentration of Arsenic in 2009

Urban, rural, traffic and industrial stations



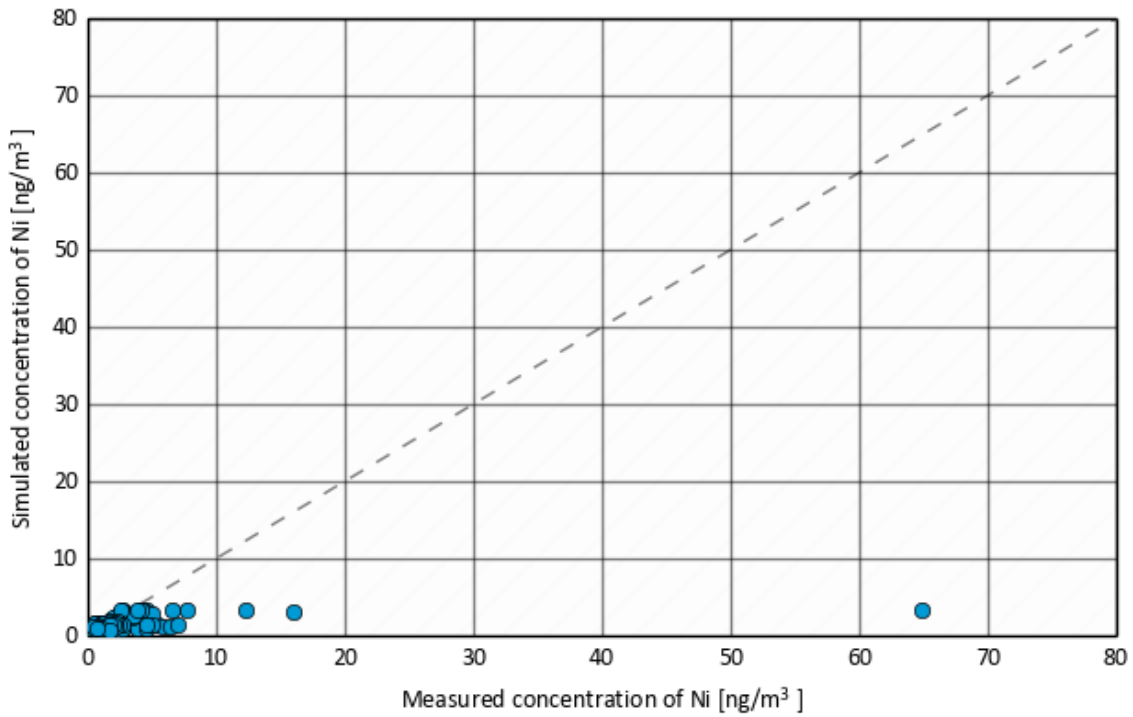
Annual concentration of Cadmium in 2009

Urban, rural, traffic and industrial stations



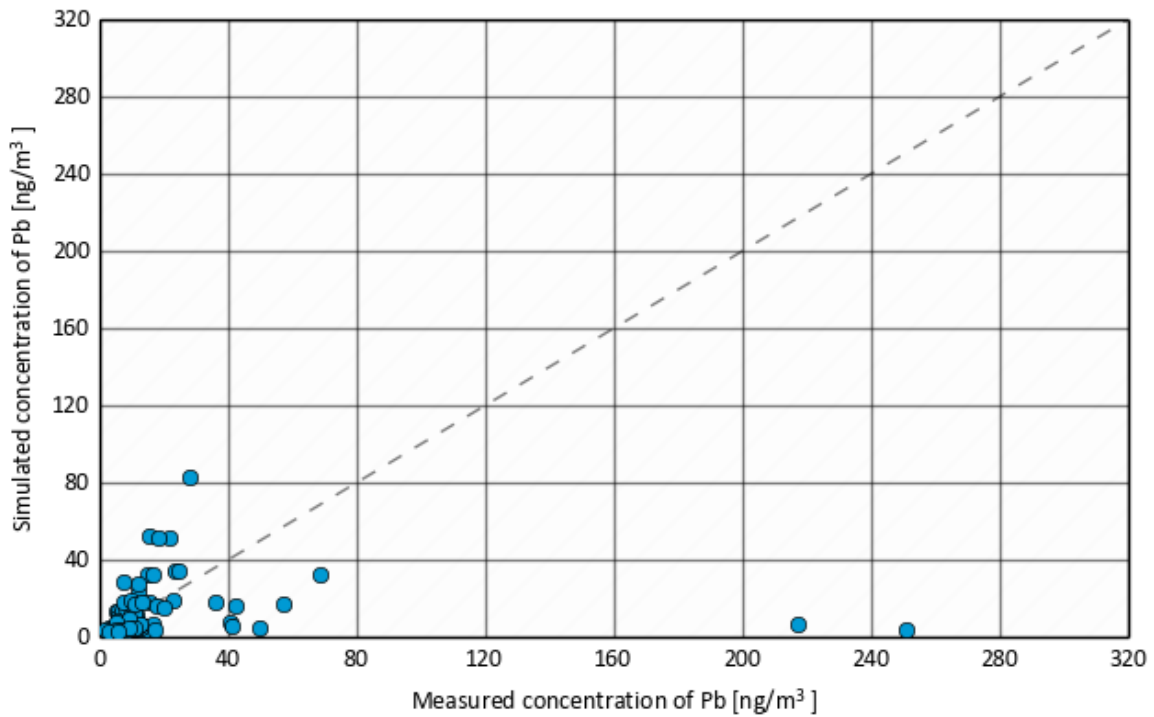
Annual concentration of Nickel in 2009

Urban, rural, traffic and industrial stations



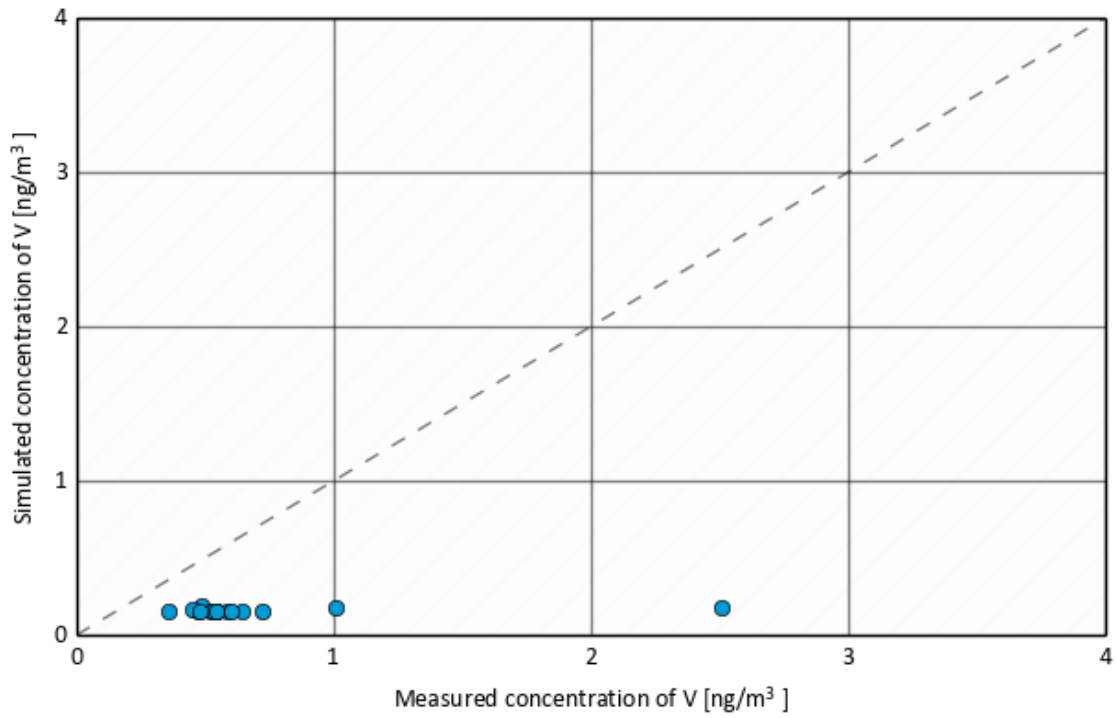
Annual concentration of Lead in 2009

Urban, rural, traffic and industrial stations



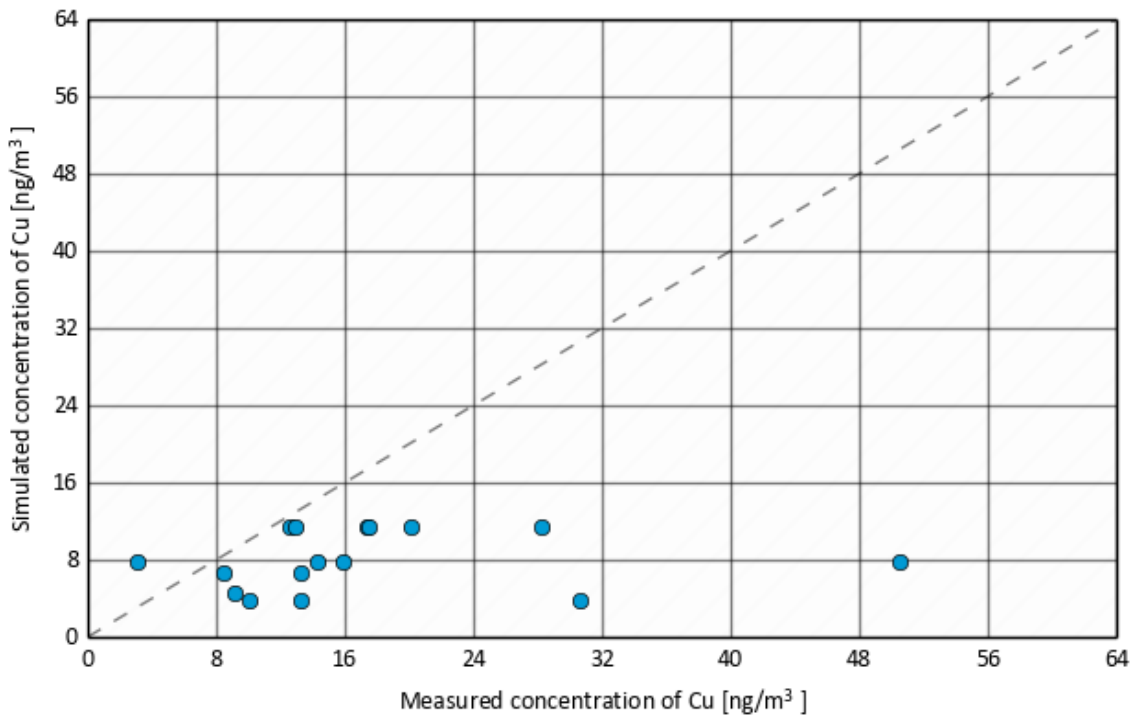
Annual concentration of Vanadium in 2011

Urban, rural, traffic and industrial stations



Annual concentration of Copper in 2011

Urban, rural, traffic and industrial stations



The comparison of modelled versus observed concentration shows reasonable agreement for cadmium and lead. The variability is similar to that of the observations. Furthermore, the systematic difference between the modelled and observed concentrations is rather small. The agreement for the other components is much worse. The model clearly predicts less spatial variability and underestimates the observations systematically. This result is in agreement with the results we found in the comparison of modelled and observed wet deposition: the model performance increases clearly when the resolution of the emission maps is increased.

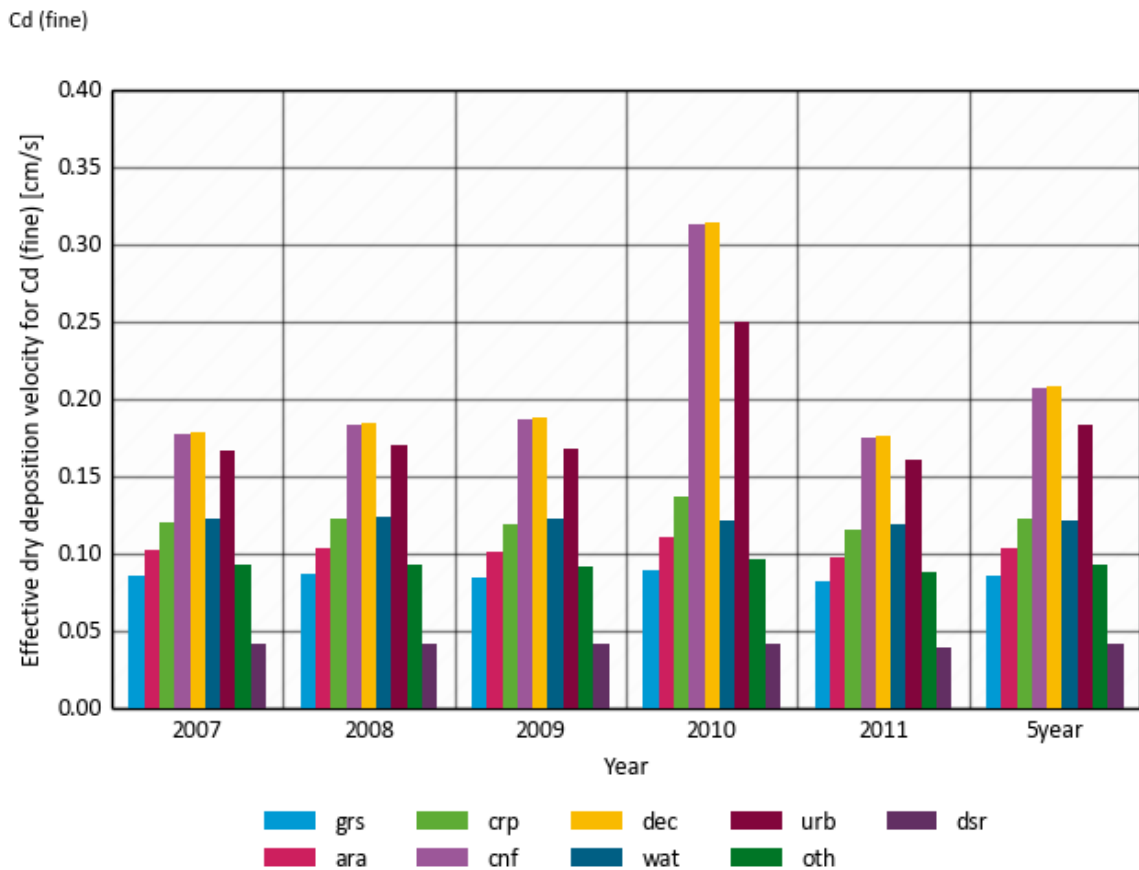
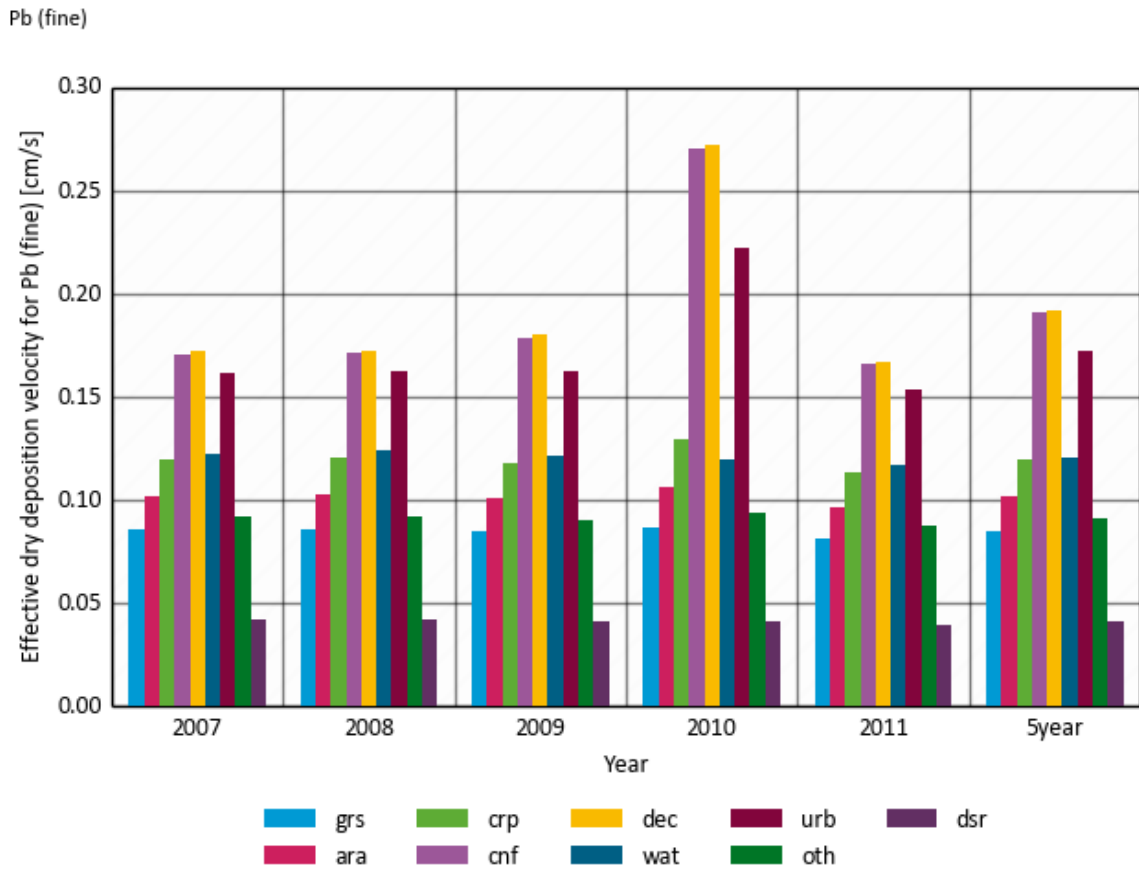
2.3.3.4 Assessment of effective dry deposition velocity

This simulation was used to determine the effective dry deposition velocity used for other metals in the empirical assessment. The five year simulation for two metals enable to address the following questions:

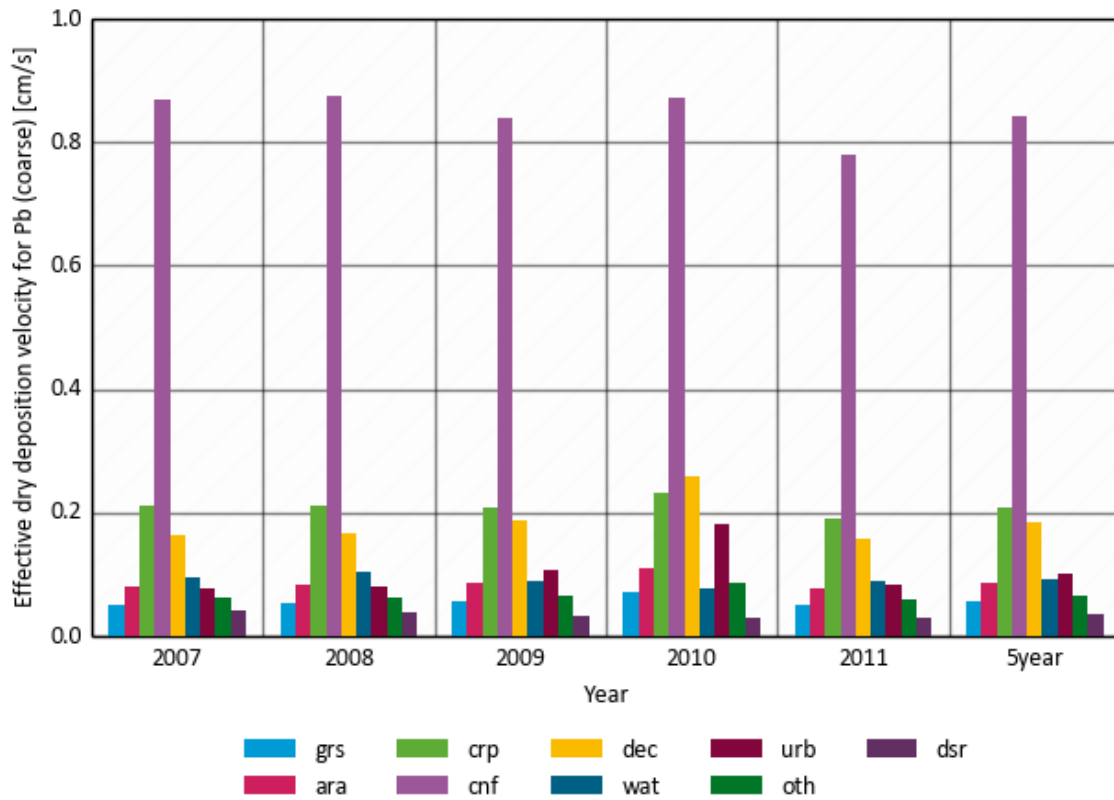
- ▶ What are the effective dry deposition velocities for the main land use categories?
- ▶ How comparable are the effective dry deposition velocities between the two metals?
- ▶ How large is the inter-annual variability in the effective dry deposition velocities?
- ▶ How representative is the value of a single year for that of the 5 year mean?

The effective dry deposition velocities of Pb and Cd in both fine and coarse fractions for the 9 land use classes are shown for five individual years and the 5-year average in Figure 25 and Figure 26. It is seen that particle dry deposition velocities are highly dependent on surface type. For small particles, the v_d values are controlled by Brownian diffusion and the aerodynamic resistance. For forests and urban surfaces with larger roughness lengths which induced more turbulent mixing, the surface resistance and aerodynamic resistance are smaller and the v_d values are higher than that for the other surface types. On average the effective deposition velocity for fine particles is around 0.1 cm s^{-1} for short vegetation and about 0.18 cm s^{-1} for taller vegetation and cities. Comparing the data for the individual years show very comparable results for four out of five years. The year 2010 seems to be quite exceptional with about 70% higher effective deposition velocities especially for the taller vegetation and cities. The higher deposition fluxes in 2010 can be linked to the impact of more frequent episodes during in the autumn and spring. These episodes largely contribute to the total deposition, but hardly count for the average annual concentration due to their short duration. These higher effective deposition velocities in 2010 are not obtained for the coarse particles, which can be explained by the fact that the coarse particles deposit quicker due to their weight, i.e., coarse particles have shorter transport distances. For the dry deposition velocity for coarse mode particles ($d_p=5 \mu\text{m}$), impaction and interception become important. Coniferous forest (i.e., needle leaf forests in Zhang et al., 2001) do not only have larger roughness lengths than most of the other land uses, but also smaller collection radii 'A', which result in larger Stokes numbers. This subsequently results in a larger impaction collection efficiency. Therefore, coniferous forest have the highest v_d values. Zhang et al. (2001) also obtain approximately 4-5 times higher effective deposition velocities for coniferous forest than for deciduous forest, but comment that observations to support these findings are sparse.

Figure 25: Effective dry deposition velocity per land use category based on each individual year and the 5 year period for the fine and coarse fractions of lead and cadmium (source: this work)



Pb (coarse)



Cd (coarse)

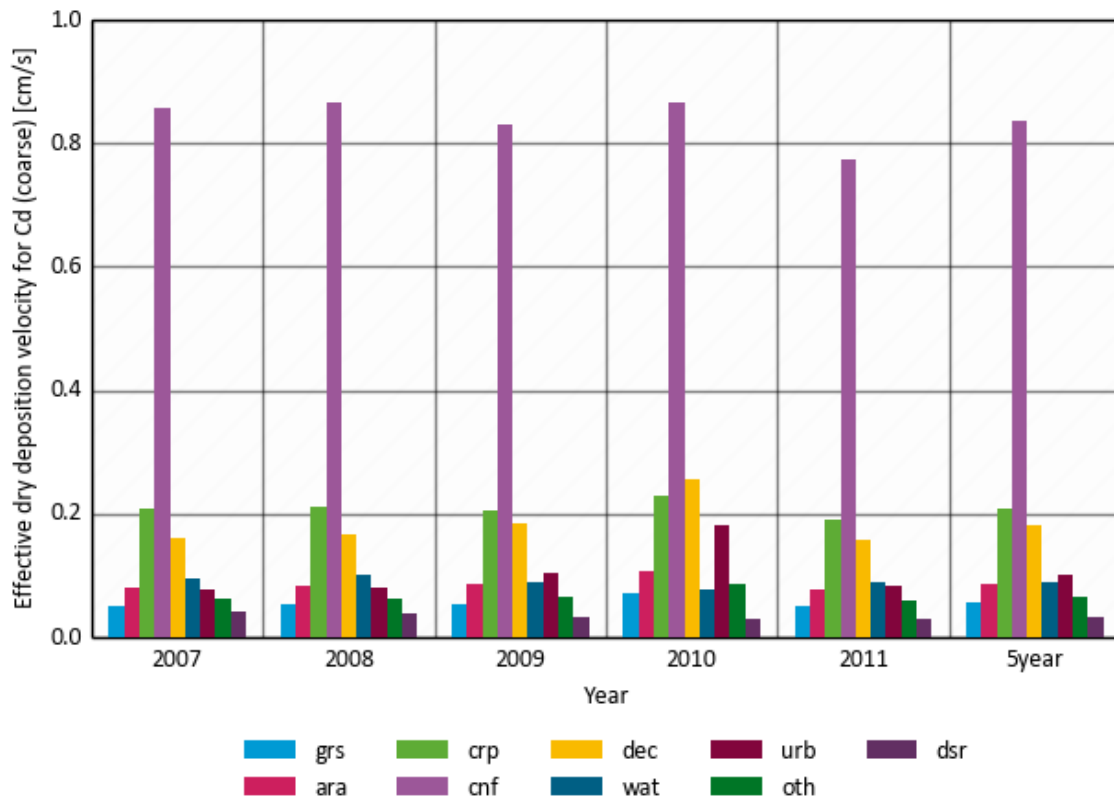
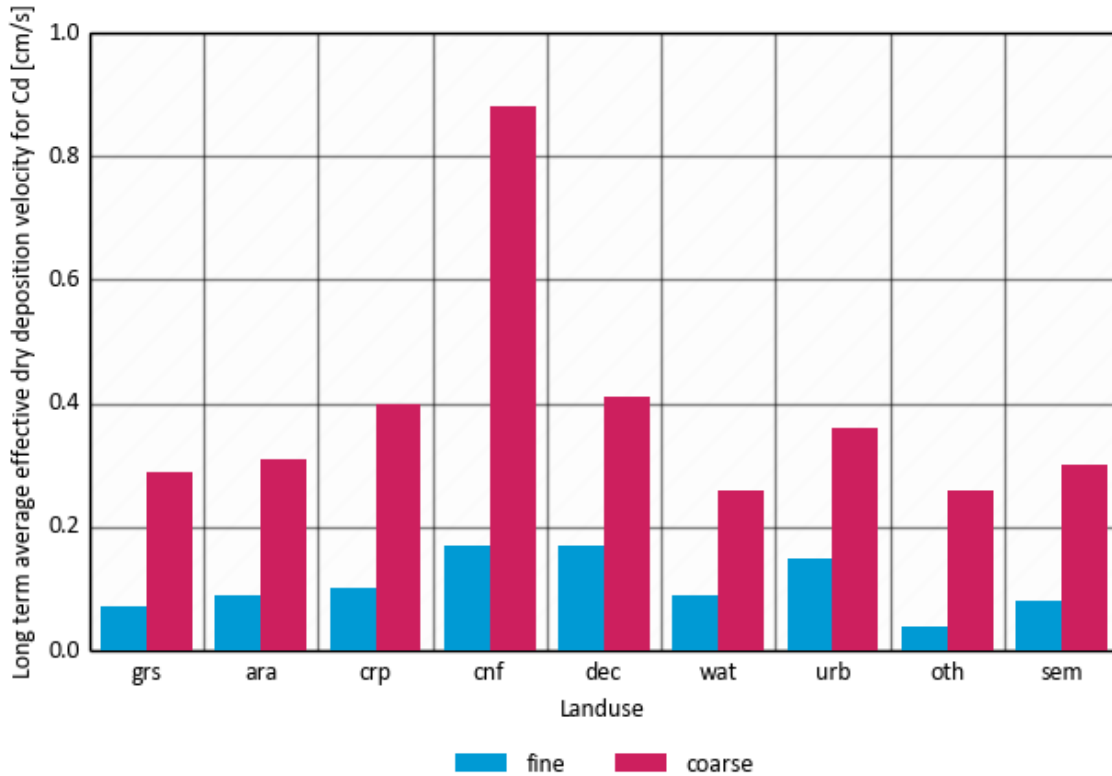
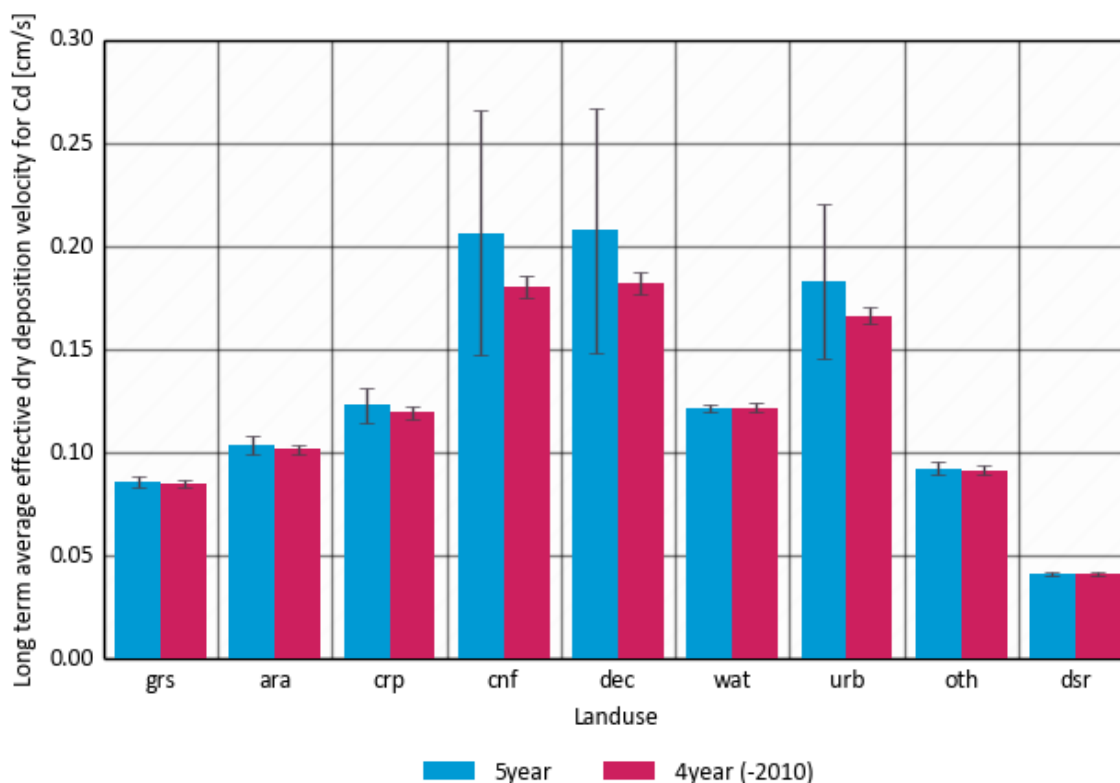


Figure 26: Comparison of the long term average effective dry deposition velocity for fine and coarse cadmium (source: this work)



The analysis shows that assessing the effective dry deposition velocities based on a single year is not advisable as it can be influenced by the number of long range transport events over a region as well as general variations in meteorological conditions such as rain fall. Overall, 2009 seems to be the year that is closest to the 5-yr mean in terms of annual concentration and deposition distributions. Although 2010 was an exceptional year, we include it in the determination of the effective dry deposition velocities used in this study. The impact is shown in Figure 27 where we compare the 5-yr mean to the 4-yr mean excluding 2010. Comparison of the two metals shows that the difference between Cd and Pb are smaller than the variability between the years and much smaller than the differences between the land use categories. As such we decided to average the data for these metals to arrive at our final effective dry deposition velocity.

Figure 27: Effective v_d for fine cadmium particles: comparison of the 5-yr mean to the 4-yr mean excluding 2010 (source: this work)



2.4 Discussion on emissions

In this study we used the emission information from Builtjes et al. (2012) for Cd and Pb and from Denier van der Gon et al. (2007) for Cu. For the other metals (Ni, Zn, As and Cr) the emission distributions at the EMEP 50 km grid from Denier van der Gon (2005) for the year 2000 were used. The inventories for Cd, Pb and Cu are updates of the Denier van der Gon (2005) database. Within the MAPESI project (Builtjes et al., 2012) a 2005 estimate for Cd and Pb was made at a 7x7 km resolution by estimating the 2005 emissions totals and gridding the emissions using proxy maps derived from the PAREST project (Jörß et al., 2010). For copper, it was recognized that the base inventory did not include brake wear as a major source, which was added by Denier van der Gon et al. (2007).

In Table 9 we compare the emission totals used in the model exercise for Germany to emission reporting by Germany to EMEP in 2016. The numbers show that the emission data show large differences for the individual metals. For Cd, Pb, Ni and As the European emission inventory used in the modelling provides considerably larger emissions than reported. The values for Cr and Zn are relatively similar, whereas for copper the reported emissions are a factor 10 higher than used in the model. The background of the differences is shortly discussed below.

Table 10: Comparison of the 2005 emission totals for heavy metals as used in LOTOS-EUROS (Denier van der Gon et al., 2005; Bultjes et al., 2012) and officially reporting by Germany in 2016 (www.emep.int).

	Pb	Cd	Ni	Zn	As	Cu	Cr
Model input	620	21	248	1658	34	273	74
Reported	277	9.1	133	1899	5.8	2113	57

The Denier van der Gon (2005) database, in the following called TNO-off, is a so-called hybrid emission database, which consists of both officially reported emission data and expert estimates. Officially reported emissions are screened for completeness and obvious outliers, which are then filled/replaced by expert estimates. At the time the database was compiled, officially reported emission data for Germany were such that the German emissions were largely derived by expert estimates from the TNO bottom-up reference inventory. The expert estimates are a factor two higher than currently reported. In Table 10 we compare the emission data of the TNO-off to the emission estimates of the FP6-ESPreme project, the only other bottom-up expert inventory for Europe. The ESPreme project built a hybrid (ESP-off) and a pure expert (ESP-exp) inventory. The results show that expert estimates for metals tend to be considerably higher than officially reported by countries. For lead ESPreme and TNO-off are very close together, showing a large consistency between the expert estimates. For cadmium, ESPreme took national reporting into account in the hybrid database, but shows much larger expert estimates.

These results illustrate the well-known large variety in emission estimations for heavy metals. Since the heavy metal content of fuels and raw materials is highly variable and mostly unknown, the variation in estimated contents in the emission inventory preparation can be very high. It is not possible to simply assess which emission factor is better or more reliable – hence differences might perhaps better be represented as “uncertainties”. The TNO bottom-up inventory used by Denier van der Gon (2005) is based on established but older information from the 2006 CORINAIR Guidebook and the 1993 Parcom Atmos Emission Factor Manual. In this respect information underlying ESPreme might partially be newer. The fact that official country reports and two truly independent methodologies to estimate heavy metal emissions can result in differences of the indicated magnitudes clearly demonstrates that more research is needed for heavy metal emissions.

Table 11: Comparison of Cadmium and Lead emissions for the year 2000 from TNO-official and ESPreme-official and ESPreme-expert inventories.

Code	Country	TNO-off	ESP-off	ESP-exp	TNO-off	ESP-off	ESP-exp
		Cd	Cd	Cd	Pb	Pb	Pb
AUT	Austria	1.4	1.4	5.7	13.9	13.9	64.1
BEL	Belgium	2.8	2.3	13.5	133.8	123.0	268.8
CHE	Switzerland	2.2	2.2	4.9	113.6	113.6	107.0
CZE	Czech Rep.	2.8	2.9	13.2	107.7	107.7	185.9
DEU	Germany	21.1	11.0	66.3	587.6	632.0	942.4
DNK	Denmark	1.0	0.7	3.6	9.6	7.0	38.5
NLD	Netherlands	1.2	1.2	10.7	44.1	44.1	183.0
POL	Poland	50.4	50.4	39.4	647.5	647.5	437.1

The modelling results provide hints as to how likely it is that the official emission reporting may indeed underestimate the actual cadmium and lead emissions. The comparisons for air concentrations and wet deposition fluxes at sites away from the direct sources (industrial areas) show a general agreement between modelled and observed concentrations ranges. There is no indication of a large overestimation. In contrast, EMEP modelling results using the officially reported emissions indicate a general underestimation of both Cd and Pb concentrations of at least a factor 2 for most stations in Europe. Hence, it appears that the officially reported emission totals cannot explain the observed concentration and deposition fluxes. For this reason, the EMEP model also includes a methodology to include resuspension or secondary emissions from enriched soils into account. Dust emissions from urban areas are estimated and connected to soil metal contents and an additional enrichment of metals. In fact, these emissions dominate over the inventoried emission data and close the gap between observed and modelled concentrations with the EMEP model.

Explorative simulations were performed using the dust resuspension scheme of LOTOS-EUROS. This scheme calculates the resuspension emissions from both traffic and agricultural activities. For Germany emissions of 86 and 31 kton PM₁₀ were estimated for agriculture and traffic, respectively. Combined with the FOREGS lead soil content distribution (typically 25 mg Pb/kg soil) a contribution of about 0.5 % of the lead emissions in the inventory was found. There are indications that the lead concentrations in equilibrium PM₁₀ dust loads on urban streets may be a factor 10 higher than the lead soil content used here (Shatalov et al., 2016), which would increase the estimate to about 2%. Considering the results with LOTOS-EUROS, it appears that the additional enrichment of metals assumed in urban areas results in the large secondary emissions within the EMEP model. In the newest EMEP model version the lead enrichment in soils was reduced in north western Europe to get rid of overestimations in the area and it was noted that the currently assumed enrichment may be too high. The latter was supported by a comparison of the assumed lead content in resuspended dust against the street dust concentration measurements showing more than 10 times higher metal concentrations in the model than in the observations (Shatalov et al., 2016).

On the other range of the spectrum we see the large difference for copper. The German copper emissions reported to EMEP (2113 tonnes/yr) are ten times higher than expert estimates by Denier van der Gon et al. (2007). The reason is found in the reported emissions for brake wear. In Table 11 the reported brake wear emissions for copper and PM₁₀ from different countries is provided. Comparing the estimates of Germany and the Netherlands shows that although the PM emissions from brake wear are a factor 10 apart, the copper emissions are a factor 100 apart, although the car fleet and associated brake systems are not very different between these countries. The Dutch reporting follows the assumption of 5% of the brake pads to be copper (Denier van der Gon et al., 2007) and a wear ratio between brake pads and disk of 1:2. The disks mainly contain iron. Recent, brake pad composition measurements hint at a high average copper content in the order of 10 % (Hulskotte et al., 2014). Hence, values ranging between 1 and 3 % of brake wear emissions to be copper appear to be in the range of current understanding. With 16 % the reported emissions seem too high and the expert emission inventory was used here. The modelling results indicate that the expert inventory is in the right order of magnitude.

Note that the reported emissions of Copper from Germany did not change between different reporting years in the last decade, whereas those of some other countries, e.g. the Netherlands, have been updated as a consequence of the new publications. In addition, a number of countries do not even report copper or PM emissions from brake wear. This example for copper clearly illustrates that the emissions of heavy metals need attention.

Table 12: Emissions of Copper and PM10 (tonnes/yr) from brake wear from transport as well as the implied percentage (%) of Copper.

	AUT	BEL	DNK	FRA	DEU	ITA	NLD	PT	ESP	SWE	UK
Cu	-	18	380	130	2011	102	21	-	148	44	24
PM10	-	1977	1035	9084	12273	9823	1376	-	6333	1625	9230
Cu/ PM ₁₀	-	0.9	3.7	1.4	16	1.0	1.5	-	2.3	2.7	0.3

In short, we feel that the officially reported emissions for Cd and Pb are underestimating the real emission situation in Europe. It is likely that existing sources are underestimated or that important sources are not on our radar. Although there might be missing sources, it is unlikely that resuspension of dust contributes a large part of the missing mass. A thorough analysis of the official emission reporting and expert estimates from TNO and ESPREME seems to be necessary to further elucidate the reasons behind the deviations. Subsequently, a new emission inventory should be derived including a detailed uncertainty analysis, taking new knowledge into account. The model results using the expert estimates for Ni, Cd, Pb and Cu seem to be consistent with observations of air concentrations and wet deposition data.

2.5 Conclusions

In this work, an empirical assessment was made of the deposition fluxes of 17 heavy metals for different land use classes. Industrial, urban, traffic and rural conditions were considered separately. Since measurement data for heavy metal concentration and deposition are scarce, the assessment is based on a limited amount of observation data and locations. The resulting deposition estimates should therefore be considered rough large-scale estimates that could be biased significantly because of the selection of measurements available.

To estimate the dry deposition flux, the most appropriate available air concentration measurements per station type were averaged to get a representative concentration for average rural, urban, traffic and industrial locations in Germany. When possible, only German measurements were used, but for some metals measurements were so scarce data from neighboring countries was taken into account as well. These concentrations were multiplied by the effective deposition velocity for particles as modelled by LOTOS-EUROS, arriving at an estimate of the dry deposition flux.

For wet deposition, observed concentrations of heavy metals in rain and observed total rain at measurement stations was combined to arrive at the wet deposition flux. Also for wet deposition, limited data availability, with the available data often skewed towards one or a few Bundesländer, makes it difficult to come to a reliable estimate for the country as a whole. While many of the observations are done using bulk samplers rather than wet-only samplers, the wet deposition estimate derived from these measurements should be treated as an upper estimate of the true wet deposition.

The results for dry and wet deposition of heavy metals found during this study were compared to Knappe et al., (2008), who used roughly the same approach but different observation data and v_d estimates. The wet deposition estimates for the different heavy metals agree quite well between both studies. However, the dry deposition estimates found in this work are often much lower than those found by Knappe et al. (2008). For coniferous forests, the difference in dry deposition estimates is a factor 2-8, whereas for urban areas the estimates are a factor 6-39 apart. Both the effective v_{dS} calculated for this study as well as the air concentrations of heavy metals based on observations are lower than those reported and used by Knappe et al. (2008). This shows that the method used in both studies is very sensitive to the selection and/or availability of measurements.

The comparison between modelled to observed concentrations in air and precipitation show that for Cd, Pb, Ni and Cu the model results are in general agreement with observed values. For As, Zn, V the modelled values underestimate the observations by far, leading to the advice to use the empirically derived estimates. For all metals the fluxes near industrial sites are dominated by local sources and thus largely underestimated by the model. For such locations it is advised to take the range as deduced from the observed concentrations above.

A comparison of the differences between emissions from national reporting and expert estimates shows the well-known large variety in emission estimates for heavy metals. Uncertainties for single metals are a factor 3 or more. A thorough revision of the emission information for heavy metals is highly needed. A new consistently derived inventory could be used to perform (simple) inverse modelling studies to further detail the source strength and deposition patterns of the metals at hand.

3 Case Study: Mercury

3.1 Introduction

Mercury (Hg) is a naturally occurring element. Trace amounts of mercury are found in most plants, animals and soils. Almost all mercury compounds are toxic and can be dangerous at very low levels in both aquatic and terrestrial ecosystems. Nonetheless, mercury has many practical properties from conducting electricity, expanding evenly with changes in temperature or pressure, being a dense and heavy liquid that flows, and even for its reflectivity. Even its toxic properties have been used as a preservative or a fungicide. These properties make it extremely useful in electronics and other industries, medicine and for household use. Mercury is a by-product of combustion for energy as old organic matter is burned, the trapped mercury is then released. Over 40 percent of anthropogenic mercury released into the atmosphere is from the generation of electricity through coal burning. Experimental data from lake sediments and ice cores indicate that atmospheric Hg deposition has increased globally by a factor of 3 since preindustrial times, with larger increases in regions receiving elevated deposition from regional sources (Drevnick et al., 2012; Lindberg et al., 2007). As such human activities have significantly altered the natural global mercury cycle through emissions to the atmosphere from anthropogenic activities.

The atmosphere is the foremost transport pathway of Hg emissions, whereas land and ocean processes play an important role in the redistribution of Hg in terrestrial, freshwater, and marine ecosystems. The temporal and spatial scales of Hg transport in the atmosphere and its transfer to aquatic and terrestrial ecosystems depend primarily on its chemical and physical forms. Following emission, gaseous elemental mercury (GEM) can be transported long distances before oxidation and removal by particle and gas-phase dry deposition or scavenging by precipitation. The atmospheric residence time of GEM is several months to a year. Mercury can therefore be transported and deposited to remote locations such as the Arctic and Antarctic. Gaseous oxidized mercury (GOM) and particulate bound mercury (PBM) have a shorter atmospheric residence time than GEM ranging from hours to days, and as a result are generally deposited locally or regionally.

An important distinction between mercury and most other atmospheric pollutants is that environmental and health impacts are only indirectly related to ambient atmospheric concentrations of Mercury. Once deposited to land or oceans, mercury can be converted by microorganisms to the extremely toxic methylmercury (MeHg), which is much more toxic than the inorganic mercury forms (Clarkson and Magos, 2006). Mercury from the environment is transformed by bacteria into methylmercury and begins its rise in the food chain (Oken et al., 2012). Small fish feed on the plankton and pick-up small amounts of mercury, which accumulate in the small fish. The little fish get eaten by larger fish, which accumulate the mercury of their smaller prey, thus adding to their burden. Since these fish eat a lot of smaller fish, they have many times more mercury in them than the smaller fish they eat. In turn, these fish then get eaten by others and so on up the food chain. The top of the lake food chain can have hundreds of thousands of times higher mercury concentration than the water column that they are in. Humans catch these top predators, such as tuna and swordfish and consume them (Sunderland, 2007). This process of bioaccumulation, in living organisms, inflicting increasing levels of harm on higher order species such as predatory fish and fish eating birds and mammals is known as "biomagnification".

Over time humans can accumulate levels of mercury in our bodies that can be harmful to us. After consumption, MeHg is transported by blood and can easily pass the blood-brain barrier and cause neurotoxic dysfunctions. It is reported that even relatively low doses can damage the nervous system. The symptoms which can be observed are: blurred vision, malaise, dysarthria, paraesthesia, ataxia, impairment of hearing and difficulty in walking. Symptoms appear slowly and increase gradually along with amount of mercury accumulated in body (AMAP/UNEP, 2008).

It should be highlighted, that mercury also passes the placental barrier and has immense negative impact on foetus decreasing the child's IQ. In this way the development of the whole population is influenced (Rice, 2008). It is reported that methyl mercury can be cause of a cancer, kidney dysfunction, heart and blood system diseases (AMAP/UNEP, 2008). In short, mercury pollution is therefore a threat to ecosystem health on a global scale and is now being addressed as such following the negotiations to produce an international agreement, known as the Minamata Convention (UNEP 2013b).

Although the long-term effects of mercury on whole ecosystems are unclear, the survival of some affected populations and overall biodiversity are at risk. To evaluate the impact of mercury it is necessary to be able to assess the atmospheric deposition to the relevant eco-system. The experimental data on atmospheric mercury is very limited, making it very difficult to provide an empirical assessment of mercury deposition. Hence, one normally relies on modelling work to estimate deposition fluxes. In this report we provide an overview of the atmospheric mercury cycle with the aim to assess which model set-up can be used to quantify mercury deposition over a given ecosystem or area.

3.2 Mercury components

Most mercury in the atmosphere is in the gaseous state, although a small fraction is attached to particulate matter. Gaseous mercury is mostly elemental mercury. Only a small percentage is present in the form of oxidized mercury compounds. Here we present the main characteristics of these components.

Gaseous elemental mercury (GEM) is a shiny, silver, odourless, liquid metal. In its metallic form it is a silvery liquid that looks like it has a chrome-like polish. Elemental or metallic mercury is the common liquid metal used in thermometers, dental fillings, blood pressure cuffs, fluorescent light bulbs, barometers, batteries and auto and home switches. At room temperature, metallic mercury will vaporize, forming mercury vapours. Mercury vapours are colourless, do not have a smell and are harmful to health. Elemental mercury, has a very low water solubility making it very stable in the atmosphere, with an estimated residence time of between six months and two years. This life time makes elemental mercury a global pollutant with concentrations to be fairly uniform in the atmosphere. The more industrially developed Northern Hemisphere, however, has ~30% higher atmospheric elemental mercury concentrations than does the Southern Hemisphere.

Gaseous oxidized mercury compounds (GOM) are often referred to as reactive gaseous mercury. Important gaseous mercury "salts" are mercury chloride (HgCl_2), and mercury oxide (HgO). The mercury is present in the form of Hg^{2+} . These compounds undergo chemical transformations and are mostly soluble in water. Hence, their atmospheric life time is rather short as rain and other forms of precipitation can remove them from the atmosphere. In addition, they are removed by dry deposition at the earth's surface.

Particulate-bound mercury (PBM) is mercury that is found attached to particulate matter, in particular in combustion particles. The lifetime in the atmosphere is governed by that of the particle which means that it is also relatively short due to removal by both wet and dry deposition. PBM is best viewed as part of GOM, with gas-particle partitioning of GOM occurring in the atmosphere on the basis of local particle concentrations and temperature.

Organic mercury is mercury that is combined with carbon (and hydrogen) to make an organic mercury compound. The most commonly discussed organic mercury compound is methylmercury. Methylmercury is produced by microscopic bacteria that live on the bottom of lakes and ponds. These bacteria transform mercury that is present in the water into methylmercury.

Figure 28 gives an overview of the types, sources and fates of atmospheric mercury.

Anthropogenic sources include intentional and unintentional sources:

Intentional sources: These sources arise when an intentional decision is made to create a product that contains mercury or to operate a process that uses mercury. Examples of products that contain mercury or a mercury compound include fluorescent lamps, some thermometers, batteries and switches, and other similar products. A non-industrial process that uses mercury is large-scale and small-scale gold mining. Most of the mercury emissions from large-scale gold mining are the result of mercury impurities in the gold ores themselves, whereas small-scale gold miners purchase and use elemental to capture gold from mixtures of crushed rocks, sediments, soils, or other particles. The Mercury is then released into the environment during the mining and refining process. Of all the intentional uses of mercury, artisanal and small-scale gold mining appears to be, by far, the largest global source of mercury pollution (not only to air). This mining practice also seriously harms miners and their families, as well as local and regional ecosystems.

Unintentional sources: These sources arise from activities that burn or process fossil fuels, ores, or minerals that contain mercury as an unwanted impurity. Examples include coal-fired power plants, cement kilns, large-scale metal mining and refining, and fossil fuel extraction for coal, oil, oil shale and tar sands. Incinerators and landfills that are used to dispose of mercury-containing end-of-use products and wastes also release mercury into the environment and are categorized by some as unintentional sources.

Besides these sources mercury can be emitted through **remobilization activities**. These sources to air arise from human activities that burn or clear forests. The biomass and organic surface soils in forests often contain mercury that has fallen out from the air. Burning or clearing forests—especially boreal or tropical forests—releases large quantities of this mercury back into the air.

Recent global assessments and associated modeling have improved understanding of Hg emissions from both primary and secondary sources as well as their atmospheric transport and deposition (Travnikov et al., 2010; Ryaboshapko et al., 2007). Overall, total global Hg emissions to the atmosphere range from 6500 to 8200 Mg yr⁻¹, of which 4600 to 5300 Mg yr⁻¹ are from natural processes and sources (primary geogenic plus secondary emissions). Primary anthropogenic sources release 1400–2900 Mg yr⁻¹ compared with primary natural (geogenic) inputs of 80–600 Mg yr⁻¹ (Pirrone et al., 2010).

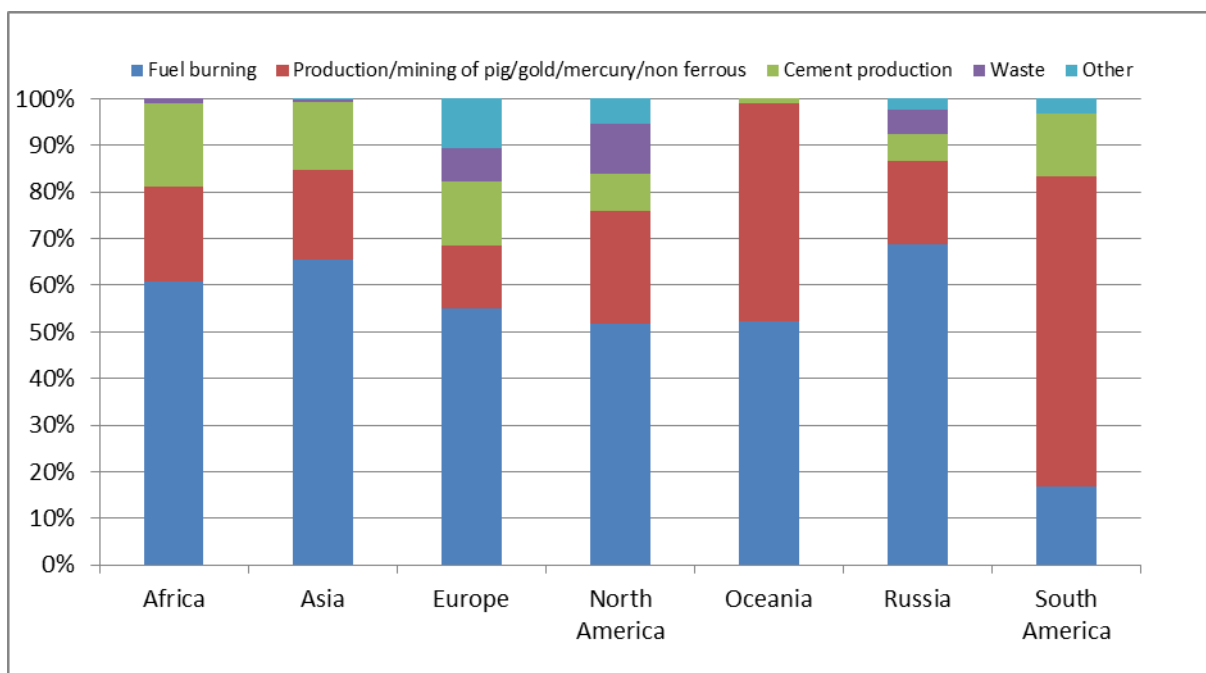
The yearly natural emissions (included remission) were estimated at approx. 2000 Mg from land and approx. 2600 Mg from oceans ((Selin et al., 2007), (Mason and Sheu, 2002)). The global anthropogenic mercury emissions in 2005 were estimated at c.a. 1400 Mg (AMAP/UNEP, 2008). Lohman et al. (2008) and Pacyna et al. (2006) estimated anthropogenic emission at c.a. 2200 Mg in 2000, whereas Pirrone et al. (2009) arrive at 2900 Mg. The majority of anthropogenic mercury is emitted from coal combustion, and a large part of the range in emission estimates is explained by differences for fossil fuel combustion. In addition to anthropogenic mercury emissions (~2000 Mg yr⁻¹), reemitted mercury from soils and aquatic ecosystems presently contribute approximately 2/3 of global emissions to the atmosphere (Corbitt et al., 2011). Pirrone et al. (2010) estimated that mercury evasion from terrestrial surfaces is about 2430 Mg yr⁻¹ and that from surface waters (oceans and lakes) is about 2780 Mg yr⁻¹.

Globally, energy production is the largest source for mercury, followed by gold mining activities, non-ferrous metal production and cement production. Other sources include combustion of waste and cremations. Figure 29 gives an overview.

Table 13: Overview of global anthropogenic Hg emissions (Mg/yr)

Emission area	Emission total	Source
Global	2000	Selin et al., 2007
Global	1554	Rafaj et al., 2013
Global	2254	Pacyna et al., 2006; Lohmann et al., 2008
Global	1400	AMAP/UNEP, 2008
Global	2900	Pirrone et al., 2009
Global	1926	Pacyna et al., 2010

Figure 29: Global emission of mercury by activity sector in 2005 (source: Rafaj et al., 2013)



European mercury emissions to air were reported to be 65 tonnes for 2010. The power sector and other stationary combustion emissions are the major contributor to mercury emissions in most of the countries. Germany is held responsible for the largest emission within the EU-28 (Figure 30).

The German emission inventory reports about 9 tonnes of mercury emitted to air in 2015. Seventy percent is related to the energy sector, whereas combustion of fuels in transport and households contributes another 10%. The remaining twenty percent derives from industrial activities including cement production and metal industries. Compared to 1990 emissions have come down by about two thirds, equally strong for industrial and energy production sectors (see Table 14).

Figure 30: Officially reported annual emission of mercury to air for the EU28 in 2010 (tonnes/yr).
Source: this work

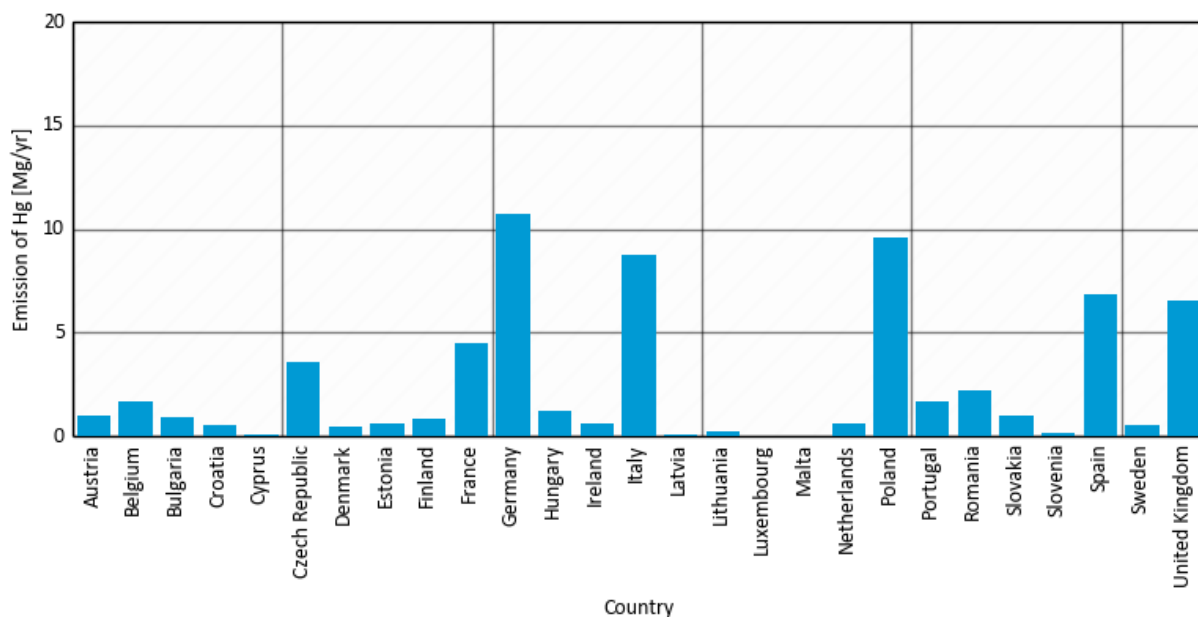
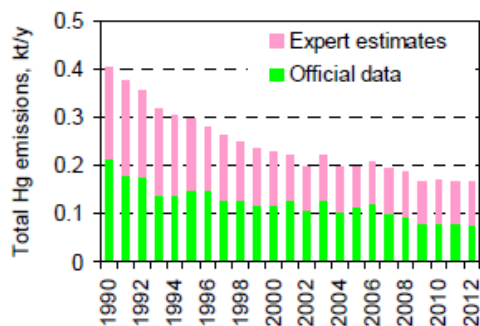


Table 14: Overview of German mercury emissions (tonnes) in the period 1990-2015 (UBA, 2017).

Emission source categories	1990	1995	2000	2005	2010	2015
Total Emissions	34.85	19.84	17.83	13.68	10.89	9.09
1. Energy	26.45	11.31	9.67	8.84	8.53	7.09
A. Fuel Combustion	26.45	11.31	9.67	8.84	8.53	7.09
1. Energy Industries	19.04	9.33	8.24	7.62	7.17	5.94
2. Manufacturing Industries and Construction	5.23	0.73	0.37	0.33	0.33	0.34
3. Transport	0.45	0.49	0.50	0.45	0.43	0.44
<i>thereof Road transportation</i>	0.43	0.47	0.49	0.44	0.42	0.43
4. Other Sectors	1.72	0.76	0.55	0.44	0.59	0.36
<i>thereof Commercial/Institutional</i>	0.28	0.15	0.09	0.05	0.06	0.02
<i>thereof Residential</i>	1.36	0.59	0.44	0.38	0.50	0.32
5. Other (military)	0.01	0.00	0.00	0.00	0.00	0.00
B. Fugitive Emissions from fuels						
1. Solid Fuels						
2. Oil and Natural Gas						
2. Industry	8.39	8.50	8.13	4.8	2.32	1.96
A. Mineral Industry	0.83	0.72	0.79	0.74	0.65	0.58
B. Chemical Industry	3.01	2.94	1.85	1.14	0.60	0.35
C. Metal Industry	4.55	4.84	5.49	2.91	1.07	1.02
D. Non-energy Products from Fuels						
G. Other Product Manufacture and Use	0.00	0.00	0.00	0.00	0.00	0.00
H. Other (Pulp & Paper, Food)						
I. Wood Processing						
K. Consumption of POPs and Heavy Metals						
3. Agriculture						
B. Manure Management						
D. Agricultural Soils						
5. Waste	0.02	0.03	0.03	0.03	0.04	0.05
C. Waste Incineration	0.02	0.03	0.03	0.03	0.04	0.05

Figure 31: Reported and expert emission estimates for Germany (source: EMEP, 2015).



The official emissions for Europe are lower than most scientific studies report (Figure 31). Pacyna et al. (2006) report almost twice as much mercury emissions within Europe, leading to EMEP expert emissions twice as high as the official reporting (EMEP, 2015).

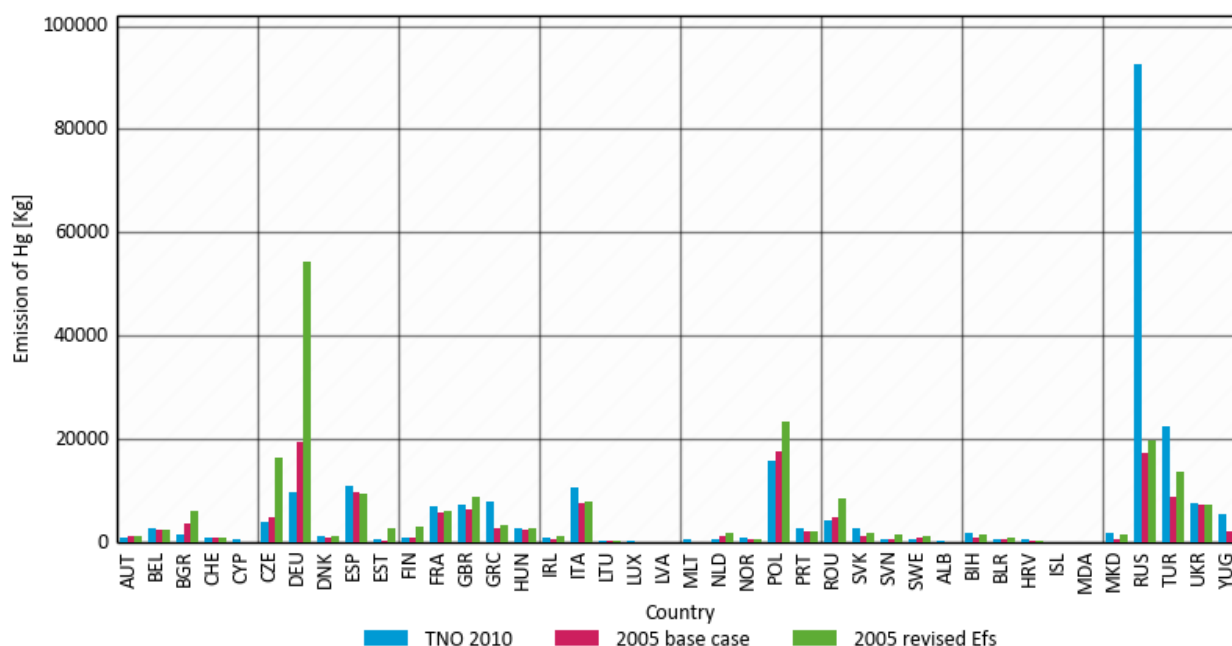
Coal-fired power plants are a major source of mercury emissions in Europe. For Poland, Zyśk et al. (2011) reported revised emission factors for mercury emissions from coal combustion based on measurements in Polish power plants. The conclusion was that current emission factors were heavily underestimating the emissions especially when using brown coal (see Table 15). Within the EnerGEO project it was investigated what the impact on European mercury emissions would be if the emission factors reported by Zyśk et al. (2011) would be applied to all coal-fired power plants in Europe (Figure 32). The 2005 base case emissions were taken from the GAINS model as reported in Rafaj et al., 2014. The impact of the adapted emission factors is huge for countries with a large use of brown coal. For Germany and Czech Republic the emissions would increase manifold. For Poland the impact is about 40% higher emissions with the new factors. It needs to be mentioned here that the application of the revised emission factors to all countries may not be appropriate. These emission factors of Zyśk et al. (2011) were generated for Poland, taking into account the technology and control strategies used in Polish power plants. For instance in Germany, emission control measures are likely to be more stringent leading to lower emissions. Hence, the comparison should be seen as an indication that the uncertainty in the (brown) coal emission factors is a key factor to determine the national emissions of Germany. It should be also mentioned, that in Germany many measurement data is available. Several coal fired plants measure continuously, many power plants provide annual data based on single measurements. This could mean that uncertainties around mercury emissions in Germany are lower than in other countries and for other heavy metals.

Based on these studies we rate the uncertainty in European emissions to be a factor 2.

Table 15: Emission factors from IIASA and Zyśk et al. (2011) for Hg (kg.PJ⁻¹)

	IIASA (implied emission factor)	Zyśk et al., 2011
Hard coal	1.6	4.1
Brown coal	5.3	27.7

Figure 32: Mercury emissions by country according to several emission databases. Efs = emission factors. Source: this work



Gridded emission data for Europe are provided by the (EMEP) program as well as by TNO. EMEP yearly emission fluxes are provided with a horizontal resolution of approximately 50 x 50 km based on emission data reported by the membership countries. In the near future enhanced resolution is expected to become available. TNO prepared an emission inventory with a horizontal resolution of approximately 7 x 7 km (Visschedijk et al., 2010). The location and emission of 3977 main point sources were provided. Additionally the Standardized Nomenclature for Air Pollutants (SNAP) categories of emission sources are specified. Although these data are available many regional modelling studies currently still use the AMAP mercury emission inventory (Pacyna et al. 2005) for the year 2000 (<http://amap.no/Resources/HgEmissions/>). Hence, many modelling groups are not aware of the improved emission database presented above.

Non-combustion processes emit Hg as GEM, but combustion processes (including fuel use, waste incineration, open fires) emit about half of their Hg as GOM and BPM. This partitioning of emissions is of considerable importance because the emitted GOM can be deposited regionally downwind of the source, resulting in a local deposition enhancement in contrast to the global influence associated with emissions of GEM. Emission inventories also generally include a particulate component of mercury (BPM) in addition to GEM and GOM. BPM is best viewed as part of GOM, with gas-particle partitioning of GOM occurring in the atmosphere on the basis of local particle concentrations and temperature.

The speciation of mercury emitted from coal-fired power plants to atmosphere depends on coal characteristics (e.g. chlorine, sulphur content), combustion temperature, type of installed post-combustion controls and flue gas cooling rate in the pathway from boiler to the stack. Table 16 provides an overview of speciation information based on stack measurements. In the stack about 60 % of the Hg is present as GEM and 40 % as GOM+PBM. Coal combustion tends to have slightly more GOM than average, whereas cement and metal production emit more GEM than average.

Note that in models GOM needs to be specified into different components. It seems most authors take the easiest assumption and are equally distributed into the following mercury compounds: HgBr₂, HgO, HgCl₂ and Hg(OH)₂.

It needs to be mentioned here that it is currently debated that a considerable in-plume reduction takes place after emission converting GOM into GEM downwind of the stack (see below).

Table 16: Specific splitting factors of total mercury into its main forms – literature review

Reference	Hg form	General [%]	SNAP categories [%]										
			01	02	03	04	05	06	07	08	09	10	11
(Pacyna et al., 2006a)	GEM	61	50	50	80	73					25		80
	GOM	32	40	40	17	24					58		13
	PBM	7	10	10	3	3					17		7
(Zyśk et al., 2011)	GEM		75										
	GOM		20										
	PBM		5										
(Ryaboshapko and Korolev, 1997)	GEM	57											
	GOM	30											
	PBM	13											
(Lindqvist et al., 1991)	GEM		50								20		
	GOM		30								60		
	PBM		20								20		
(AMAP/UNEP, 2008)	GEM		50	50	80	80					20		80
	GOM		40	40	15	15					60		15
	PBM		10	10	5	5					20		5
Proposed factors	GEM	60	50	50	80	80					20		80
	GOM	33	40	40	15	15					60		15
	PBM	7	10	10	5	5					20		5

3.3.2 Atmospheric transformation processes

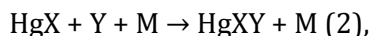
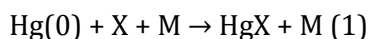
Mercury cycling between different environmental compartments depends on the dynamic of chemical and physical processes (oxidation, dry deposition, wet scavenging) which influence its transport and residence time in the global environment. In this chapter we summarize the processes that determine the fate of mercury in the atmosphere.

There is considerable uncertainty regarding the atmospheric redox chemistry of Hg. Until about 20 years ago, the conventional view based on experiments and expressed in atmospheric models was that oxidation of Hg(0) would principally occur by OH and O₃, and that reduction of Hg(II) would occur by reaction with HO₂ (aq) in clouds. However, recent laboratory experiments and thermodynamic and kinetic constraints indicate that these reactions are unlikely to be significant in the atmosphere (Schroeder and Munthe, 1998). Still, observations of a weak summer minimum in Hg(0) concentrations at northern mid-latitudes are consistent with a photochemical sink.

Holmes et al. (2010) suggested that Br atoms could provide the dominant global atmospheric oxidant for Hg(0). Known sources of Br atoms to the troposphere include photolysis and oxidation of bromoform (CHBr₃), dimethylbromide (CH₂Br₂), and methyl bromide (CH₃Br), as well as debromination of sea salt aerosol. CHBr₃ and CH₂Br₂ are emitted from the marine biosphere, while CH₃Br has both biogenic and anthropogenic sources. The Bromine chemistry is well established from earlier studies of stratospheric chemistry. Consensus is growing that homogeneous reactions with atomic bromine and bromine containing radicals are the most important atmospheric oxidation processes even at mid-latitudes and not just in the Arctic (Holmes et al., 2010; Obrist et al., 2011).

3.3.2.1 Oxidation

Halogen atoms are important oxidants for Hg(0) in the atmosphere because the overall oxidation reactions are exothermic, involving a two-step process:



where $\text{X} \equiv \text{Cl}, \text{Br}, \text{I}$ is a halogen atom and Y is another radical, either a halogen atom or another species such as OH, OH₂, or NO₂. Cl could thus also be a particularly efficient oxidant, but its tropospheric concentration is low because reaction with methane results in stable HCl.

Hence, modelling the oxidation of mercury requires to model the halogen cycles and sea salt. Many regional model systems for mercury (e.g. polyphemus) do not incorporate these processes, but rather prescribe concentrations (at ppt level). Note that many CTMs that currently are used for Hg modelling include the oxidation pathways with OH and O₃. For example, Gencarelli et al. (2015) conclude that the oxidation of Hg(0) in their implementation in WRF-CHEM is too fast.

The aqueous oxidation of mercury by halogen compounds in the atmosphere is less well understood, as are the reactions that reduce oxidized mercury compounds, although it is generally agreed that reduction occurs predominantly in the water phase, two recent reviews by Subir et al. (2011, 2012) give a thorough overview of some of the uncertainties in atmospheric mercury chemistry.

3.3.2.2 Reduction

Slow reduction reactions of Hg(II) to Hg(0) are incorporated in the chemistry schemes. There is some evidence for rapid Hg(II) reduction taking place in power plant plumes. Atmospheric observations in plumes and in polluted regions show much lower Hg(II)/Hg(0) concentration ratios than inferred from emission inventories (Amos et al., 2012; Edgerton et al., 2006; Lohman et al., 2006) and observed atmospheric deposition patterns do not show the regional enhancements that would be expected from power plant Hg(II) emissions (Zhang et al., 2012). In addition, Edgerton et al. (2006) observed that Hg(0) accounted for about 84% of total mercury emissions from power plant plumes at three surface sites. Therefore, Zhang et al. (2012) substituted an 86.5 : 9.9 : 3.6 (Hg(0) : Hg(II) : Hg(P)) speciation for the 50 : 40 : 10 speciation used for fossil fuel combustion, which comprised 46% of the total anthropogenic emissions in the inventory from Pacyna et al. (2010), and demonstrated significant improvements of their in-plume reduction simulations while comparing with the mercury concentrations observed at 19 surface sites and wet deposition observed at US sites. In a recent study, Kos et al. (2013) observed large improvements in model performance, both for concentration and wet deposition, by reducing the amount of GOM emissions from power plants even further from 40 to 2 %.

In case the in-plume reduction is actually important as suggested here, the nature of mercury pollution would be increasingly global, with much lower gradients between source regions and natural areas than previously assumed.

3.3.2.3 Mercury partitioning between aerosol and gas phase

Observations of RGM and Hg(p) suggest that Hg(II) behaves as a semivolatile compound, partitioning between the gas and aerosol phases in a manner dependent on local aerosol concentration and composition and ambient temperature.129,130 As limiting cases, Hg(II) is mainly in the gas phase in warm environments with low aerosols and mainly in the particle phase in cold environments with high aerosols. Efficient uptake of Hg(II) by sea salt particles makes sea salt deposition a major process for delivery of Hg to the surface ocean.

Recently, modelling systems such as GEOS-CHEM and GLEMOS have updated their schemes to include an empirically derived parameterization of the gas-particle partitioning developed by Amos et al. [2012].

In the literature a dry deposition parameterization with parameters for GEM is presented by Zhang et al. (2009), although some authors neglect it (Gencarelli et al., 2014).

Dry deposition of PBM depends on particle size, being slow for submicrometer particles but fast for supermicrometer particles. Observations indicate that PBM in continental air is mostly in the submicrometer size range, while PBM in marine air is mostly in the supermicrometer size range of sea salt particles (Malcolm et al., 2003). The process description for particle deposition are incorporated in every chemistry transport model and dry deposition velocities can be assumed to be the same as those for other metals (fine and coarse mode). In many models, e.g. LOTOS-EUROS, the scheme of Zhang et al. (2001) is used.

Assuming that GOM and PBM act as nitric acid and fine aerosol we can take the typical dry deposition velocities from the PINETI project. For Germany these are about 1.6 cm/s and 0.16 cm/s for forest, respectively. For lower vegetation the values are lower, but the relative behavior between GOM and PBM remains the same (Table 17). The phase partitioning of GOM thus has important implications for removal by deposition. Efficient uptake of GOM by sea salt particles may cause sea salt deposition to be a major process for input of Hg to coastal ecosystems.

Estimated annual Vd for GEM mostly range between 0.05–0.08 cm s⁻¹ over vegetated surfaces and below 0.05 cm s⁻¹ over urban areas, which is generally 20–30 times smaller than those of GOM, and 2–6 times smaller than PBM (Zhang et al., 2012).

Table 17: Estimated effective and average dry deposition velocities for GOM and PBM based on Schaap et al. (2015).

Vd [cm/s]	GOM		PBM	
	Eff	Ave	Eff	Ave
ara	1.20	1.04	0.08	0.09
cnf	1.63	1.52	0.16	0.20
dec	1.63	1.52	0.16	0.20
grs	1.11	0.98	0.07	0.08
oth	0.89	0.81	0.04	0.04
crp	1.42	1.22	0.10	0.11
sem	1.24	1.08	0.10	0.12
wat	0.67	0.62	0.08	0.09
urb	2.94	2.58	0.14	0.17
mix	1.63	1.52	0.16	0.20

In chemical transport models, the approach for the calculation of the dry deposition velocities of GEM, GOM, and PBM varies between models. For example, in GRAHM (Dastoor et al., 2015), GEOS-Chem (Song et al., 2015), ECHMERIT (De Simone et al., 2014), and GNAQPMS-Hg (Chen et al., 2015), the dry deposition velocity for GEM is calculated using the multiple resistance analogy approach described in Wesely (1989), Zhang et al. (2003) or Kerkweg et al. (2006). Due to uncertainties presented in Zhang et al. (2009), ECHMERIT sets a maximum allowed Vd for GEM of 0.03 cm s⁻¹ equal to the annual mean GEM deposition velocity from Selin et al. (2008). Assumed values of 0.01 cm s⁻¹ over land and 0 cm s⁻¹ over the ocean for the dry deposition velocity of GEM have been implemented in CTM-Hg (Seigneur et al., 2004). In the case of many regional models, GEM is still not considered in the simulations under the assumption that the dry deposition of GEM is not important considering it is also emitted from the surface, for example WRF/Chem-Hg (Gencarelli et al., 2015), TEAM (Seigneur et al., 2006), REMSAD

(Bullock et al., 2008), and CAMx (De Foy et al., 2014). CMAQ has implemented the bi-directional scheme of Bash (2010) for its treatment of GEM (Bash et al., 2014). No wonder, model intercomparison studies show differences of a factor 2-10 between model estimates (Travnikov et al., 2010; Ryaboshapko et al., 2007b).

3.4 Atmospheric mercury levels in Germany

3.4.1 Atmospheric concentration levels

Background atmospheric concentrations of elemental mercury typically range from 1.3 to 1.7 ng m⁻³ in the Northern Hemisphere, whereas concentration levels are about 30% less in the southern hemisphere (Figure 34). Measured GEM concentrations in Germany are at the higher end of the northern hemispheric range. GOM+PBM concentrations are typically a factor 100-200 lower than GEM, as illustrated for Waldhof in Table 18. At Waldhof 11.2 pg/m GOM+PBM is measured with most of the reactive mercury in the form of PBM.

Figure 34: Mercury concentrations in air (left; ng/m³) and precipitation (right; ng/L) from the EMEP network (www.emep.int).

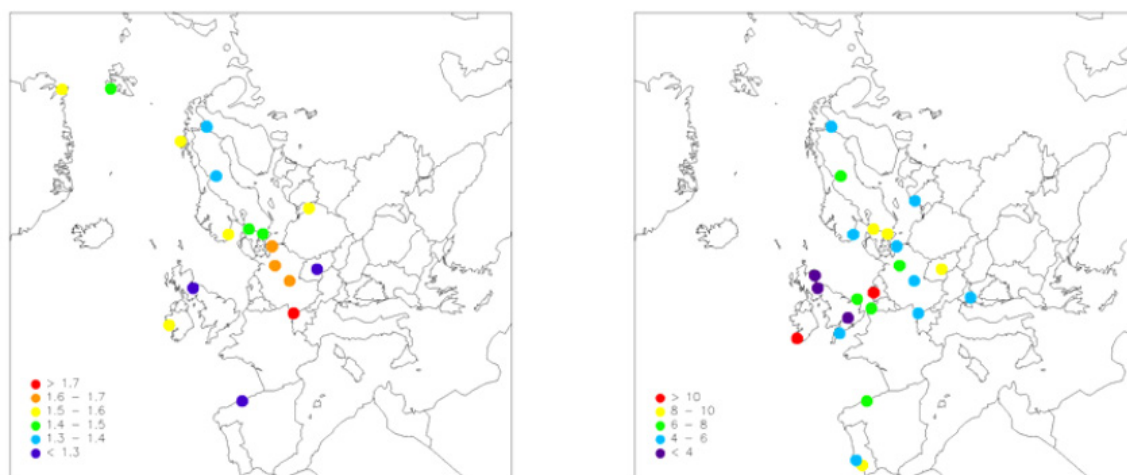


Table 18: Mercury levels (pg/m³) for 2009-2011 at Waldhof (Weigelt et al., 2013).

Station	Period	GEM	GOM	PBM
Waldhof - mean	2009-2011	1.7e3	1.6	9.6
Waldhof - median	2009-2011	1.6e3	0.6	6.2

3.4.2 Dry deposition

Dry deposition of Hg has been estimated using surrogate surface measurements (e.g. Huang et al., 2012), micrometeorological measurements (e.g. Lindberg et al., 1998), litterfall and throughfall measurements (e.g. Demers et al., 2007), and the inferential method (e.g. Lyman et al., 2007). Due to the constant cycling of Hg between different atmosphere-surface media, as well as technological limitations, direct measurements of dry deposition are difficult and subject to larger errors (Zhang et al., 2009; Huang et al., 2012). It is believed that the uncertainties in dry deposition estimates are larger than those in wet deposition estimates (Lindberg et al., 2007).

Table 19: Estimates of mercury deposition to forest and grassland in the surrounding of Waldhof.

	GEM		GOM		PBM	
	Grass	Forest	Grass	Forest	Grass	Forest
Concentration (pg/m ³)	1610	1610	1	1	6.3	6.3
Vd (cm/s)	0.03	0.07	1.1	1.6	0.07	0.16
Flux (ug/m ²)	15.2	35.5	0.3	0.5	0.1	0.3

In most studies, dry deposition of GOM has been estimated to be much higher than PBM due to the much higher deposition velocities of GOM than PBM (Huang et al., 2012; Zhang et al., 2012). In contrast, for Waldhof they appear to be almost equal (Table 19), which may be due to the distance to sources and the partitioning of GOM and PBM, favoring the latter.

Zhang et al (2012) estimated dry deposition of mercury for the year 2008–2009 at 19 monitoring locations in eastern and central North America. Annual dry deposition of GOM+PBM was estimated to be in the range of 0.4 to 8.1 $\mu\text{g m}^{-2}$ at these locations with GOM deposition being mostly five to ten times higher than PBM deposition, due to their different modeled Vd values. Annual average concentrations among the sites during 2008–2009 ranged from 1.1 to 22.6 pg m^{-3} for GOM, 2.9 to 17.1 pg m^{-3} for PBM, and 1.2 to 2.1 ng m^{-3} for GEM. As expected, the species having the shortest lifetimes (i.e. GOM) had the largest geographical variations. The Waldhof estimates are at the low edge of the range, particularly due to the comparably low GOM concentrations.

GOM and PBM concentrations and dry deposition fluxes have been observed to be 5-10-20 times greater at urban and industrial sites due to the close proximity to, or downwind from, point source emissions (Sakata and Marumoto, 2005; Liu et al., 2007; Sakata and Asakura, 2008; Fang et al., 2012a; Huang et al., 2012; Sather et al., 2014) than at rural sites (Sakata and Marumoto, 2005; Sakata and Asakura, 2008; Castro et al., 2012; Sather et al., 2014). Hence, the estimates for Waldhof should be multiplied by a factor of at least 5 to arrive at dry deposition estimates for source areas.

Net annual GEM dry deposition Zhang et al. (2012) estimated to be in the range of 5 to 26 $\mu\text{g m}^{-2}$ at 18 sites, which is much higher than originally assumed in many previous studies. Earlier studies either simply excluded GEM in the dry deposition budget or used extremely small Vd values (Engle et al., 2010; Baker and Bash, 2012). The high dry deposition fluxes of GEM are certainly due to the two to three orders of magnitude higher concentrations of GEM compared to those of GOM+PBM. The much higher litterfall mercury than GOM plus PBM dry deposition suggests the important contribution of gaseous elemental mercury (GEM) to mercury dry deposition to vegetated canopies. (Wright et al., 2016).

As discussed in Zhang et al. (2012), GEM re-emission is normally around half of the GEM dry deposition on regional scales in eastern North America, although the relative importance of re-emission/dry deposition varied significantly with location. Applying the same factor to Waldhof still indicates that the GEM input is the highest one.

Dry deposition is often assumed to be less important than wet deposition since earlier studies only estimated GOM and PBM dry deposition. Given the data below one can see that the new assumptions on GEM deposition make dry deposition the larger term.

3.4.3 Wet deposition of mercury

Wet deposition of mercury is due to rain out of Hg(p) and Hg(II) as elementary mercury is not water soluble.

Long time series of mercury concentrations in precipitation exist at 4 sites in Germany. As for many sites in Europe, the mercury concentration data do not show a trend since the mid-nineties. Hence, we have averaged the Hg-concentration in rain water to obtain typical concentration values for background conditions. The obtained values range between 9 and 13 ng/L at the four locations (Table 20). Here we take 11 ng/L as a central value. Given the range of precipitation occurring in Germany (from 450 mm in eastern Germany to 1800 mm on the alpine range) a typical range of 5 – 20 ug/m² or g/Km² is obtained.

Only in the Ruhr area, with a higher density of sources for atmospheric Hg, a higher background is expected. The enhanced deposition across the Ruhr-area is found in all model results across Europe. Similarly, close to installations emitting mercury local enhancements above the mentioned range may be found.

Table 20: Mean Hg-concentration in precipitation at four locations in Germany (www.emep.int).

Station	Period	Conc (ng/L)
Schmücke	2007-2013	8.9
Schauinsland	2010-2013	10.9
Waldhof	2007-2012	10.5
Zingst	2003-2006	12.8

3.4.4 Total deposition estimate for Germany

The interpretation of the current literature study is provided in Table 21. Traditional studies provide only deposition estimates for reactive mercury. For background conditions we provide the dry deposition estimate for Waldhof combined with a typical wet deposition flux for Germany (10 µg/m²) resulting in an estimate of nearly 11 µg/m². Assuming that reactive mercury in source areas may be 10 times higher than observed in Waldhof we arrive at typical values of 14 and 18 µg/m² for grass and forests across Germany. In areas with large precipitation amounts the wet deposition could be higher. Although rain water concentrations typically decrease with increasing precipitation amounts, we feel the linear extrapolation is warranted as in areas with enhanced orographic precipitation. The reason is that in these areas also occult deposition could contribute considerably (Blackwell et al., 2015). Hence, in these areas the reactive mercury deposition could be up to 10 µg/m² higher.

Including the new insight that GEM contributes largely to dry deposition of mercury a contribution of 15-35 µg/m² is derived. Literature studies arrive at the conclusion that about 50% of this flux is re-emitted on average. Only for water surfaces the deposition is estimated to be much lower.

Table 21: Estimates of typical total deposition for reactive mercury in background and polluted conditions as well as GEM deposition for the German situation [$\mu\text{g}/\text{m}^2$].

	Background GOM+PBM		Polluted GOM+PBM		GEM	
	Grass	Forest	Grass	Forest	Grass	Forest
Dry	0.4	0.8	4	8	15	35
Wet	10	10	10	10	-	-
Total	10.4	10.8	14	18	15	35

3.5 Establishing the mercury input of two plants in Bavaria to the catchments of the Isar and Salzach.

To be able to develop mitigation strategies for the improvement of water quality a modelling framework for the budget of pollutants across a catchment is necessary. Within Germany the MoRE (Modelling of Regionalized Emissions) system is used to quantify the pollutant input to surface waters. The MoRE system (Fuchs et al., 2010) comprises approaches for different input pathways: municipal wastewater treatment plants, industrial direct dischargers and emissions of historic mining for pathways related to point sources and the following pathways related to diffuse sources: sewer systems, surface runoff, erosion, groundwater, tile drainage, direct atmospheric deposition onto water surfaces and inland navigation. In addition to the modelling of inputs into the water bodies an estimation of the river load is carried out to verify the model results.

Atmospheric deposition is a significant source of mercury (and other metals) in a river basin. In this case study the aim was to quantify in how far regional emission source contribute to the mercury deposition in a catchment area and in how far the estimates provided above are in line with the current atmospheric input data of the MoRe system. During this study the Isar and Salzach catchments were selected as for these catchments more detailed measurement data on the water concentrations of mercury were available. To this end a cooperation with Karlsruher Institut für Technik (KIT) was established. As a case study indicative calculations were performed to generate a first estimate of the regional deposition of two power plants in Bavaria and the results are combined with the empirical findings described above.

In the following sections the case study is detailed further.

3.5.1 Plants under consideration

To estimate the deposition of mercury for the Salzach region, we examined the TNO and E-PRTR emission inventories for mercury emission sources in Bavaria. The E-PRTR data include the points for the reportings for 2007, 2011 and 2013, whereas the TNO-inventory is representative for 2005. In the TNO inventory there are a few point sources near Burghausen, located at the Salzach. Within the E-PRTR-2007 these are not present, but a few source appear at sites located only 8 km away. However, these point sources disappear in E-PRTR2011 and 2013 and are presumably not present anymore. Looking at additional emission sources we noticed substantial differences between TNO-2005 and E-PRTR, but as well year to year differences in E-PRTR (comparing 2007, 2011 and 2013). We therefore used E-PRTR emission estimates for two locations, which are relatively high and are present in the reporting for 2007, 2011 and 2013. In vicinity of the Salzach, we did not find sources that fulfil these criteria. Hence, two emission source in the Munich areas were chosen to perform the local scale modelling. The two sources are the SWM Heizkraftwerk Nord in Munich and the GDF SUEZ Standort Kraftwerk in Zolling. The reported Hg emissions for these locations are listed in Table 22; pictures of the locations are shown in Figures 35 and 36.

Table 22: Reported mercury emissions (kg/yr) for the two selected point sources in Bavaria.

Point Source	Location	2007	2011	2013
SWM Heizkraftwerk Nord	München	32	62	40
GDF SUEZ Standort Kraftwerk	Zolling	148	42	11

Figure 35: Google earth picture of SWM Heizkraftwerk Nord

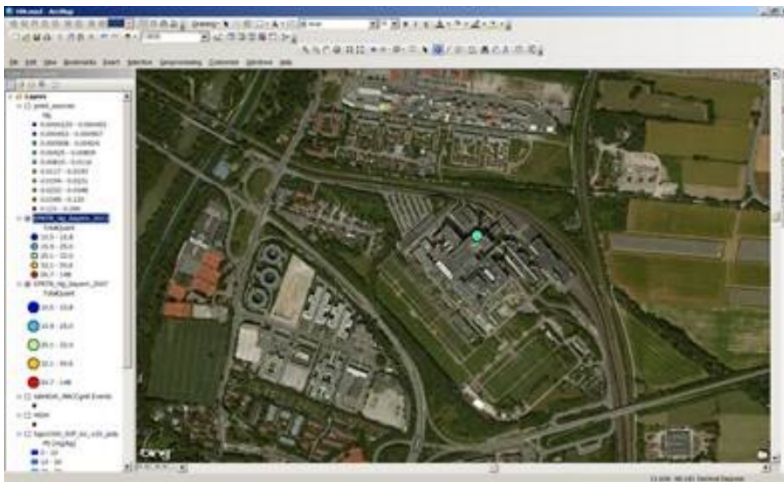


Figure 36: Google earth picture of GDF SUEZ Kraftwerk

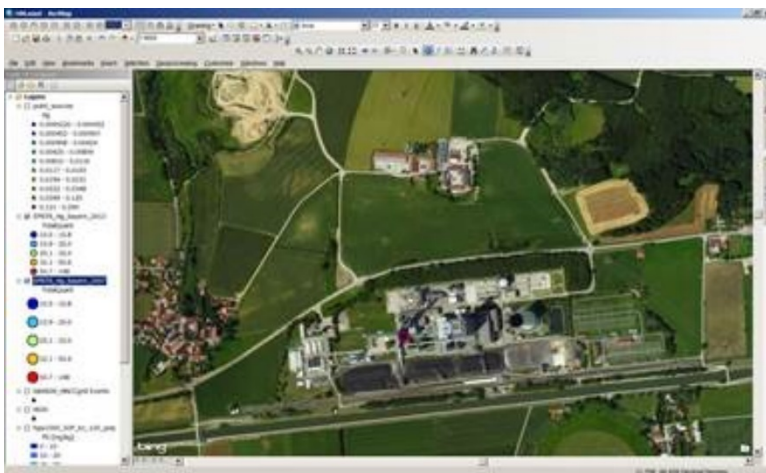
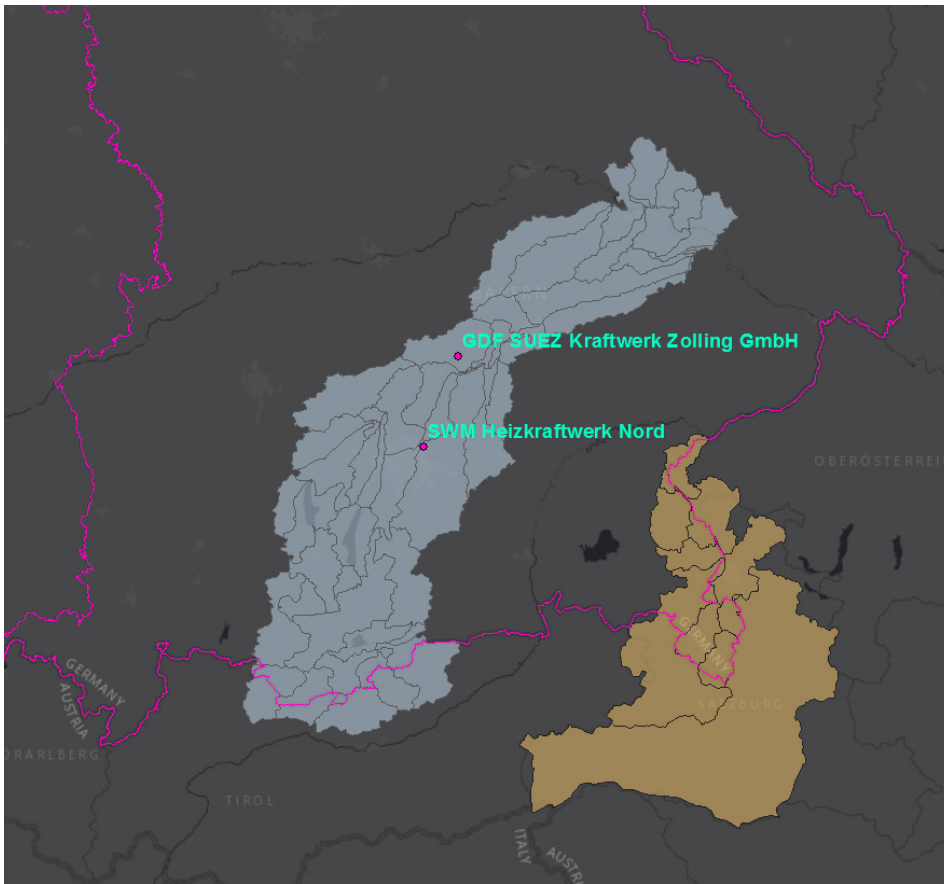


Figure 37: Locations of Kraftwerk Zolling and Heizkraftwerk Nord. In pink : the German Länder borders; light grey: the Isar area, brown: the Salzach area. Source: this project.



3.5.2 Local scale dispersion calculations

Dispersion over spatial scale scales up to 10 km can be modelled with a Gaussian Plume model. The Gaussian plume formulation gives a direct relation between the emission, the wind speed and the atmospheric stability (van Ham and Pulles, 1998):

$$C_p = \frac{q}{2\pi \cdot \sigma_x \cdot \sigma_y \cdot u} e^{-\frac{y^2}{2\sigma_y^2}} \cdot \left(e^{-\frac{(z-h)^2}{2\sigma_z^2}} - e^{-\frac{(z+h)^2}{2\sigma_z^2}} \right)$$

With

C_p	concentration contribution	$\mu\text{g}/\text{m}^3$
q	emission strength	$\mu\text{g}\cdot\text{s}^{-1}$
$\sigma_{y,z}$	stability dependent plume width (horizontal or vertical)	m
y	horizontal distance off plume axis	m
z	receptor height	m
h	source height	m
u	wind vector	m/s

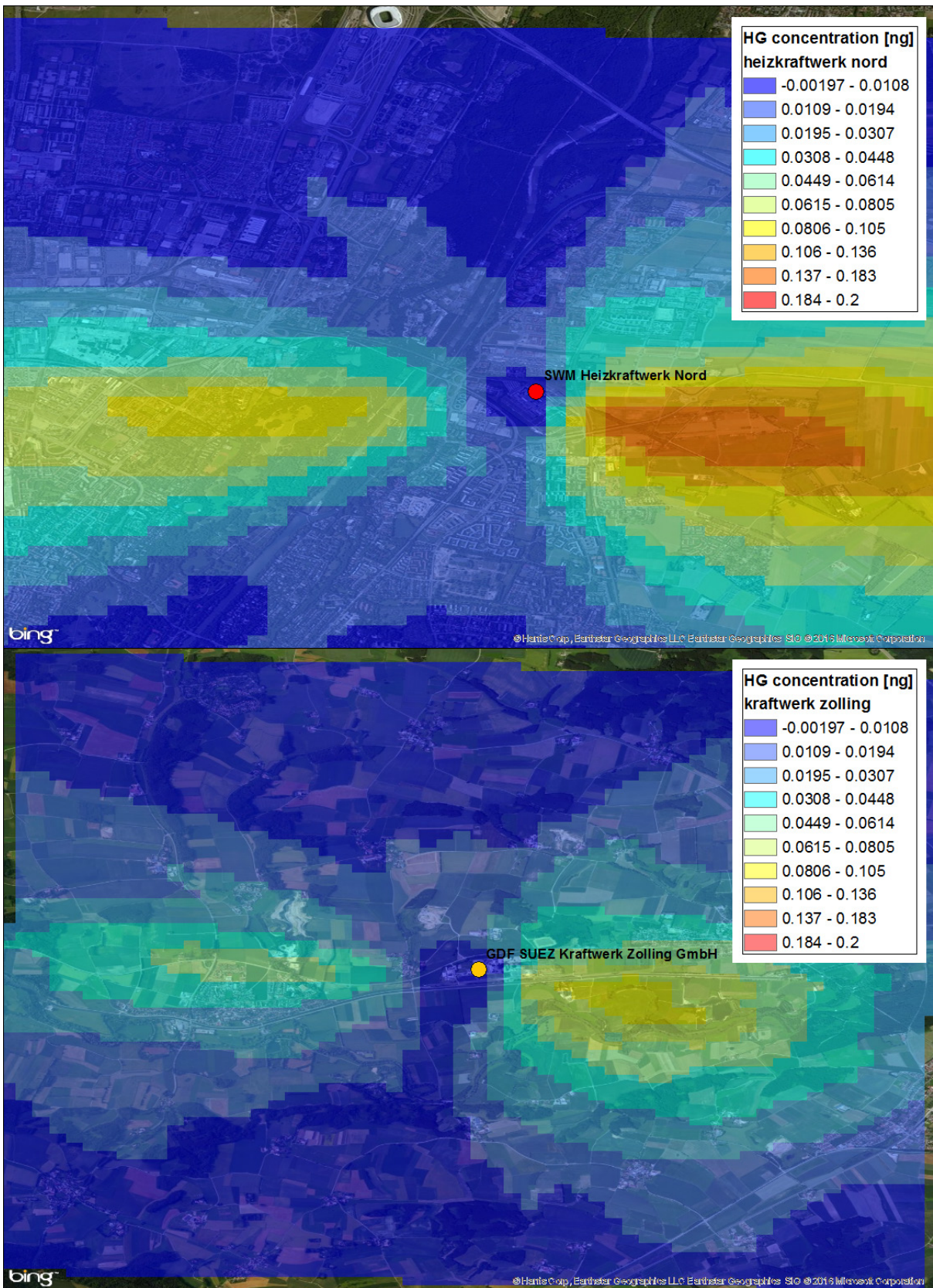
When the dispersion from stack emission is modelled, the source height is increased due to plume rise¹. The plume rise results from the relative heat of the plume compared to its direct surrounding. Plumes from fossil fuel-fired power stations very often have a significant plume rise.

For the modelling of the local Hg increments resulting from the power plants Kraftwerk Zolling and Heizkraftwerk Nord (see Figure 37) we used the Gaussian plume model. Meteorological data ($\sigma_{y,z}$ and u) were taken from the ECMWF model to be consistent with the regional scale modelling. The emission strength was taken as listed in the EPRTR 2011 registration for Kraftwerk Zolling (42kg/yr) and Heizkraftwerk Nord (62kg/yr). For the exploratory calculation the central value (293m) of the SNAP code dependent height distribution as applied in the EMEP model was taken. This height includes the average plume rise due to the heat output. For the receptor height the default value of 1.5 m was taken.

The resulting concentration distribution for total mercury is shown in Figure 38. The modelled distributions clearly show that the dominating wind directions are either easterly or westerly flows. Hence, in these directions the maxima are found. For SWM Heizkraftwerk Nord the additional Hg concentration within 10 Km east of the plant is up to 180 pg/m³. Assuming that roughly 50% is emitted as reactive primary mercury the additional concentration is up to 10 times higher than the background measured at Waldhof. The difference between the sites scales roughly with the emission amount. These calculations confirm the concentration ranges found in source areas in literature.

¹ This is an approach to include plume rise in Gaussian modelling.

Figure 38: Local scale dispersion modelling results (source: this work)

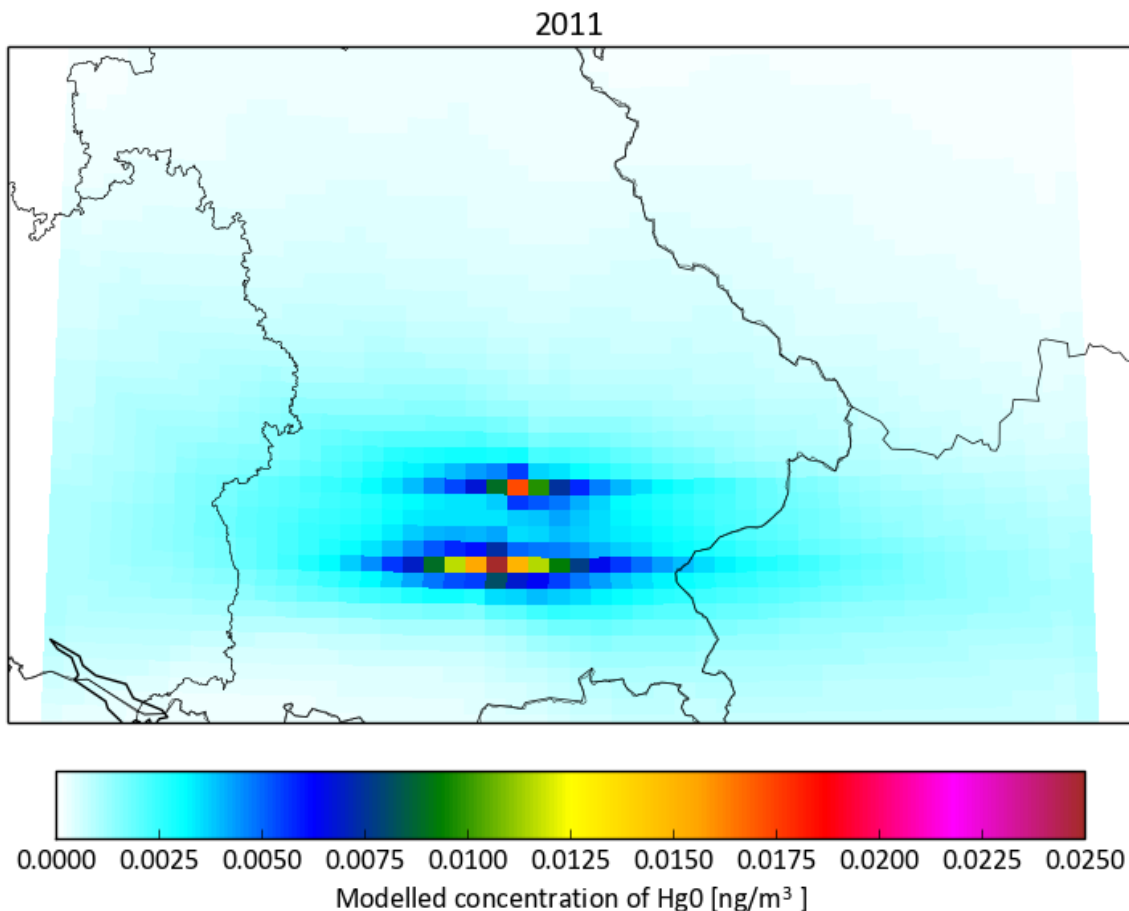


3.5.3 Regional calculation with LOTOS-EUROS

As a next step a simple simulation was performed using the LOTOS-EUROS model at 7x7 km resolution to provide an overview of the large scale dispersion. The LOTOS-EUROS model does not incorporate mercury chemistry, so the calculations were performed taking gaseous elemental mercury into account as a passive tracer. In addition, half of the mercury was emitted as reactive mercury and given the same deposition properties as fine mode aerosol. Due to the simple nature of the simulation we emphasize that this calculation should be considered to be indicative.

The modelled mercury distribution is shown in Figure 39. As the dominant wind origin is from west and east the distribution shows a larger transport in these directions. Within 25 km from the plants more than 10 pg/m³ is modelled which is more than a doubling of the background concentration at Waldhof. Note that due to artificial dilution within the grid cell of emission, the near source concentrations are much lower than computed with the Gaussian plume model. Given the dominant east-west dispersion and the north-south orientation of the catchments large parts of the catchments do not show enhanced mercury concentration levels.

As a next step we simply averaged the modelled concentration and deposition values over the catchment areas. Atmospheric surface concentrations of reactive mercury induced by the plants are on average 1.1 and 0.35 pg/m³ in the Isar and Salzach catchment areas. These are in the order of 10% and 2% of the surface concentration on average, which hints at similar contributions to the dry deposition. Modelled total deposition from the two plants arrives at about 1.1 ug/m²/yr and 0.5 ug/m²/yr for Isar and Salzach, respectively. These estimates are in the order of 7 and 3 % above the background values, respectively.

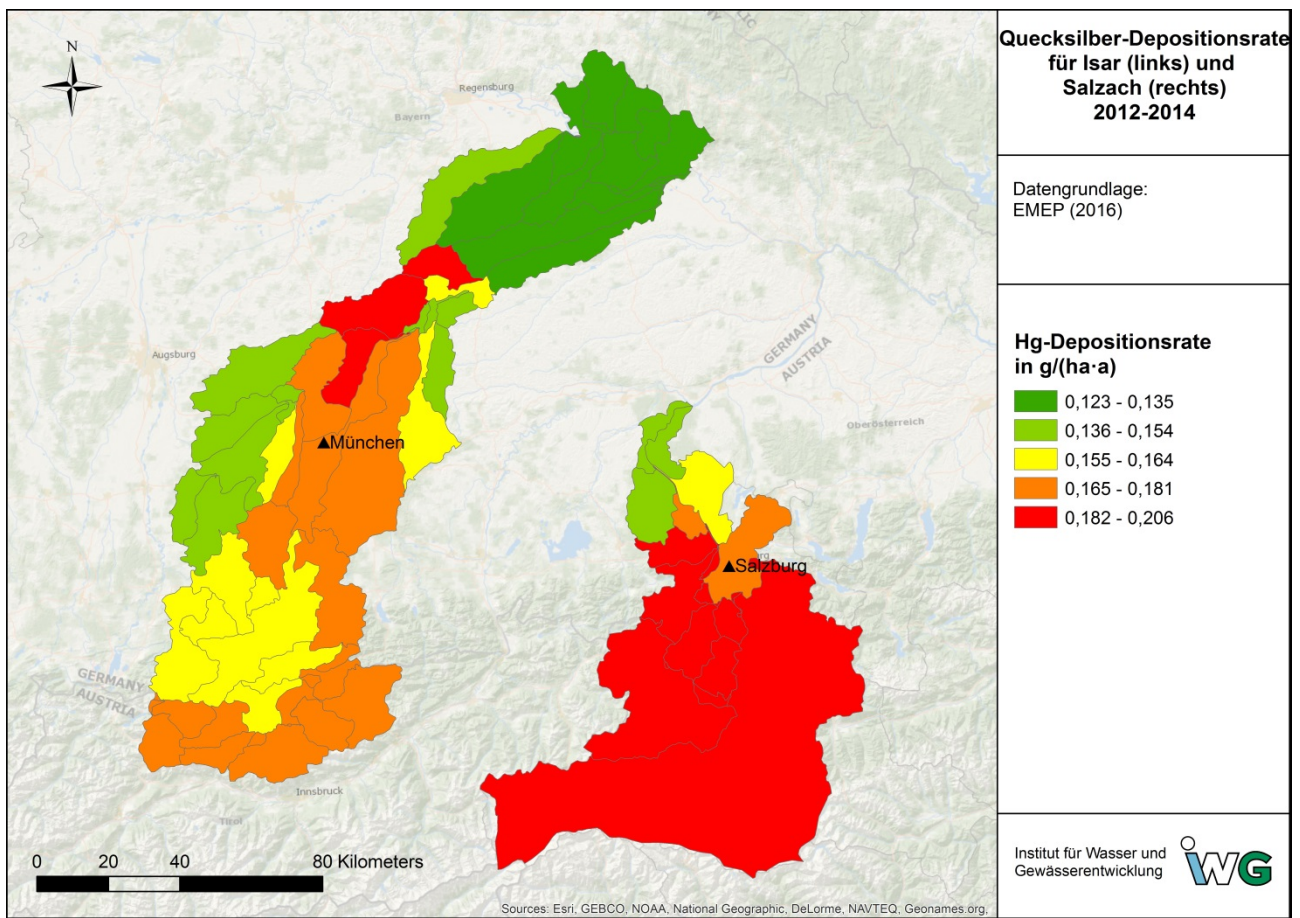
Figure 39: Modelled mercury concentrations (ng/m³) with LOTOS-EUROS.

3.5.4 Comparison to deposition estimates used in MoRe for Salsach and Isar

The atmospheric mercury deposition distribution currently used in the MoRe system are derived from the EMEP-MSC-East model results for 2012-2013 (www.emep.int). The EMEP model results are available in a 50 x 50 km resolution. The EMEP deposition values were matched to the MoRe areas using a simple area dependent averaging. The range of deposition fluxes obtained for the Isar and Salsach basins is between 0.12 and 0.21 g/(ha·yr), see Figure 40. This translates to a range between 12 and 21 $\mu\text{g}/\text{m}^2/\text{yr}$. The total deposition counts 174 kg/yr for the Isar catchment and 130 kg/yr for the Salsach catchment.

The central estimation for background conditions as derived based on data at Waldhof fits very well to the depositions used within the MoRe modelling (Figure 40). The central value of 11 $\mu\text{g}/\text{m}^2/\text{yr}$ or 0.11 g/ha/yr is surprisingly almost the lower value in the mapped range. Taking into account that the precipitation amounts in the pre-alpine region are above average the higher modelled values by EMEP are defensible. Inspecting the resulting deposition distribution within the catchments shows that the variability is rather low, as anticipated given the 50x50 km resolution of the EMEP model. Given the importance of wet deposition we would expect that signal of the precipitation amounts should be clearly visible in the maps. Hence, as a first step we recommend to improve the spatial disaggregation of the EMEP deposition maps onto the MoRe units using high resolution precipitation maps. Ideally, one would expand the LOTOS-EUROS model with mercury to be able to perform higher resolution simulations across the full MoRe domain, which include Germany and the foreign parts of the river basins present inside Germany.

Figure 40: Mercury deposition rates as used within MoRe



3.6 Conclusions

Mercury is an element and is naturally occurring. Trace amounts of mercury are found in most plants, animals and soils. Almost all mercury compounds are toxic and can be dangerous at very low levels in both aquatic and terrestrial ecosystems. The atmosphere is the foremost transport pathway of Hg, whereas land and ocean processes play an important role in the redistribution of Hg in ecosystems. Once deposited to land or oceans, mercury can be converted by microorganisms to the extremely toxic methylmercury, and begins its rise in the food chain. This process of bioaccumulation, in living organisms, inflicting increasing levels of harm on higher order species such as predatory fish, birds and mammals is known as "biomagnification".

The temporal and spatial scales of Hg transport in the atmosphere and its transfer to aquatic and terrestrial ecosystems depend primarily on its chemical and physical forms. Following emission, gaseous elemental mercury (GEM) can be transported long distances before oxidation and removal by particle and gas-phase dry deposition or scavenging by precipitation. The atmospheric residence time of GEM is several months to a year. Mercury can therefore be transported and deposited to remote locations such as the Arctic and Antarctic. Gaseous oxidized mercury (GOM) and particulate bound mercury (PBM) have a shorter atmospheric residence time than GEM ranging from hours to days, and as a result are generally deposited locally or regionally.

Sources of Hg to the atmosphere can be from either primary natural and anthropogenic sources or can be due to reemission of deposited Hg (secondary emission). Overall, total global Hg emissions to the atmosphere range from 6500 to 8200 Mg yr⁻¹, of which 4600 to 5300 Mg yr⁻¹ are from natural processes and sources (primary geogenic plus secondary emissions). Primary anthropogenic sources release 1400–2900 Mg yr⁻¹ compared with primary natural (geogenic) inputs of 80–600 Mg yr⁻¹. Hence, roughly one-third of the mercury emissions to the atmosphere are of primary anthropogenic nature. Globally, energy production is the largest source for mercury, followed by gold mining activities, non-ferrous metal production and cement production. Other sources include combustion of waste and cremations. With an emission of 10 Mg Hg per year the German contribution to the global emission is about 0.5 % (relative to a central global estimate of 2000 Mg/yr). In the stack about 60 % of the Hg is present as elemental mercury and 40 % as reactive mercury (GOM+PBM). Hence, a large part of the emission occurs as a global pollutant. For the behaviour of reactive mercury a parallel with oxidized nitrogen, of which it is estimated that 30% of the German emission is deposited within the country, can be drawn. Applying this share to the reactive mercury emissions indicates that only about 15 % of the German emissions deposit on Germany territory.

There is considerable uncertainty regarding the atmospheric redox chemistry of mercury. Common understanding is that halogen atoms, most importantly bromine but also chlorine and iodine, are important oxidants for Hg(0) in the atmosphere. Hence, modelling the oxidation of mercury requires to model the halogen cycles and sea salt. Many regional model systems for mercury, however, do not incorporate these processes, but rather prescribe the halogen concentrations. The aqueous oxidation of mercury by halogen compounds in the atmosphere is less well understood, as are the reactions that reduce oxidized mercury compounds. Slow reduction reactions of Hg(II) to Hg(0) are incorporated in current chemistry schemes. However, there is appearing evidence for rapid Hg(II) reduction taking place in power plant plumes. Atmospheric observations in plumes and in polluted regions show much lower reactive to elemental concentration ratios than inferred from emission inventories, which could be explained by a fast reduction of reactive to elemental mercury. In case in-plume reduction is important, the nature of mercury pollution would be increasingly global, with much lower gradients between source regions and natural areas than previously assumed.

The removal from the atmosphere is mostly governed by the solubility of the different mercury forms. Wet deposition by rain provides an efficient sink for GOM as the components are very soluble in water. In addition, rain out is the primary loss process for particle bound mercury.

Elemental mercury is not soluble and therefore does not rain out. For dry deposition it is often assumed that GOM and PBM act as nitric acid and fine aerosol, respectively. For Germany typical dry deposition velocities are about 1.6 cm/s and 0.16 cm/s for forest, respectively. Estimated annual Vd for GEM mostly range between 0.05–0.08 cm s⁻¹ over vegetated surfaces and below 0.05 cm s⁻¹ over urban areas, which is generally 20–30 times smaller than those of GOM, and 2–6 times smaller than PBM.

Background atmospheric concentrations of elemental mercury typically range from 1.3 to 1.7 ng m⁻³ in the Northern Hemisphere, whereas concentration levels are about 30% less in the southern hemisphere. Measured GEM concentrations in Germany are at the higher end of the northern Hemispheric range. GOM+PBM concentrations are typically a factor 100-200 lower than GEM. For background conditions we provide a dry deposition estimate based on measurement at Waldhof of almost 1 µg/m²/a combined with a typical wet deposition flux for Germany of 10 µg/m²/a resulting in an estimate of nearly 11 µg/m²/a. Assuming that reactive mercury in source areas may be 10 times higher than observed in Waldhof we arrive at typical values of 14 and 18 µg/m²/a for grass and forests across Germany. Hence, only near sources the dry deposition process becomes important. Deposition of elemental mercury may be in the same order, but is assumed to partly be re-emitted.

Atmospheric deposition is a significant source of mercury in a catchment area. As a case study the regional deposition of two power plants in Bavaria was discussed with indicative calculations using the LOTOS-EUROS model and a local dispersion model. The dispersion model indicates that within the first ten kilometers from a large power plant an annual mean concentration can be up to 90 pg/m³, up to 10 times higher than the background measured at Waldhof. Atmospheric surface concentrations of reactive mercury induced by the plants are on average 1.1 and 0.35 pg/m³ in the Isar and Salzach catchment areas. These are in the order of 10% and 2% of the surface concentration on average, which hints at similar contributions to the dry and wet deposition. Modelled total deposition from the two plants arrives at about 1.1 ug/m²/yr and 0.5 ug/m²/yr for Isar and Salzach, respectively. These estimates are in the order of 7 and 3 % above the background values, respectively.

These results were compared to the MoRE model input which is derived from the EMEP model. The EMEP model provides an input of 174 kg/a for the catchment of the Isar and 130 kg/a for the Salzach catchment. The central estimation for background conditions as derived based on data at Waldhof fits very well to the depositions used within the MoRe modelling. The central value of 11 ug/m²/yr or 0.11 g/ha/yr is surprisingly the central value in the mapped range used in MoRE. The spatial disaggregation of the EMEP model results on 50x50 km resolution occurred via topology. Inspecting the resulting deposition distribution within the catchments shows that the variability is rather low. Given the importance of the wet deposition we would expect that signal of the precipitation amounts should be clearly visible in the distributions. Hence, we would advise to update the spatial disaggregation by using high resolution rain fall data in contrast to topology.

Recommendations

The assessment presented here assumed that primary fraction of reactive mercury is about 40%. However, there is appearing evidence for rapid reduction of reactive mercury to elemental mercury taking place in power plant plumes. In case this reduction is important it make mercury an even larger global issue. Hence, we recommend to perform an experimental study to the mercury speciation in a source region to assess if primary fraction of reactive mercury can be consolidated to be 40% or considerably less. It is advised to perform measurements at several sites at variable distance to a source region such as the Ruhr area and perform supporting modelling work to analyze the results. Potentially, dedicated flight campaign could be organized, although the limited data availability and high costs may favor a more traditional set-up.

To provide high resolution estimates of mercury deposition patterns we recommend to expand the LOTOS-EUROS model with the mercury cycle relevant for the regional scale.

This would enable to generate consistent distributions for mercury, cadmium and lead as well as nitrogen for Germany. Proper attention to the global scale modelling used for boundary conditions should be given.

On the 3rd of February, 2017, a small workshop with KIT was held to start a discussion on the quantification of the atmospheric deposition pathway in MoRe. At this workshop the availability of the deposition data for mercury and other metals was discussed. In general, the numbers used in MoRe are derived based on similar considerations as in this project. The availability of modelled distributions for a number of metals was welcomed as a potential improvement to include spatial differentiation. In addition, it was recognized that a number of easy adoptions, such as the use of high resolution precipitation maps in the spatial allocation could provide significant improvements. Hence, a systematic review of the deposition fields and identification of possible improvements was recommended. Finally, benzo-a-pyrene (BaP) was identified as a component for which the atmospheric deposition is highly relevant. It is recommended to include BaP in a future study as new atmospheric emission information is present. Note that for provision of atmospheric deposition data for metals and other components to MoRE the assessment domain should be extended beyond the German territory.

4 References

- AMAP/UNEP, (2008): Technical Background Report to the Global Atmospheric Mercury Assessment. Arctic Monitoring and Assessment Programme / UNEP Chemicals Branch. 159 pp. Online at: www.chem.unep.ch/mercury/Atmospheric_Emissions/Technical_background_report.pdf
- Amos, H.M., Jacob, D.J., Holmes, C.D., Fisher, J.A., Wang, Q., Yantosca, R.M., Corbitt, E.S., Galarneau, E., Rutter, A.P., Gustin, M.S., Steffen, A., Schauer, J.J., Graydon, J.A., St. Louis V.L., Talbot, R.W., Edgerton, E.S., Zhang, Y., Sunderland, E. M. (2012): Gas-particle partitioning of atmospheric Hg(II) and its effect on global mercury deposition, *Atmos. Chem. Phys.*, Vol. 12, pp. 591–603.
- Andersen, Z.J., Wahlin, P., Raaschou-Nielsen, O., Scheike, T., Loft, S., (2007): Ambient particle source apportionment and daily hospital admissions among children and elderly in Copenhagen, *Journal of Exposure Science and Environmental Epidemiology*, Vol. 17, pp. 625-636.
- Banzhaf, S., Schaap, M., Kranenburg, R., Manders, A.M.M., Segers, A.J., Visschedijk, A.J.H., Van Der Gon, H.A.C.D., Kuenen, J.J.P., Van Meijgaard, E., Van Ulft, L.H., Cofala, J., Builtjes, P.J.H., (2015): Dynamic model evaluation for secondary inorganic aerosol and its precursors over Europe between 1990 and 2009, *Geoscientific Model Development*, Vol. 8, No. 4, pp. 1047-1070.
- Becker K., Schroeter-Kermani C., Seiwert M. et al., (2013): German health-related environmental monitoring: Assessing time trends of the general population's exposure to heavy metals, *International Journal of Hygiene and Environmental Health* 2013, Vol. 216, No. 3, pp. 250-254.
- Bieser, J., De Simone, F., Gencarelli, C., Geyer, B., Hedgecock, I., Matthias, V., Travnikov, O., Weigelt, A., (2014): A diagnostic evaluation of modeled mercury wet depositions in Europe using atmospheric speciated high-resolution observations, *Environ. Sci. Pollut. Res.* 21, pp. 9995-10012.
- Beltman, J.B., Hendriks, C., Tum, M., Schaap, M., (2013): The impact of large scale biomass production on ozone air pollution in Europe, *Atmospheric Environment*, Vol. 71, pp. 352-363, doi:10.1016/j.atmosenv.2013.02.019.
- Bender, J., Bergmann, E. Weigel, H-J, Grünhage, L., Schröder, M., Builtjes, P., Schaap, M., Kranenburg, R., Wichink Kruit, R., Stern, R., Baumgarten, M., Matyssek, R., (2015): Anwendung und Überprüfung neuer Methoden zur flächenhaften Bewertung der Auswirkung von bodennahem Ozon auf die Biodiversität terrestrischer Ökosysteme, Abschlussbericht Förderkennzeichen (UFOPLAN), 3711 63 235, UBA Texte 70/2015.
- Beuck, H., Quass, U., Klemm, O., Kuhlbusch, T.A.J., (2011): Assessment of sea salt and mineral dust contributions to PM10 in NW Germany using tracer models and positive matrix factorization, *Atmospheric Environment*, Vol. 45, pp. 5813-5821.
- Builtjes, P., Hendriks, E., Koenen, M., Schaap, M., Banzhaf, S., Kerschbaumer, A., Gauger, T., Nagel, H.-D., Scheuschner, T., Schlutow, A., (2011): Erfassung, Prognose und Bewertung von Stoffeinträgen und ihren Wirkungen in Deutschland; Modelling of Air Pollutants and Ecosystem Impact (MAPESI), Abschlussbericht Förderkennzeichen (UFOPLAN) 3707 64 200, Umweltbundesamt, Dessau.
- Clarkson, T. W., Magos, L., (2006): The toxicology of mercury and its chemical compounds, *Critical Reviews in Toxicology*, Vol. 36, No. 8, pp. 609-662.
- Curier, R.L., Timmermans, R., Calabretta-Jongen, S., Eskes, H., Segers, A., Swart, D., Schaap, M., (2012): Improving ozone forecasts over Europe by synergistic use of the LOTOS-EUROS chemical transport model and in-situ measurements, *Atmospheric Environment*, Vol. 60, pp. 217-226, doi:10.1016/j.atmosenv.2012.06.017.
- Curier, R.L., Kranenburg, R., Segers, A.J., Timmermans, R.M.A., Schaap, M., (2014): Synergistic use of OMI NO2 tropospheric columns and LOTOS-EUROS to evaluate the NOx emission trends across Europe, *Remote Sensing of Environment*, Vol. 149, pp. 58-69, doi:10.1016/j.rse.2014.03.032.
- Cyrys, J., Stolzel, M., Heinrich, J., Kreyling, W.G., Menzel, N., Wittmaack, K., Tuch, T., Wichmann, H.-E., (2003): Elemental composition and sources of fine and ultrafine ambient particles in Erfurt, Germany, *The Science of the total Environment*, Vol. 305, pp. 143-156.
- Drevnick, P.E., Engstrom, D.R., Driscoll, C.T., Balogh, S.J., Kamman, N.C., Long, D.T., Muir, D.G.C., Parsons, M.J., Rolfhus, K. R., Rossmann, R., Swain, E.B., (2012): Spatial and temporal patterns of mercury accumulation in lacustrine sediments across the Laurentian Great Lakes region, *Environment and Pollution*, DOI: 10.1016/j.envpol. 2011.05.025.
- Edgerton, E.S., Hartsell, B.E., Jansen, J.J., (2006): Mercury speciation in coal-fired power plant plumes observed at three surface sites in the southeastern US, *Environ. Sci. Technol*, Vol. 40, No. 15, pp. 4563–4570.

- Erismann, J.W. and Schaap, M., (2004): The need for ammonia abatement with respect to secondary PM reductions in Europe, *Environmental Pollution*, Vol. 129, pp. 159–163.
- European Commission, DG Environment, (2013): Guidance on the Commission Implementing Decision laying down rules for Directives 2004/107/EC and 2008/50/EC of the European Parliament and of the Council as regards the reciprocal exchange of information and reporting on ambient air (Decision 2011/850/EU).
- Fuchs, S., Scherer, U., Wander, R., Behrendt, H., Venohr, M., Opitz, D., Hillenbrand, Th., Marscheider-Weidemann, F., Götz, Th. (2010): Calculation of Emissions into Rivers in Germany using the MONERIS Model, Nutrients, heavy metals and polycyclic aromatic hydrocarbons. UBA-Texte 46/2010, Dessau.
- Gauger, T., Anshelm, F., Köble, R., (2000): Kritische Luftschadstoff-Konzentrationen und Eintragsraten sowie ihre Überschreitung für Wald und Agrarökosysteme sowie naturnahe waldfreie Ökosysteme, UBA-FB 297 85 079.
- Gauger, T., Anshelm, F., Schuster, H., Erismann, J.W., Vermeulen, A.T., Draaijers, G.P.J., Bleeker, A., Nagel, H.-D., (2002): Mapping of ecosystem specific long-term trends in deposition loads and concentration of air pollutants in Germany and their comparison with critical loads and critical levels, Part 1: deposition loads 1990-1999. Inst. f. Navigation, Stuttgart, pp. 1-207.
- Gu, J., Pitz, M., Schnelle-Kreis, J., Diemer, J., Reller, A., Zimmermann, R., Soentgen, J., Stoelzel, M., Wichmann, H.E., Peters, A., Cyrus, J., (2011): Source apportionment of ambient particles: Comparison of positive matrix factorization analysis applied to particle size distribution and chemical composition data, *Atmospheric Environment*, Vol. 45, pp.1849-1857.
- Harmens, H., Buse, A., Büker, P., et al. (2004): Heavy Metal Concentrations in European Mosses: 2000/2001 Survey, *Journal of Atmospheric Chemistry*, Vol. 49, pp. 425-436.
- Harmens, H., Norris, D. & the participants of the moss survey, (2008): Spatial and temporal trends in heavy metal accumulation in mosses in Europe (1990-2005), Programme Coordination Centre for the ICP Vegetation, Centre for Ecology and Hydrology, Bangor, UK.
- Harmens, H., Norris, D., Steinnes, E. et al. (2010): Mosses as biomonitors of atmospheric heavy metal deposition: Spatial patterns and temporal trends in Europe, *Environmental Pollution*, Vol. 158, pp. 3144-3156.
- Hendriks, C., Kranenburg, R., Kuenen, J., Van Gijlswijk, R., Wichink Kruit, R., Segers, A., Denier van der Gon, H., Schaap, M., (2013): The origin of ambient particulate matter concentrations in the Netherlands, *Atmospheric Environment*, Vol. 69, pp. 289-303. doi:10.1016/j.atmosenv.2012.12.017.
- Holmes, C.D., Jacob, D.J., Corbitt, E.S., Mao, J., Yang, X., Talbot, R., Slemr, F., (2010): Global atmospheric model for mercury including oxidation by bromine atoms, *Atmospheric Chemistry and Physics*, Vol. 10, No. 24, pp. 12037-12057.
- Hueglin, C., Gehrig, R., Baltensperger, U., Gysel, M., Monn, C., Vonmont, H., (2005): Chemical characterisation of PM_{2.5}, PM₁₀ and coarse particles at urban, near-city and rural sites in Switzerland, *Atmospheric Environment*, Vol. 39, pp.637-651.
- John, A.C., Kuhlbusch, T.A.J., Fissan, H., Schmidt, K.-G., (2001): Size-fractionated sampling and chemical analysis by total-reflection X-ray fluorescence spectrometry of PM_x in ambient air and emissions, *Spectrochimica Acta Part B*, Vol. 56, pp. 2137-2146.
- Jörß, W., Kugler, U., Theloke, J., (2010): Emissionen im PAREST Referenzszenario 2005-2020, Teilbericht zum F&E-Vorhaben „Strategien zur Verminderung der Feinstaubbelastung - PAREST“. UBA-FB 001524/ANH,4. ISSN 1862-4804.
- Knappe, F., Möhler, S., Ostermayer, A., Lazar, S., Kaufmann, C., (2008): Vergleichende Auswertung von Stoffeinträgen in Böden über verschiedene Eintragspfade, *Forschungsbericht 203 74 275*, UBA-FB 001168. ISSN 1862-4804.
- Kos, G., Ryzhkov, A., Dastoor, A., Narayan, J., Steffen, A., Ariya, P. A., and Zhang, L., (2013): Evaluation of discrepancy between measured and modelled oxidized mercury species, *Atmos. Chem. Phys.*, Vol.13, pp. 4839–4863.
- Kuhlbusch, T.A.J., John, A.C., (2000): Korngrossenabhängige Untersuchungen van Schwebstaub und Inhaltstoffen.
- Lindberg, S., Bullock, R., Ebinghaus, R., Engstrom, D., Feng, X.B., Fitzgerald, W., Pirrone, N., Prestbo, E., Seigneur, C.A., (2007): Synthesis of progress and uncertainties in attributing the sources of mercury in deposition, *Ambio*, Vol. 36, No. 1, pp. 19–32.
- Lohman, K., Seigneur, C., Edgerton, E., Jansen, J., (2006): Modeling mercury in power plant plumes, *Environ. Sci. Technol.*, Vol. 40, No.12, pp. 3848–3854.
- Lohman, K., Seigneur, C., Gustin, M., Lindberg, S., Mar. (2008): Sensitivity of the global atmospheric cycle of mercury to emissions, *Applied Geochemistry*, Vol. 23, No. 3, pp. 454-466.

- Lohman, K., Seigneur, C., Edgerton, E., Jansen, J., (2006): Modeling mercury in power plant plumes, *Environ. Sci. Technol.* Vol. 40, No.12, pp. 3848–3854.
- Malcolm, E.G., Keeler, G.J., Landis, M.S., (2003): The effects of the coastal environment on the atmospheric mercury cycle, *J. Geophys. Res.*, Vol. 108, No. D12, ACH 4–1–ACH 4–9.
- Manders, A.M.M., Schaap, M., Hoogerbrugge, R., (2009): Testing the capability of the chemistry transport model LOTOS-EUROS to forecast PM10 levels in the Netherlands, *Atmospheric Environment*, Vol. 43, pp. 4050-4059, doi:10.1016/j.atmosenv.2009.05.006.
- Manders, A.M.M., Schaap, M., Querol, X., Albert, M.F.M.A., Vercauteren, J., Kuhlbusch, T.A.J. & Hoogerbrugge, R., (2010): Sea salt concentrations across the European continent. *Atmospheric Environment*, Vol. 44, pp. 2434-2442.
- Oken, E., Choi, A., Karagas, M., Mariën, K., Rheinberger, C., Schoeny, R., Sunderland, E., Korrick, S., (2012): Which fish should I eat?, perspectives influencing fish consumption choices, *Environmental Health Perspectives*, Vol. 120, No.6, pp. 790e798.
- Obrist, D., Tas, E., Peleg, M., Matveev, V., Fain, X., Asaf, D., Luria, M., (Jan. 2011): Bromine-induced oxidation of mercury in the mid-latitude atmosphere, *Nature Geoscience*, Vol. 4, No. 1, pp. 22-26.
- Pacyna, E.G., Pacyna, J.M., Steenhuisen, F., and Wilson, S., (2006): Global anthropogenic mercury emission inventory for 2000, *Atmospheric Environment*, Vol. 40, pp. 4048-4063.
- Pacyna, E. G., et al. (2010): Global emission of mercury to the atmosphere from anthropogenic sources in 2005 and projections to 2020, *Atmospheric Environment*, Vol. 40, No.20, pp. 2487-2499.
- Pirrone, N., et al. (2009): Global mercury emissions to the atmosphere from natural and anthropogenic sources, in *Mercury Fate and Transport in the Global Atmosphere: Emissions, Measurements, and Models*, edited by Pirrone, N., and Mason, R. P., pp. 3-49, Springer, Dordrecht.
- Pirrone, N.; Cinnirella, S.; Feng, X.; Finkelman, R.B.; Friedli, H.R.; Leaner, J.; Mason, R.; Mukherjee, A.B.; Stracher, G.B.; Streets, D. G.; Telmer, K.; (2010): Global mercury emissions to the atmosphere from anthropogenic and natural sources, *Atmos. Chem. Phys*, Vol. 10, No.13, pp. 5951–5964.
- Rafaj, P., Cofala, J., Kuenen, J., Wyrwa, A., Zyśk, J., (2014): Benefits of European climate policies for mercury air pollution, *Atmosphere*, Vol. 5, No.1, pp. 45-59.
- Rice, D.C., (2008): Overview of modifiers of methylmercury neurotoxicity, *Chemicals, nutrients, and the social environment, Neuro-Toxicology*, Vol. 29, pp. 761–766.
- Richard, A., Gianini, M.F.D., Mohr, C., Furger, M., Bukowiecki, N., Minguillon, M.C., Lienemann, P., Flechsig, U., Appel, K., DeCarlo, P.F., Heringa, M.F., Chirico, R., Baltensperger, U., Prevot, A.S.H., (2011): Source apportionment of size and time resolved trace elements and organic aerosols from an urban courtyard site in Switzerland, *Atmos. Chem. Phys.*, Vol. 11, pp. 8945-8963.
- Rogula-Kozłowska, W., Blaszcak, B., Dzopa, S., Klejnowski, K., Sowka, I., Zwodziazak, A., Jablonska, M., Mathews, B., (2011): PM2.5 in the central part of Upper Silesia, Poland: concentrations, elemental composition, and mobility of components, *Environ Monit Assess*, Vol. 185, pp. 581-601.
- Schaap, M., Denier Van Der Gon, H.A.C., Dentener, F.J., Visschedijk, A.J.H., Van Loon, M., Ten Brink, H.M., Putaud, J.-P., Guillaume, B., Liousse C., Builtjes, P.J.H., (2004a): Anthropogenic Black Carbon and Fine Aerosol Distribution over Europe, *Journal of Geophysical Research*, Vol. 109, D18201, doi: 10.1029/2003JD004330.
- Schaap, M., van Loon, M., ten Brink, H.M., Dentener, F.D., Builtjes, P.J.H., (2004b): Secondary inorganic aerosol simulations for Europe with special attention to nitrate, *Atmospheric Chemistry and Physics*, Vol. 4, pp. 857-874.
- Schaap, M., Sauter, F., Timmermans, R.M.A., Roemer, M., Velders, G., Beck, J., Builtjes, P.J.H., (2008): The LOTOS-EUROS model: description, validation and latest developments, *International Journal of Environment and Pollution*, Vol. 32, No. 2, pp. 270–290.
- Schaap, M., Weijers, E.P., Mooibroek, D., Nguyen, L., Hoogerbrugge, R., (2010): Composition and origin of Particulate Matter in the Netherlands, BOP report 5000099007/2010.
- Schaap, M., Kranenburg, R., Curier, L., Jozwicka, M., Dammers, E., Timmermans, R., (2013): Assessing the sensitivity of the OMI-NO2 product to emission changes across Europe, *Remote Sensing*, Vol. 5, No. 9, pp. 4187-4208, doi:10.3390/rs5094187.

- Schaap, M., Wichink Kruit, R., Banzhaf, S., Scheuschner, T., Hendriks, C., Kranenburg, R., Segers A., Bultjes, P. (2015): Atmospheric deposition to German naturaland semi-natural ecosystems during 2009, Report to PINETI II Project (Project No. FKZ 371263240-1), Umweltbundesamt, Dessau.
- Scheider, J., Lorbeer, G., (2002): Inhaltsstoffe vna PM10 und PM2.5 and zwei messstationen, Umweltbundesamt GmbH, Wien. ISBN 3-85457-649-8.
- Schroeder, W. H.; Munthe, J.; (1998): Atmospheric mercury – An overview, *Atmos. Environ.*, Vol. 32, pp. 809–822.
- Seigneur, C., Vijayaraghavan, K., Lohman, K., Levin, L., (2009): The AER/EPRI Global Chemical Transport Model for Mercury (CTM-HG), in: Pirrone, N., Mason, R. (Eds.), *Mercury Fate and Transport in the Global Atmosphere*, Springer, London, New York, pp. 589-602.
- Shatalov V., Ilyin I., Gusev A., Rozovskaya O., Travnikov O. (2015): Heavy Metals and Persistent Organic Pollutants: Development of multi-scale modeling and trend analysis methodology, EMEP/MSC-E Technical report 1/2015.
- Sprovieri, F., Pirrone, N., Ebinghaus, R., Kock, H., and Dommergue, A. (2010): Worldwide atmospheric mercury measurements: a review and synthesis of spatial and temporal trends, *Atmos. Chem. Phys.*, Vol.10, pp. 8245-8265.
- Sunderland, E. M. (2007): Mercury exposure from domestic and imported estuarine and marine fish in the US seafood market, *Environmental Health Perspectives*, Vol. 115, No.2, pp. 235-242.
- Swielicki, E., Krejci, R., (1996): Source characterisation of the Central European atmospheric aerosol using multivariate statistical methods, *Nuclear Instruments and Methods in Physics Research B*, Vol. 109/110, pp. 519-525.
- Travnikov O. (2011): Atmospheric Transport of Mercury, in *Environmental Chemistry and Toxicology of Mercury* (eds G. Liu, Y. Cai and N. O'Driscoll), John Wiley & Sons, Inc., Hoboken, NJ, USA. doi:10.1002/9781118146644.ch10.
- Truhaut R. (1977): Ecotoxicology: objectives, principles, and perspectives, *Ecotoxicol Environ Saf*, Vol. 1, pp. 151-173.
- UBA (2017): National Trend Tables for the German Atmospheric Emission Reporting (Heavy Metals) 1990 – 2015, www.uba.de
- Vallius, M., Janssen, N.A.H., Heinrich, J., Hoek, G., Ruuskanen, J., Cyrys, J., Van Grieken, R., De Hartog, J.J., Kreyling, W.G., Pekkanen, J., (2005): Sources and elemental composition of ambient PM2.5 in three European cities, *Science of the Total Environment*, Vol. 337, pp. 147-162.
- Van Damme, M., Wichink Kruit, R.J., Schaap, M., Clarisse, L., Clerbaux, C., Coheur, P.-F., Dammers, E., Dolman, A.J., Erisman, J.W., (2014): Evaluating 4 years of atmospheric ammonia (NH3) over Europe using IASI satellite observations and LOTOS-EUROS model results, *Journal of Geophysical Research: Atmospheres*, Vol. 119, No. 15, pp. 9549-9566.
- Van Ham, J/ and Pulles, T., (1998): The Dutch New National Model (in Dutch), TNO Milieu, Energie en Procesinnovatie - Apeldoorn 1998, Infomil, Den Haag, ISBN 90-76323-00-3; <http://www.infomil.nl/onderwerpen/klimaat-lucht/luchtkwaliteit/rekenen-meten/nnm/paarse-boekje/>
- VMM (2010): Chemkar PM10 'hotspots': Chemische karakterisatie van fijn stof in Vlaanderen, 2008-2009.
- VMM (2011): Chemkar PM10, Chemische karakterisering van fijn stof in Vlaanderen - 2010VMM (2009), Chemkar PM10: Chemische karakterisatie van fijn stof in Vlaanderen, 2006-2007.
- VMM (2013): Chemkar PM10, Chemische karakterisering van fijn stof in Vlaanderen, 2011-2012.
- Weigelt, A., Temme, C., Bieber, E., Schwerin, A., Schuetze, M., Ebinghaus, R., Kock, H.K., Measurements of atmospheric mercury species at a German rural background site from 2009 to 2011 – methods and results. *Environ. Chem.*, Vol.10, pp. 102–110, 10 2013. <http://dx.doi.org/10.1071/EN12107>.
- Wichink Kruit, R., Schaap, M., Segers, A., Banzhaf, S., Schauschner, T., Bultjes, P., Heslinga, D., (2014): PINETI (Pollutant INput and EcosysTem Impact) report, Modelling and mapping of atmospheric nitrogen and sulphur deposition and critical loads for ecosystem specific assessment of threats to biodiversity in Germany, Abschlussbericht Förderkennzeichen (UFOPLAN) 3710 63 246, Umweltbundesamt, Dessau.
- Wichink Kruit, R.J., Schaap, M., Sauter, F., Van Zanten, M.C., Van Pul, W.A.J., (2012): Modelling the distribution of ammonia across Europe including bi-directional surface-atmosphere exchange, *Biogeosciences*, Vol. 9, pp. 5261-5277. doi:10.5194/bg-9-5261-2012.

Wichink Kruit, R., Schaap, M., Segers, A., Banzhaf, S., Scheuschner, T., Bultjes, P. and Heslinga, D.: PINETI (Pollutant INput and EcosysTEM Impact) report, Modelling and mapping of atmospheric nitrogen and sulphur deposition and critical loads for ecosystem specific assessment of threats to biodiversity in Germany, Dessau., 2014.

Wright et al. (2016) : Atmos. Chem. Phys. Discuss., doi:10.5194/acp-2016-474, 2016.

Zhang, L., Gong, S., Padro, J., Barrie, L., (2001): A size-segregated particle dry deposition scheme for an atmospheric aerosol module, Atmospheric Environment, Vol. 35, pp. 549-560.

Zhang, L., Brook, J.R., Vet, R., (2003): A revised parameterization for gaseous dry deposition in air-quality models, Atmos. Chem. Phys., Vol. 3, pp. 2067–2082.

Zhang, L., Gong, S., Padro, J., Berrie, L., (2001): A size-segregated particle dry deposition scheme for an atmospheric aerosol module, Atmospheric Environment, Vol. 35, pp. 549-560.

Zhang, Y.; Jaeglé, L.; van Donkelaar, A.; Martin, R. V.; Holmes, C. D.; Amos, H. M.; Wang, Q.; Talbot, R.; Artz, R.; Brooks, S.; Luke, W.; Holsen, T. M.; Felton, D.; Miller, E. K.; Perry, K. D.; Schmeltz, D.; Steffen, A.; Tordon, R.; Weiss-Penzias, P.; Zsolway, R., (2012): Nested-grid simulation of mercury over North America, Atmos. Chem. Phys. Discuss., Vol. 12, pp. 2603-2646.

5 List of Annexes

- ▶ Annex 1: Dry deposition fluxes (in $\mu\text{g}/\text{m}^2/\text{year}$) based on empirical approach and modelled deposition velocities
- ▶ Annex 2: Total deposition fluxes (in $\mu\text{g}/\text{m}^2/\text{year}$) based on empirical approach and modelled deposition velocities

Annex 1: Dry deposition fluxes (in $\mu\text{g}/\text{m}^2/\text{year}$) based on empirical approach and modelled deposition velocities

Table A1.1: Industrial stations

Metal	grs	ara	crp	cnf	dec	wat	urb	oth	sem
Cd	44.00	48.54	61.53	129.59	68.75	41.71	59.65	36.73	45.66
Pb	1889.47	2116.11	2641.71	5345.58	3256.83	1894.35	2815.45	1456.19	1972.92
As	71.25	80.08	99.61	199.59	125.55	72.36	108.45	53.82	74.50
Ni	501.21	550.37	700.91	1493.81	758.59	466.83	659.05	428.16	519.06
Zn	2915.39	3233.09	4076.52	8469.32	4717.75	2818.80	4087.92	2369.09	3031.63

Comments under table, for e.g. references and explanations

Table A1.2: Rural stations

Metal	grs	ara	crp	cnf	dec	wat	urb	oth	sem
Cd	7.27	8.11	10.16	20.79	12.22	7.18	10.57	5.72	7.58
Pb	280.39	312.79	392.04	801.81	471.46	277.11	407.93	220.81	292.30
As	23.23	26.31	32.48	63.74	42.81	24.23	36.92	16.81	24.37
Cr	122.16	139.03	170.77	330.30	231.85	129.69	199.77	85.69	128.43
Cu	216.55	246.45	302.71	585.50	410.99	229.89	354.12	151.89	227.65
Ni	60.02	66.86	83.92	172.30	100.00	59.01	86.56	47.63	62.53
Zn	3642.78	4007.97	5094.06	10802.20	5589.50	3418.68	4853.37	3081.60	3775.58
V	18.65	21.57	26.06	47.96	38.79	20.95	33.33	11.72	19.74
Mn	362.65	399.88	507.12	1069.36	564.84	343.18	490.16	303.45	376.21
Sb	52.16	58.68	72.92	145.73	92.46	53.16	79.85	39.18	54.57
Ti	306.03	337.44	427.94	902.40	476.65	289.60	413.63	256.07	317.47
Mo	44.01	49.51	61.52	122.95	78.00	44.85	67.37	33.06	46.04

Table A1.3: Traffic stations

Metal	grs	ara	crp	cnf	dec	wat	urb	oth	sem
Cd	7.39	8.55	10.33	19.01	15.38	8.31	13.22	4.65	7.83
Pb	390.14	438.93	545.44	1090.03	691.57	397.62	597.25	293.09	408.15
As	40.89	46.00	57.17	114.25	72.48	41.67	62.60	30.72	42.78
Cr	175.02	199.19	244.65	473.21	332.16	185.80	286.20	122.76	183.99
Cu	2155.27	2366.66	3014.00	6423.58	3262.06	2007.44	2834.02	1841.15	2232.02
Ni	111.74	124.65	156.23	319.53	187.88	110.43	162.57	88.00	116.48
Zn	1579.95	1828.16	2208.13	4063.87	3287.37	1775.07	2824.37	993.33	1672.69
V	99.64	115.29	139.25	256.28	207.31	111.94	178.12	62.64	105.49
Mn	914.50	1004.19	1278.86	2725.57	1384.12	851.77	1202.49	781.21	947.06
Sb	274.57	300.46	383.98	825.48	405.61	252.36	352.74	238.50	283.94
Ti	694.88	763.03	971.74	2071.01	1051.71	647.21	913.71	593.60	719.62
Mo	144.88	159.09	202.61	431.81	219.28	134.95	190.51	123.77	150.04

Table A1.4: Urban stations

Metal	grs	ara	crp	cnf	dec	wat	urb	oth	sem
Cd	5.29	6.28	7.39	12.49	12.55	6.47	10.74	2.71	5.66
Pb	334.53	383.57	467.59	884.74	662.32	364.42	569.90	223.74	352.79
As	30.38	34.57	42.47	82.14	57.65	32.25	49.68	21.31	31.94
Cr	254.42	283.82	355.73	727.54	427.79	251.44	370.15	200.36	265.22
Cu	1065.77	1181.22	1490.25	3100.84	1718.06	1028.23	1488.91	868.68	1107.99
Ni	82.99	94.45	116.01	224.39	157.50	88.10	135.71	58.21	87.24
Zn	1740.61	2014.06	2432.68	4477.13	3621.67	1955.57	3111.59	1094.34	1842.79
V	26.69	30.37	37.31	72.16	50.65	28.33	43.64	18.72	28.06
Mn	909.88	1003.28	1272.35	2683.00	1417.16	861.03	1229.78	761.35	943.91
Sb	168.46	186.70	235.55	490.12	271.56	162.52	235.34	137.30	175.13
Ti	555.26	612.26	776.46	1637.31	864.83	525.45	750.48	464.62	576.03
Mo	120.30	133.34	168.22	350.02	193.93	116.07	168.07	98.06	125.07

Annex 2: Total deposition fluxes (in $\mu\text{g}/\text{m}^2/\text{yr}$) based on empirical approach and modelled deposition velocities

Table A2.1: Industrial stations

Metal	grs	ara	crp	cnf	dec	wat	urb	oth	sem
Cd	71.12	75.66	88.65	156.71	95.87	68.83	86.77	63.85	72.77
Pb	2498.08	2724.71	3250.32	5954.18	3865.43	2502.96	3424.06	2064.79	2581.52
Hg*	11.15	11.15	11.15	11.15	11.15	11.15	11.15	11.15	11.15
As	141.64	150.47	170.00	269.98	195.94	142.75	178.84	124.21	144.90
Cr*	81.85	81.85	81.85	81.85	81.85	81.85	81.85	81.85	81.85
Cu*	1197.45	1197.45	1197.45	1197.45	1197.45	1197.45	1197.45	1197.45	1197.45
Ni	934.12	983.28	1133.82	1926.71	1191.50	899.74	1091.96	861.07	951.96
Zn	59768.93	60086.63	60930.07	65322.87	61571.30	59672.35	60941.46	59222.64	59885.17
V*	130.62	130.62	130.62	130.62	130.62	130.62	130.62	130.62	130.62
Mn*	1295.45	1295.45	1295.45	1295.45	1295.45	1295.45	1295.45	1295.45	1295.45
Sb*	57.01	57.01	57.01	57.01	57.01	57.01	57.01	57.01	57.01
Co*	12.80	12.80	12.80	12.80	12.80	12.80	12.80	12.80	12.80
Mo*	113.71	113.71	113.71	113.71	113.71	113.71	113.71	113.71	113.71

*Only wet deposition data available

Table A2.2: Rural stations

Metal	grs	ara	crp	cnf	dec	wat	urb	oth	sem
Cd	34.39	35.23	37.28	47.90	39.34	34.30	37.69	32.84	34.69
Pb	889.00	921.40	1000.65	1410.41	1080.06	885.71	1016.54	829.41	900.90
Hg*	11.15	11.15	11.15	11.15	11.15	11.15	11.15	11.15	11.15
As	93.62	96.70	102.87	134.13	113.20	94.62	107.31	87.20	94.76
Cr	204.01	220.88	252.62	412.15	313.70	211.53	281.62	167.54	210.27
Cu	1414.00	1443.90	1500.16	1782.95	1608.43	1427.34	1551.57	1349.34	1425.10
Ni	492.93	499.77	516.83	605.21	532.91	491.92	519.47	480.54	495.44
Zn	60496.32	60861.52	61947.61	67655.75	62443.05	60272.23	61706.92	59935.15	60629.13
V	149.27	152.20	156.68	178.58	169.42	151.57	163.95	142.35	150.36
Mn	1658.10	1695.33	1802.57	2364.81	1860.29	1638.63	1785.61	1598.90	1671.66
Sb	109.17	115.69	129.93	202.74	149.47	110.17	136.86	96.19	111.58
Ti**	306.03	337.44	427.94	902.40	476.65	289.60	413.63	256.07	317.47
Co*	12.80	12.80	12.80	12.80	12.80	12.80	12.80	12.80	12.80
Mo	157.71	163.21	175.23	236.66	191.71	158.55	181.07	146.76	159.74

*Only wet deposition data available; ** Only dry deposition data available

Table A2.3: Traffic stations

Metal	grs	ara	crp	cnf	dec	wat	urb	oth	sem
Cd	34.51	35.67	37.45	46.13	42.50	35.42	40.33	31.77	34.94
Pb	998.75	1047.53	1154.05	1698.64	1300.17	1006.22	1205.86	901.69	1016.76
Hg*	11.15	11.15	11.15	11.15	11.15	11.15	11.15	11.15	11.15
As	111.28	116.40	127.56	184.64	142.88	112.07	132.99	101.11	113.17
Cr	256.87	281.03	326.50	555.06	414.01	267.65	368.05	204.61	265.84
Cu	3352.72	3564.11	4211.45	7621.03	4459.51	3204.89	4031.47	3038.59	3429.47
Ni	544.65	557.56	589.14	752.44	620.79	543.34	595.47	520.90	549.39
Zn	58433.49	58681.70	59061.68	60917.42	60140.92	58628.61	59677.92	57846.88	58526.24
V	230.26	245.91	269.88	386.91	337.94	242.57	308.74	193.27	236.11
Mn	2209.95	2299.64	2574.31	4021.02	2679.57	2147.22	2497.94	2076.66	2242.51
Sb	331.58	357.47	440.99	882.49	462.62	309.37	409.75	295.52	340.95
Ti**	694.88	763.03	971.74	2071.01	1051.71	647.21	913.71	593.60	719.62
Co*	12.80	12.80	12.80	12.80	12.80	12.80	12.80	12.80	12.80
Mo	258.59	272.80	316.32	545.52	332.99	248.65	304.22	237.47	263.75

*Only wet deposition data available; ** Only dry deposition data available

Table A2.4: Urban stations

Metal	grs	ara	crp	cnf	dec	wat	urb	oth	sem
Cd	32.41	33.40	34.51	39.61	39.67	33.58	37.86	29.83	32.78
Pb	943.13	992.18	1076.19	1493.34	1270.92	973.02	1178.51	832.34	961.40
Hg*	11.15	11.15	11.15	11.15	11.15	11.15	11.15	11.15	11.15
As	100.77	104.96	112.86	152.53	128.05	102.64	120.07	91.70	102.33
Cr	336.27	365.67	437.58	809.39	509.64	333.29	452.00	282.21	347.07
Cu	2263.21	2378.67	2687.70	4298.28	2915.51	2225.68	2686.36	2066.13	2305.44
Ni	515.90	527.36	548.92	657.29	590.41	521.01	568.62	491.12	520.15
Zn	58594.16	58867.61	59286.22	61330.68	60475.21	58809.12	59965.13	57947.89	58696.34
V	157.31	161.00	167.93	202.78	181.27	158.96	174.27	149.34	158.68
Mn	2205.33	2298.73	2567.80	3978.45	2712.61	2156.48	2525.23	2056.80	2239.36
Sb	225.47	243.72	292.56	547.13	328.57	219.53	292.35	194.32	232.14
Ti**	555.26	612.26	776.46	1637.31	864.83	525.45	750.48	464.62	576.03
Co*	12.80	12.80	12.80	12.80	12.80	12.80	12.80	12.80	12.80
Mo	234.01	247.04	281.92	463.73	307.64	229.77	281.77	211.76	238.78

*Only wet deposition data available; ** Only dry deposition data available